

An-Najah National University

Faculty of Graduate Studies

**Synthesis, Characterization, Antibacterial Activities of Novel
Polydentate Schiff's Bases and Their Transition Metal
Complexes**

By

Yasmeen Azam Aldomere

Supervisor

Prof. Ismail Warad

**This Thesis is submitted in Partial Fulfillment of the Requirements for
the Degree of Master in Chemistry, Faculty of Graduate Studies,
An- Najah National University, Nablus, Palestine.**

2015

**Synthesis, Characterization, Antibacterial Activities of Novel
Polydentate Schiff's Bases and Their Transition Metal
Complexe**

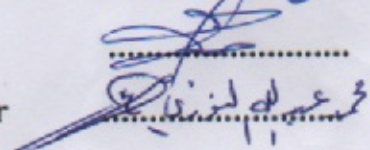
**By
Yasmeen Azam Aldomere**

This Thesis was Defended Successfully on 26/3/2015 and approved by:

Defense Committee Members

Signature

1. Prof. Ismail Warad / Supervisor
2. Dr. Nizam Diab / External Examiner
3. Dr. Ashraf Sawafta / Internal Examiner
4. Prof. Mohammed Al-Nuri / Internal Examiner


.....
N. Diab
.....

.....
محمد عبد النور النوري

iii
DIDICATION

To my loved Husband , for love, care and support all the time.

To my Son , with hope for bright future.

To my beloved Parents, for their prayers to me.

To my dear sister and brothers.

To all my dear friends

*My Doctors at both the university of Jordan and An-Najah
National University*

*I dedicate this ‘All the people in my life who touch my heart
research.*

ACKNOWLEDGEMENTS

Foremost, I am highly grateful thank Allah for everything in my life , In the Name of Allah, the Most Merciful, the Most Compassionate all praise be to Allah, the Lord of the worlds; and prayers and peace be upon Mohamed His servant and messenger.

I wish to express my deep appreciation to Prof. Ismail Warad, who was my advisor, for all the support and guidance. I also appreciate his positive comments and advices throughout my research and I am proud to work with him.

Also, I would like to give my heartfelt appreciation to my husband Dr. Said Shahwan, the greatest orthopedist in the world, who has accompanied me with his love, unlimited patience, understanding, helping and encouragement. Without his support, I would never be able to accomplish this work. So, I want to dedicate this thesis to my husband.

I would also like to thank the members of the examination committee for their help and valuable comments on this thesis. And many thanks to the Hamdi Mango Research Center at the University of Jordan for Scientific XRD measurement.

My parents, my little sister, my baby, my close friends ,thank you all for your love, and endless support in everything in my life.

And to the technical staff in the laboratories and all employees at the chemistry department at An-najah National University, for the help and the encouragement they provide at all times.

Thanks for Dr. Motasem Al-Masri for his efforts in the biological activities work.

Many thanks for Prof. Mohammed Al-Nuri and his family for their help and encouragement.

And the final appreciation to Dr. Mousa Al-Noaimi at the Hashemite University / Jordan for his helping in NMR, TG/DTA measurement data, and encouragement.

الإقرار

أنا الموقع أدناه مقدم الرسالة التي تحمل العنوان:

Synthesis, Characterization, Antibacterial Activities of Novel

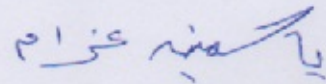
Polydentate Schiff's Bases and Their Transition Metal Complexes

أقر بأن ما اشتملت عليه هذه الرسالة هو نتاج جهدي الخاص ، باستثناء ما تمت الإشارة إليه
حيثما ورد ، وأن هذه الرسالة ككل أو أي جزء منها لم يقدم من قبل لنيل أي درجة أو لقب علمي
أو بحثي لدى أي مؤسسة تعليمية أو بحثية أخرى.

Declaration

The work provided in this thesis, unless otherwise referenced, is the researcher's own work, and has not been submitted elsewhere for any other degrees or qualifications.

Student's name:

اسم الطالب: 

Signature:

التوقيع: 

Date:

التاريخ: ٢٦ / ٣ / ٢٠١٥

List of contents

No	Content	Page
	Dedication	lii
	Acknowledgements	lv
	Declaration	vi
	List of contents	vii
	List of Tables	x
	List of Figures	xi
	List of Schemes	xiv
	List of charts	xiv
	List of abbreviations	xv
	Abstract	xvi
	Chapter One : Introduction	1
1.1	Coordination Chemistry	2
1.2	Application of Transition Metals and their Complexes	4
1.3	Properties and Application of Some. Nobel Transition Metals and their influence in pharmacological industries	7
1.4	Schiff's base ligand	7
1.5	Chemistry of Schiff's bases ligand	9
1.6	Mechanism of Schiff's base (Imine) formation	10
1.7	Why Schiff's bases ligand are attractive ligands	11
1.8	Schiff's bases and their complexes	11
1.9	General method and history of preparation of Schiff's bases and their complexes	12
1.10	Applications of Schiff's bases and their metal complexes	13
1.11	Biological activity of Schiff's bases ligand and their complexes	15
1.12	Bacteria and Bacterial Infections	15
1.12.1	<i>Escherichia coli</i>	16
1.12.2	<i>Staphylococcus aureus</i>	17
1.12.3	<i>Pseudomonas aeruginosa</i>	18
1.13	Methods of Antimicrobial Susceptibility Testing	19
1.14	Objectives	20
1.15	Novelty	21
	Chapter Tow: Materials and Methods	21
2.1	Chemicals	21

2.2	Methods and Physical Measurements	22
2.3	General procedure for synthesis of [L ₁ , L ₂ , L ₃ , L ₄ , L ₅ , L ₆] and their Complexes	22
2.4	General procedure to synthesis of the L ₁ & L ₂	23
2.5	General procedure to synthesis of L ₃	24
2.6	General procedure for synthesis of L ₄ , L ₅ , and L ₆	26
2.7	General procedure for synthesis the Copper(II) and Cadmium(II) complexes	26
2.8	General procedure for synthesis the Copper (II) complexes	27
2.9	General procedure to synthesis the Cadmium(II) complexes	28
	Chapter Three: Results and Discussion	28
3.1	Physical data of the prepared Ligands	30
3.2	Ligands synthetic investigations	30
3.2.1	Investigation about synthesis L ₁	31
3.2.2	Investigation about synthesis L ₂	31
3.2.3	Investigation about synthesis L ₃	33
3.2.3	Investigation about synthesis L ₄	33
3.2.4	Investigation about synthesis L ₅	34
3.2.5	Investigation about synthesis L ₆	35
3.3	Complexes synthetic investigations	35
3.3.1	Copper Complexes synthesis	36
3.3.2	Cadmium Complexes synthesis	36
3.4	Spectroscopic analysis	36
3.4.1	IR Spectra Investigations	37
3.4.1.1	The general investigations about free ligands spectra	37
3.4.1.2	The general investigations about metal complexes with ligand spectra	38
3.4.1.3	IR spectrum of L ₁	40
3.4.1.4	IR spectra of L ₂	42
3.4.1.5	IR spectrum of L ₃	45
3.4.1.6	IR spectra of L ₄	47
3.4.1.7	IR spectrum of L ₅	49
3.4.1.8	IR spectrum of L ₆	51
3.4.2	UV-VISIBLE Spectra Investigations	51
3.4.2.1	UV-Visible spectra of L ₂	54
3.4.2.2	UV-Visible spectra of L ₄	54
3.4.2.2.1	UV-Visible spectrum of Free L ₄ and its complex with	56

	CuBr ₂	
3.4.2.2.2	UV-Visible spectrum of Free L ₄ and its complex with CdCl ₂	56
3.4.2.3	UV-Visible spectra of L ₅	57
3.4.2.3.1	UV-Visible spectrum of Free ligand and L ₅ with CuBr ₂	57
3.4.2.3.2	UV-Visible spectrum of Free ligand and L ₅ with CdCl ₂	59
3.4.2.4	UV-Visible spectrum of L ₆	60
3.4.3	¹ H- NMR investigations of Schiff's bases L ₁ -L ₆	61
3.4.3.1	¹ H- NMR spectra of L ₁	61
3.4.3.2	¹ H- NMR spectra of L ₂	64
3.4.3.3	¹ H- NMR spectrum of L ₃	66
3.4.3.4	¹ H- NMR spectra of L ₄	67
3.4.3.5	¹ H- NMR spectrum of L ₅	68
3.4.3.6	¹ H- NMR spectrum of L ₆	69
3.4.4	¹³ C-NMR investigations	70
3.4.4.1	¹³ C-NMR spectrum of L ₁	71
3.4.4.2	¹³ C-NMR spectrum of L ₂	72
3.4.4.3	¹³ C-NMR spectrum of L ₃	73
3.4.4.4	¹³ C-NMR spectrum of L ₄	74
3.4.4.5	¹³ C-NMR spectrum of L ₅	75
3.4.4.6	¹³ C-NMR spectrum of L ₆	76
3.5	Thermogravimetric analyses of L ₄ and their CuBr ₂ and CdCl ₂ complexes	77
3.6	Single-Crystal X-Ray Data collection	81
3.6.1	X-Ray Crystal Structure of L ₃	81
3.6.2	X-Ray Crystal Structure of L ₅	89
3.7	Antibacterial activity	95
3.7.1	Discussion about figures (3.45-3.56)	96
	Chapter Four : Conclusion	105
	References	108
	الملخص	ب

List of Table

No	Table	Page
1.1	Some Biological Uses for Metal-Containing Drugs	4
1.2	Types of Antimicrobial susceptibility testing methods	19
3.1	Physical and Elemental analysis of the Ligands	29
3.2	The crystal and experimental data of L ₃	82
3.3	Fractional atomic coordinates and isotropic or equivalent isotropic displacement parameters (A ² °)	85
3.4	Atomic displacement parameters (A ² °)	86
3.5	Geometric parameters (A ² °)	87
3.6	Hydrogen-bond geometry (A ² °)	89
3.7	Crystal data and structure refinement for L ₅	90
3.8	Selected geometric parameters (A ² °) for L ₅	91
3.9	Hydrogen bonding data for L ₅	92

List of Figures

No	Figure	Page
1.1	Tetradentate (N,N'-bis(2-pyridinecarboxalidene)-1,2-cyclohexanedi-amine) ligand	6
1.2	Some examples of Schiff's bases	8
1.3	Benzothiazole derivatives	15
1.4	<i>Escherichia coli</i>	16
1.5	<i>Staphylococcus aureus</i> bacteria	17
1.6	<i>Pseudomonas aeruginosa</i> bacteria	18
3.1	IR spectrum of L ₁	39
3.2	IR spectrum of L ₂	41
3.3	IR spectrum of L ₂ , the region (2800-3400)cm ⁻¹	41
3.4	IR spectrum of L ₂ the region (1500-2000)cm ⁻¹	42
3.5	IR spectrum of L ₃	44
3.6	IR spectrum of L ₄	46
3.7	IR spectrum of L ₄ , the region (2500-3500)cm ⁻¹	46
3.8	IR spectrum of L ₄ , the region (1500-1800)cm ⁻¹	47
3.9	IR spectrum of L ₅	48
3.10	IR spectrum of L ₆	50
3.11	UV-Visible spectrum of L ₂ (a), and L ₂ CuBr ₂ (b)	52
3.12	UV-Visible spectrum of L ₂	53
3.13	UV-Visible spectrum of L ₄ (a), L ₄ CuBr ₂ (b)	55
3.14	UV-Visible spectrum L ₄ (a), and L ₄ CdCl ₂ (b)	57
3.15	UV-Visible spectrum of L ₅ (a), L ₅ CuBr ₂ (b)	58
3.16	UV-Visible spectrum of L ₅ (a), L ₅ CdCl ₂ (b)	60
3.17	UV-Visible spectrum of L ₆ (a), L ₆ CuBr ₂ (b)	61
3.18	¹ H-NMR spectrum of L ₁	62
3.19	¹ H-NMR spectrum of L ₁ , the region (2-4.5)ppm	63
3.20	¹ H-NMR spectrum of L ₁ , the region (7-9)ppm	63
3.21	¹ H-NMR spectrum of L ₂	64
3.22	¹ H-NMR spectrum of L ₂ , the region (0-3)ppm	65
3.23	¹ H-NMR spectrum of L ₂ , the region (7-8.3)ppm	65
3.24	¹ H-NMR spectrum of L ₃	66
3.25	¹ H-NMR spectrum of L ₄	67
3.26	¹ H-NMR spectrum of L ₄ , the region (7-8.3) ppm	68
3.27	¹ H-NMR spectrum of L ₅	69
3.28	¹ H-NMR spectrum of L ₆	70
3.29	¹³ C-NMR spectrum of L ₁	71

3.30	¹³ C-NMR spectrum of L ₂	72
3.31	¹³ C-NMR spectrum of L ₃	73
3.32	¹³ C-NMR spectrum of L ₄	74
3.33	¹³ C-NMR spectrum of L ₅	75
3.34	¹³ C-NMR spectrum of L ₆	76
3.35	TG/DTA thermal curve of solid (L ₄ CuBr ₂) complex	78
3.36	TG/DTA thermal curve of solid L ₄	79
3.37	TG/DTA thermal curve of solid (L ₄ CdCl ₂) complex	80
3.38	Molecular conformation and atom-numbering scheme for the L ₃ . Displacement ellipsoids are drawn at the 30% probability level. H atoms are represented as small spheres of arbitrary radii.	83
3.39	Molecular conformation showing intramolecular C7—H...Cl1, C10—H...Cl1, C14—H...Cl2 and C17—H...Cl2 contacts, as well as a short intermolecular Cl1...Cl1A contact. For symmetry code (A): -x + 1, -y, -z. for L ₃	84
3.40	The ORTEP diagram of the final X-ray model of L ₅	92
3.41	Crystal packing of the L ₅	93
3.42	Crystal packing of the L ₅	93
3.43	The crystal packing of L ₅ . Only the hydrogen atoms involved in S---H bonding are marked by red bond, the S---S repulsion can be observed as green line	94
3.44	Antibacterial activity of L ₂ & L ₂ CuBr ₂ against (<i>E. coli</i>)	98
3.45	Antibacterial activity of L ₄ & L ₄ CuBr ₂ against (<i>E. coli</i>).	99
3.46	Antibacterial activity of L ₅ & L ₅ CuBr ₂ against (<i>E. coli</i>).	99
3.47	Antibacterial activity of L ₂ & L ₂ CuBr ₂ against (<i>S. aureus</i>).	100
3.48	Antibacterial activity of L ₄ & L ₄ CuBr ₂ against (<i>S. aureus</i>)	100
3.49	Antibacterial activity of L ₅ & L ₅ CuBr ₂ against (<i>S. aureus</i>)	101
3.50	Antibacterial activity of L ₂ & L ₂ CuBr ₂ against (<i>Pseudomonas</i>)	101
3.51	Antibacterial activity of L ₄ & L ₄ CuBr ₂ against (<i>Pseudomonas</i>)	102
3.52	Antibacterial activity of L ₅ & L ₅ CuBr ₂ against	102

	<i>(Pseudomonas)</i>	
3.53	Antibacterial activity of L ₂ & L ₂ CuBr ₂ against (<i>MRSA</i>).	103
3.54	Antibacterial activity of L ₄ & L ₄ CuBr ₂ against (<i>MRSA</i>).	103
3.55	Antibacterial activity of L ₅ & L ₅ CuBr ₂ against (<i>MRSA</i>).	104

List of Charts

No	chart	Page
3.1	Expected formula of L_2CuBr_2 depending on UV-Visible spectra	54
3.2	Expected formula of L_4CuBr_2 depending on UV-Visible spectra	56
3.3	Expected formula of L_5CuBr_2 depending on UV-Visible spectra	59
3.4	Decomposition steps of L_4CuBr_2	78

List of Scheme

No	Scheme	Page
1.1	The general scheme of formation of a Schiff base	7
1.2	Mechanism of Schiff's base formation	10
2.1	The chemical reaction of Schiff's base ligand (L1)	23
2.2	The chemical reaction of Schiff's base ligand (L2)	23
2.3	The chemical reaction of Schiff's base ligand (L3)	24
2.4	The chemical reaction of Schiff's base ligand (L4)	25
2.5	The chemical reaction of Schiff's base ligand (L5)	26
2.6	The chemical reaction of Schiff's base ligand (L6)	26
3.1	The chemical equation of Schiff's base ligand (L₁)	30
3.2	The chemical equation of Schiff's base ligand (L2)	31
3.3	The chemical equation of Schiff's base ligand (L3)	32
3.4	The chemical equation of Schiff's base ligand (L4)	33
3.5	The chemical equation of Schiff's base ligand (L5)	34
3.6	The chemical equation of Schiff's base ligand (L6)	35

List of Abbreviations

Symbol	Abbreviation
TG/DTA	Thermogravimetric / Differential thermal analysis
XRD	X-Ray Diffraction
DMSO	Dimethyl Sulfoxide
MRSA	<i>Methicillin-resistant Staphylococcus aureus</i>
<i>E. coli</i>	<i>Escherichia coli</i>
<i>S. aureus</i>	<i>Staphylococcus aureus</i>
<i>P. aeruginosa</i>	<i>Pseudomonas aeruginosa</i>

**Synthesis, Characterization, Antibacterial Activities of Novel
Polydentate Schiff's Bases and Their Transition Metal Complexes**

By

Yasmeen Azam Aldomere

Supervisor

Prof. Ismail Warad

Abstract

The work described in this thesis concerns the synthesis of six novel new polydentate Schiff's bases and the formation of their Metal Complexes with copper bromide and cadmium chloride.

The ligands and their metal complexes were characterized by IR, UV-VIS spectroscopy, EA, $^1\text{H-NMR}$, $^{13}\text{C-NMR}$, TG/DTA.

The structure of free ligand.

$\text{L}_5(\text{N}^1\text{E},\text{N}^2\text{E})\text{-N}^1,\text{N}^2\text{-bis}((5\text{-bromothiophen-2-yl)methylene)ethane-1,2\text{-diamine}$ & $\text{L}_3[(\text{N}^1\text{E},\text{N}^2\text{E})\text{-N}^1,\text{N}^2\text{-bis}(2\text{-chlorobenzylidene)cyclohexane-1,2\text{-diamine}]$ analyzed by XRD.

The potential of the ligands and their copper complexes against *E. coli*, *S. aureus*, *P. aeruginosa*, and *MRSA* bacteria were studied. So we expected to introduce to the literature a novel chemotherapy (antibacterial) drugs.

CHAPTER ONE

INTRODUCTION

1.1 Coordination Chemistry

Inorganic chemistry is one of the most important fields of chemistry and it has many divisions. Some of these are coordination chemistry, which is also called the chemistry of metal complexes; because coordination chemistry focuses on the studies of the properties of all the elements and their complexes, including the simple compounds of carbon [1].

There are no adequate researches about the time of the beginning of the first coordinated compounds, where the first known research was in the early 18th century with the discovery of Prussian Blue (a colour maker) [2]. After this, one might start searching about products of oxidation of ammoniacal cobalt solution [3]. In the years that followed, Cleve, Wolcott Gibbs, Blomstrand and Fermi did a large amount of effort towards the study of complexes.

When we are talking about coordination chemistry we have to mention Alfred Werner (he earned Nobel Prize in chemistry in 1913 for his work on coordination compounds).

Also, (M. Eigen, 1967, Wilkinson and Fischer, 1973; H. Taube 1983; Cram, Lehn and Pederson, 1987 earned Nobel prize in this field). Werner gave the basic idea about this field, in 1893 Werner described the stereochemistry of metal complexes, mechanism of isomerisation [4].

Coordination compounds have the greatest application in several fields as dyes, color photography, mineral extraction, nuclear fuels, toxicology bioinorganic chemistry, medicine, catalysis, ceramics, microelectronics, material science, photonics etc. Also, industries dealing with organic chemicals, pharmaceuticals, petrochemicals and plastics owe a lot to the findings in the field of coordination chemistry [5].

1.2 Application of Transition Metals and their Complexes

Among all the elements in the periodic table, transition metals have in general a multitask roles in terms of their applications related to humanity progression and evolution. Recently, this class of elements has found a wide range of application from the aerospace and electronic industries to health .

Metal complexes are attractive in particular organometallic compounds, they are coordinated compounds containing bonds between carbon and metal [6].

Organometallic compounds have properties that make them belong to medicinal chemistry like redox reaction and catalyst effect.

Organometallic compounds can be used in pharmaceutical industry as anticancer, antimalarial, and antibiotics for example the complexes of noble metals have found use in the treatment of diseases, such that platinum compounds for some types of cancer, gold complexes are used in the

treatment of arthritis, and there are a lot of drugs containing transition metal complexes mentioned in (**Table 1.1**) [7].

There are many researches concerned about medicinal chemistry of organometallic compounds because they exist basically in our body, here there are many examples of these compounds in human body some of these exist in proteins as hemoglobin (RBC protein that transfer oxygen from lung to the body tissues) it has iron complexes[8 , 45].

Vanadium complexes exist in hemovanadin protein (protein found in blood cells), and copper compounds present in hepatocuperin protein (protein present in liver)[8].

Also organometallic compounds present in human body as hormones like Zn complexes, that present in insulin hormone (hormone produce by pancreas to decrease glucose blood level) [8].

Also they present in enzymes, like Molybdenum complexes present in xanthine oxidase enzyme (conversion hypoxanthine to uric acid). And Zinc complexes present in Carbonic anhydrase (conversion of CO_2 to bicarbonate to maintain acid-base balance in blood) [9, 45].

Table 1.1 Some Biological Uses for Metal-Containing Drugs[7, 8, 45]

Metal	Medical Use
Au	Arthritis, gout
Ag	Antiseptic agent, prophyllacetate
As, Sb	Bactericides
Bi	Skin injuries, diarrhea, alimentary diseases
Co	Vitamine B ₁₂
Cu	Algicide, fungicide, insecticide
Ga	Antitumor agent
Hg	Antiseptic
Li	Manic depressoin
Mn	Fungicide, Parkinson's disease
Os	Antiarthritis
Pt, Pd	Antitumor agents
Rb	Substitute for K in muscular dystrophy; protective agent against adverse effects of heart drugs
Ru, Rh, Os	Experimental antitumor agents
Sn	Bactericide, fungicide
Ta, Si	Inert medical applications as gauzes, implants
Zn	Fungicide

1.3 Properties of Some Nobel Transition Metals and their influence in Pharmacological Industries

Copper

Copper is considered a bioessential transition metal because many of enzymes and hormones depend on copper for their activities. Copper complexes have significant role in a pharmacological industries [45], and they have been studied for many therapeutic purposes, such as antimalarial, antibacterial drugs, and antifungal [9], for example the

complexes of Cu(II) with Schiff bases derived from 2,6-diacetylpyridine and 2-pyridine carboxaldehyde with 4-amino-2,3-dimethyl-1-phenyl-3-pyrazolin-5-one show antibacterial and antifungal activities against *Escherichia coli*, *Staphylococcus aureus*, *Klebsiella Pneumoniae*, *Mycobacterium Smegmatis*, *Pseudomonas aeruginosa*, *Enterococcus cloacae*, *Bacillus megaterium* and *Micrococcus leteus* [9].

Copper has a neuroprotective action since it is used to treat Alzheimer's disease[10], and recently used as drugs for combat Parkinson's disease, diabetes, amyotrophic lateral sclerosis, inflammatory states (i.e., Rheumatoid arthritis), skin wounds, Cardiovascular diseases, and Leishmaniasis[11]. Also, copper (II) complexes play a significant role as anticancer agents. Especially, when copper complexes containing bi-Schiff bases as ligands are effective in reducing tumor size cells, increasing the survival of the hosts and delaying of metastasis[12, 45].

Copper(II) complexes are considered as the most promising alternatives to Cisplatin as anticancer drugs, this idea supported by a considerable number of research articles describing DNA binding, cytotoxic activities and the synthesis of copper(II) complexes [12].

Cadmium

Due to the toxic environmental impact of cadmium there is a substantial interest in the coordination chemistry of cadmium complexes, where the British Pharmaceutical Codex from 1907 indicates that cadmium iodide

(CdI₂) was used as a medicine, " for application with chilblains, and friction to enlarged joints"[13].

Also, the mobilization and immobilization of cadmium metal in the organisms, in environment, and in some technical processes (such as in ligand exchange chromatography) have been shown due to the complexation of the metal center by chelating nitrogen donor ligands [14].

When searching for the application of these metals above, I have been concerned about the Schiff's bases ligand with these metals and their biological applications. Cd(L)₂(H₂O)₂·H₂O, for example, complex has the highest potential against Streptomycin, Ampicillina, and Rifampicin, where L is salicylidene-4-chlorophenyl-2-aminothiazole [15].

Another example for the complexes of cadmium with Schiff base ligand is [Cd(L)(CH₃COO)₂].2H₂O, where L is (N,N'-bis(2-pyridinecarboxalidene)-1,2-cyclohexanedi-amine (see **Figure 1.1**), this complex acts as tetradentate with the cadmium metal ion [16].

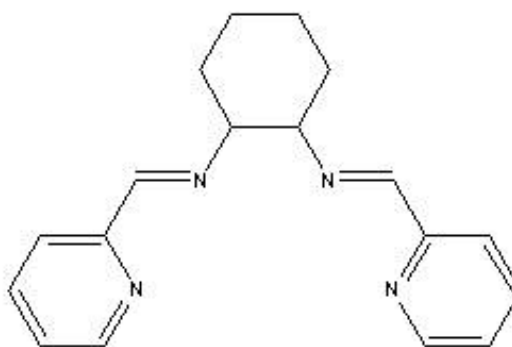


Figure (1.1): Tetradentate (N,N'-bis(2-pyridinecarboxalidene)-1,2-cyclohexanedi-amine) ligand

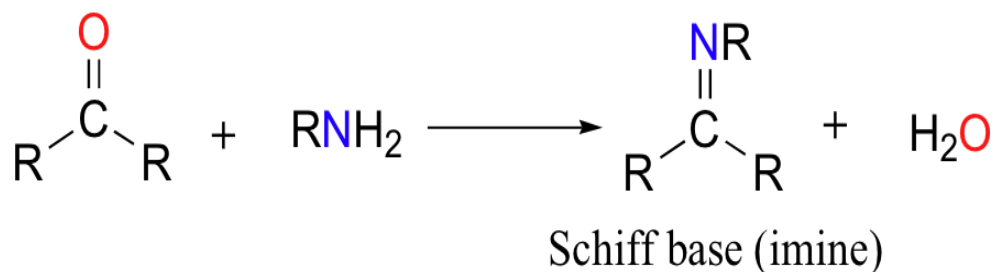
1.4 Schiff's base ligand

The studying of Schiff's bases ligand was started in 1864 by Hugo Schiff, after that this field of study was named after him.

1.5 Chemistry of Schiff's bases ligand

Schiff's bases are organic compounds arise from condensation of primary amines with carbonyl compounds (aldehyde or ketone) (Dudek, 1966), to give azomethine group having this formula $R^3R^2C=NR^1$ (**Scheme 1.1**) and also called imine or anils [15].

Azomethine or imine groups are present as natural, natural-derived, and non-natural. See ([Figure 1.2](#)) for some examples.



Scheme 1.1: The general scheme of formation of a Schiff's base.

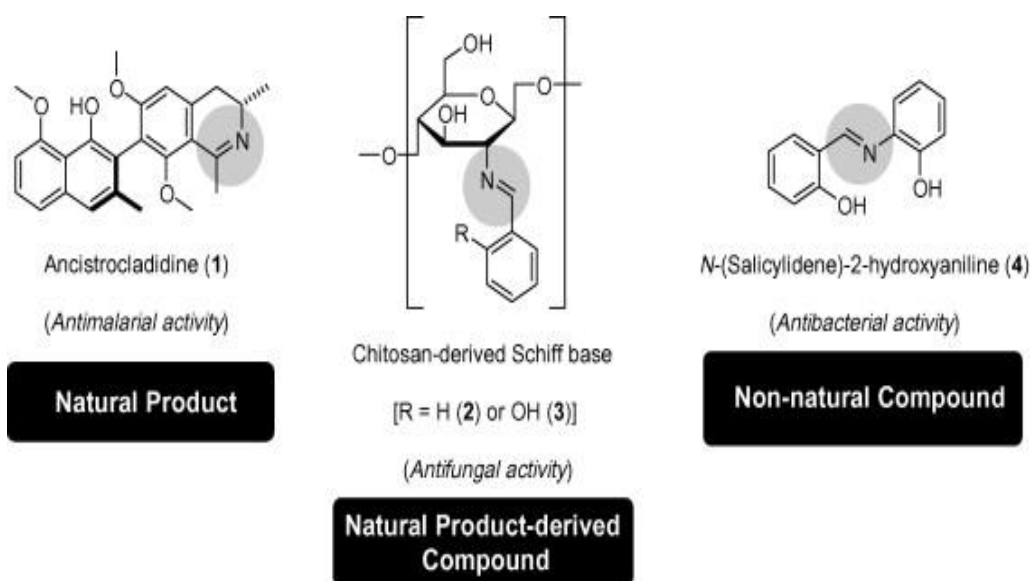


Figure 1.2 : Some examples of Schiff's bases.

The substituents R^2 and R^3 on $R^3R^2C=NR^1$ may be alkyl, cycloalkyl, aryl, heteroaryl, hydrogen, or heterocyclic groups, and the substituent at the N-imino ($C=N$) may be alkyl, aryl, heteroaryl, hydrogen, heterocyclic groups or metallo. When R^1 is hydrogen the base is called imine, if R^1 is NH_2 it is called hydrazone, when it is OH , it is called oxime, and when R^1 is an organic side chain the structure is called Schiff's base ligand.

Schiff's bases with aryl substituent are more stable and more easily synthesized. While those which contain alkyl substituents are comparatively unstable. Also, if contain aliphatic aldehydes the bases are relatively unstable and readily polymerizable, while those of aromatic aldehydes having effective conjugation are more stable [17].

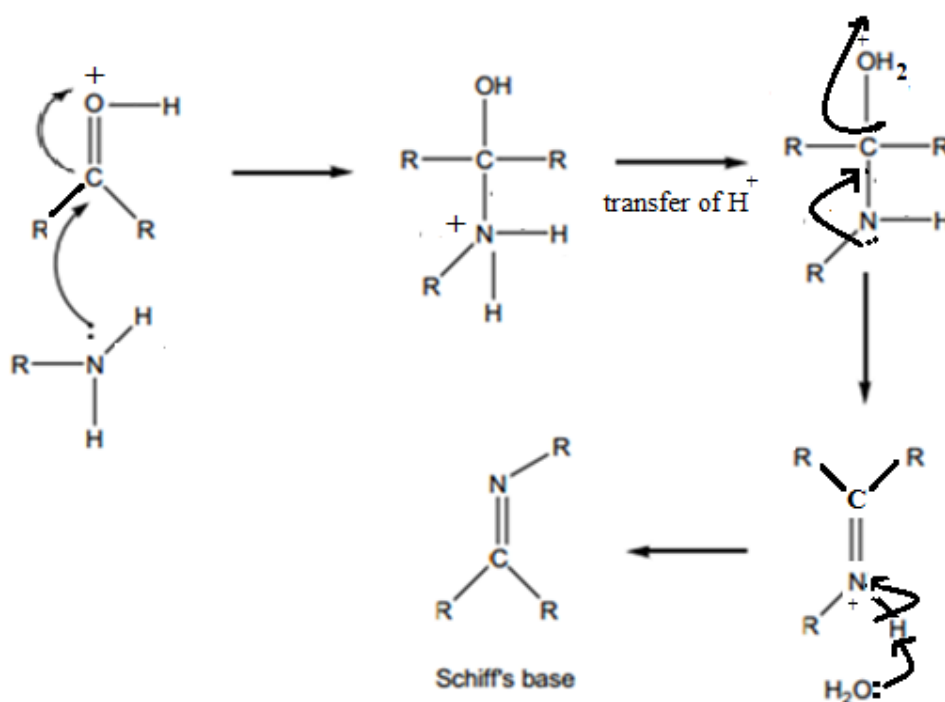
The presence of a lone pair of electrons in an sp^2 hybridized orbital of nitrogen atom of the azomethine group is considerable chemical and biological importance [17,18], particularly those in which the N-atom is a part of the aromatic system, when N is part of aromatic system, it shows activity in coordination chemistry [18].

Schiff's bases play significant role in coordination chemistry because of the relatively easy during preparation, and synthetic flexibility.

Also Schiff's bases act as chelating agents [17,18], they behave as a flexidentate ligand and act as monodentate or polydentate chelating ligand, where this chelating ligand gives the complexes extra stability due to formation of chelate ring structure with metal atom [17,18].

1.6 Mechanism of Schiff's base (Imine) formation

The first step of formation of imine ($C=N$) takes place when the amine nitrogen acts as a nucleophile, then attacking the electrophilic carbonyl carbon of aldehydes or ketones. After that, the next step the nitrogen is deprotonated, and the electrons from N-H bond push the oxygen off the carbon, and leaving a compound with a $C=N$ double bond, and the water molecule displaced (**Scheme 1.2**).



Scheme 1.2: Mechanism of Schiff's base formation.

1.7 Why Schiff's bases ligand are attractive ligands

There are several reasons make these ligands are attractive for forming complexes, they are:

- Schiff 's bases are prepared in good yield through one-step procedures via condensation of aldehydes with primary amines.
- The basicity, chelating factor, steric effects and tunable electronic of the Schiff's bases play a significant role in the stabilization of the different metals in various oxidation states.
- Schiff's bases possess similar structural with natural biological substances.

- Schiff's base complexes having stereochemical models due to their structural variety and preparative accessibility [19].
- Schiff's bases arise from the pyridyl-N and the hydroxyl groups that play an important role in the antibacterial activity[9].
- Also the Schiff's bases produced from aromatic amines with aromatic aldehydes, have been known to possess a significant role in biological applications like antibacterial, antitumor, antifungal, analgesic and anti-inflammatory activities [9].
- Schiff's base complexes show excellent catalytic activity in several reaction in the presence of moisture and at high temperature [17].

1.8 Schiff's bases and their complexes

Recently, the metal complexes of Schiff bases became widely studied due to their synthetic flexibility and sensitivity of the ligand towards central atoms [20].

Also, the general structure $R-N=C-R'$ gives the metal complexes special properties in biological activity [9,21].

1.9 General method and history of preparation of Schiff's bases and their complexes

We have previously recalled the Schiff's base synthesis that arised from condensation of a primary amine and an aldehyde or ketone under azeotropic distillation, and ethanol or methanol were commonly used as solvents. That was the classical synthetic method that was reported by

Hugo Schiff (1864) [22], where water was previously removed by molecular sieves. In 1990s, the elimination of water molecules was developed by using dehydrating solvents such as tetramethyl orthosilicate or trimethyl orthoformate [23,24].

The efficiency of this method was improved in 2004 by Chakraborti et al [25]. The method dependent on the use of highly electrophilic carbonyl compounds and strongly nucleophilic amines, they proposed an alternative use of substances that function as Bronsted- Lowry or Lewis acids to activate the carbonyl group of aldehydes, and to catalyze the nucleophilic attack by amines, and to dehydrate the system, then the eliminating water as the final step [26].

1.10 Applications of Schiff's bases and their metal complexes

Schiff's bases and their complexes have a wide range of application in food industry, dye industry, analytical chemistry, material science, catalysis, fungicidal, agrochemical, potentiometric sensors, and corrosion inhibitor [27]. Also, they have a wide application in biological activities including, antifungal, antibacterial, antimalarial, antiproliferative, anti-inflammatory, antiviral, antipyretic, anticancer and cytotoxic activities [28-32].

1.11 Biological activity of Schiff's bases ligands and their complexes

Recently, the medical field and pharmacological industries get huge development and having considerable attention by researchers due to population increase and spreading a lot of communicable diseases.

a. Antibacterial and Antifungal activities

The main essential purpose of the production and synthesis of any antimicrobial compound is to inhibit the causal microbe without any side effects on the patients.

In spite of the presence of significant progress in antibacterial and antifungal therapies, many problems still to be solved for most antimicrobial drugs available.

For example, amphotericin B, has strong antifungal activity and its serious nephrotoxicity limits its clinical applications [33].

The search and development of more effective antifungal agents are obligatory, and some Schiff's bases are known to be promising as antifungal agents, where Schiff's base complexes having potential antibacterial and antifungal interest. For example, Co(II), Ni(II) and Cu(II) complexes with Schiff base 3,3-thiodipropionic acid bis(4-amino-5-ethylimino-2,3-dimethyl-1-phenyl-3-pyrazoline) showed antifungal activity against *Alternaria brassicae*, *Fusarium Oxysprum* and *Aspergillus niger* [34].

b. Antiviral Activities

The most effective drugs for treatment of Cucumber mosaic virus are the silver complexes in oxidation state (I) with glycine salicylaldehyde Schiff base, where this complexes gave effective results up to 74% towards C.mosaic virus [9].

Also Schiff's bases of Isatin were reported to possess an antiviral activities [35].

c. Antitumor and Cytotoxic Activities

Cancer is one of the most horrible diseases in the world, it is almost a leading cause of death. Currently, one in four deaths in the United States is due to cancer [36], and this disease causes over six million deaths in each year [37].

There is a need for a knowledge of sophisticated design in new experimental treatment with drugs that reduce toxicity and improve indicators in cancer treatment. Many excellent papers have been published during the last decades on the treatment of cancer disease including Schiff's bases and their complexes, especially Schiff's bases derived from various heterocyclic systems for example 2-(4-amino-3-methylphenyl)-5-fluorobenzothiazole exhibited selective and potent anticancer activity (**Figure 1.3**)[38].

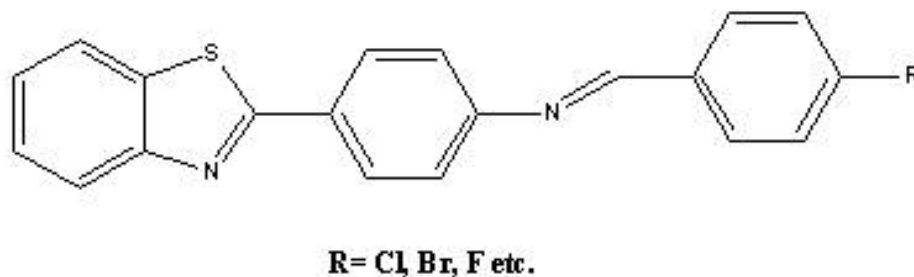


Figure 1.3: Benzothiazole derivatives

1.12 Bacteria and Bacterial Infections

1.12.1 *Escherichia coli*

A gram-negative, rod-shaped bacterium (**Fig. 1.4**) which normally lives in the intestines of human body and animals [46].

Most *E. coli* strains are inoffensive, as they form part of the normal flora of the gut in the body [46].

However, some types of *E. coli* in a particular *E. coli* 0157:H7 have caused symptoms of intestinal infection include abdominal pain, diarrhea, and fever [39].

More severe cases can lead to dehydration, bloody diarrhea or kidney failure. Some people with weakened immune systems and young children are at increased risk for developing these complications.

The intestinal infections are caused by contaminated water or food, animals and their environment [40].

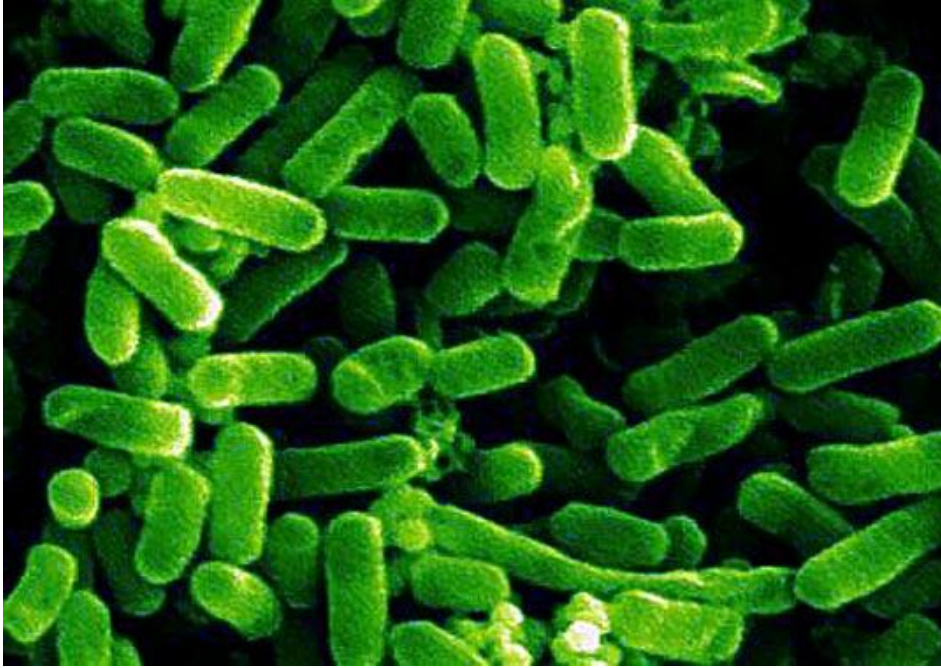


Figure 1.4 : Escherichia coli

1.12.2 Staphylococcus aureus

A gram-positive bacterium (**Figure 1.5**). This bacterium is a significant pathogen and can cause diseases in humans and animals. It is the leading cause of skin infections, such as furuncles and abscesses [41].

Where around 500,000 patients in American hospitals contract a staphylococcal infection every year [42].

Strains of *S.aureus* that have developed resistance to beta-lactam antibiotics are called *MRSA* (*Methicillin-resistant Staphylococcus aureus*). Infections caused by these strains are more difficult in treatment with standard types of antibiotics and are thus more dangerous [41].



Figure 1.5 : Staphylococcus aureus bacteria

1.12.3 Pseudomonas aeruginosa

A gram-negative, aerobic, rod-shaped bacterium (**Fig. 1.6**), which is found in skin flora in human body, water, and soil.

P.aeruginosa have caused symptoms of infection including folliculitis, hot foot syndrome, and the green nail.

Compared to other pathogens, *P. aeruginosa* is considered more difficult to eradicate as it displays high resistant to a wide variety of antibiotics [43].



Figure 1.6 : *Pseudomonas aeruginosa* bacteria

1.13 Methods of Antimicrobial Susceptibility Testing

Generally, antimicrobial susceptibility testing methods are divided into several types based on the principle applied in each system [47]. These methods are listed below in **Table 1.2**.

Table 1.2 :Types of Antimicrobial susceptibility testing methods.

Diffusion	Dilution	Diffusion&Dilution
Stokes method	Minimum Inhibitory Concentration	E-Test method
Kirby-Bauer method	i) Broth dilution ii)Agar Dilution	

In this study, we are concerned about MIC (Minimum Inhibitory Concentration) method.

Dilution susceptibility testing methods are used to determine the minimal concentration of antimicrobial to kill or inhibit the microorganism. This can be achieved through dilution of antimicrobial in an agar or broth media.

Also, the MIC value is expressed as the lowest concentration of compounds which no turbid was analogous with the negative control wells, no growth (broth only, without inoculum) [44, 47].

1.14 Objectives

The main objectives of this study are the followings :

1. To prepare and characterize new novel five types of Schiff's bases ligand and their complexes with [CuBr₂, CdCl₂].
2. The free ligands and their complexes were subjected to several physical measurements such as [EA, IR, UV-Visible, TG/DTA, NMR].
3. The structures of L₃ and L₅ were solved by [X-ray, Single crystal measurement to determine their 3D-ORTEP structure.

4. The potential of the ligands and their complexes against *E. coli*, *S. aureus*, *P. aeruginosa*, and *MRSA* were studied.

1.15 Novelty

The novelty of this work appears in the design of new six tetra and less ligands with N, S heterocyclic Schiff's bases and their metal complexes for the first time, the structure of **(N¹E,N²E)-N¹,N²-bis((5-bromothiophen-2-yl)methylene)ethane-1,2-diamine** analyzed by XRD revealed helix zig zag structure suitable for tetra dentate mononuclear and dinuclear metal complexes.

Also the structure of

[(N¹E,N²E)-N¹,N²-bis(2-chlorobenzylidene)cyclohexane-1,2-diamine] is analyzed by XRD, this ligand is racemic, in which the cyclohexane ring adopts the expected bidentate chair conformation suitable for mononuclear and dinuclear metal complexes. So we expected to introduce to the literature a novel chemotherapy (antibacterial) drugs.

CHAPTER TWO

MATERIALS AND METHODS

2.1 Chemicals

Different chemicals were used in this work. Picolinaldehyde, (R,R)-1,2-Diaminocyclohexane, ethylenediamine, 3-Bromobezaldehyde, 3-Chlorobezaldehyde, MgSO₄, CuBr₂.2H₂O, CdCl₂.2H₂O, and 2-(piperidin-1-yl)ethanamine were purchased in a pure form from Sigma-Aldrich.

5-bromothiophene-2-carbaldehyde was purchased from Alfa Aeser.

Solvents were of high purity and used as ethanol (95%), dichloromethane, n-hexane, methanol, were purchased from FRUTAROM, and diethylether was purchased from SDFCL.

2.2 Methods and Physical Measurements

Schiff bases' melting points were taken on a Stuart Melting point apparatus SMP-3. The elemental analysis were recorded with an Elementar Varrio EL analyzer, TG, DTA, ¹H and ¹³C-NMR spectra were determined in Hashemite University/ Jordan.

The X-ray structural work was carried out at the Hamdi Mango Center for Scientific Research at the University of Jordan / Jordan.

Fourier transform infrared spectrophotometer (Necolet Is5 - Id3) was used to obtain IR-Spectra and Shimadzu (UV-3101DC) UV-VIS-NIR scanning spectrometer was used for absorption measurements. Thermal analyses

were carried out with TA instrument SDT-Q600 in air. The diffraction data was collected at room temperature using an Oxford Xcalibur diffractometer (Mo K α radiation, $\lambda = 0.7107 \text{ \AA}$).

2.3 General procedure for synthesis of [L₁, L₂, L₃, L₄, L₅, L₆] and their complexes.

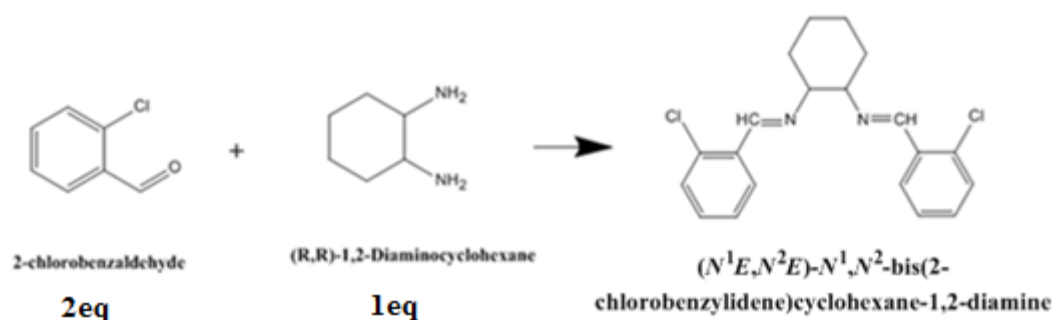
2.3.1 General procedure to synthesis of the L₁ & L₂.

L₁ [(E)-2-(piperidin-1-yl)-N-(pyridin-2-ylmethylene)ethanamine].

L₂ [(E)-N-(3-bromobenzylidene)-2-(piperidin-1-yl)ethanamine].

An 1:1 equimolar ethanolic solution of **2-(piperidin-1-yl)ethanamine** and the corresponding **aldehyde** were mixed, where **2-(piperidin-1-yl)ethanamine** was dissolved in ethanol (10 mL) and the mixture was stirred and heated gently (50°C) for 10 min, after which a solution of aldehyde in ethanol (5 mL) was added dropwise. The reaction mixture was refluxed for five hours with constant stirring, the reaction progress was monitored by thin-layer chromatography. The resulting mixture was concentrated in *vacuo* with constant stirring. Upon completion of the reaction, the mixture was cooled at room temperature and the solid obtained was filtered and washed with n-hexane. Then the solid product was dissolved in 25mL CH₂Cl₂, and 25 mL of distilled water were added with shaking in separatory funnel. This results in two layers, the organic layer was separated and 2.0g anhydrous of MgSO₄ was added to this organic layer for drying, the purified ligand left at room temperature to

The resulting mixture was concentrated in *vacuo* with constant stirring. Upon completion of the reaction, the mixture was cooled at room temperature and the solid obtained was filtered and washed with n-hexane. Then the solid product was dissolved in 25mL CH₂Cl₂, and 25 mL of distilled water were added with shaking in separatory funnel. This results in two layers, the organic layer was separated and 2.0g anhydrous of MgSO₄ was added to this organic layer for drying, the purified ligand left at room temperature to remove the solvent, then the solid product was recrystallized from ethanol (95%). The structure of ligand is given in **Scheme 2.3**.



Scheme 2.3: The chemical reaction of Schiff's base ligand (L₃)

2.3.3 General procedure for synthesis of L₄, L₅, and L₆.

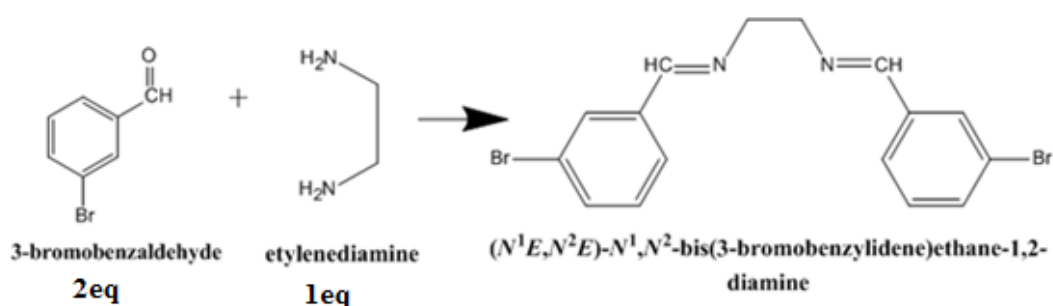
L₄ (N¹E,N²E)-N¹,N²-bis(3-bromobenzylidene)ethane-1,2-diamine.

L₅ (N¹E,N²E)-N¹,N²-bis((5-bromothiophen-2-yl)methylene)ethane-1,2-diamine.

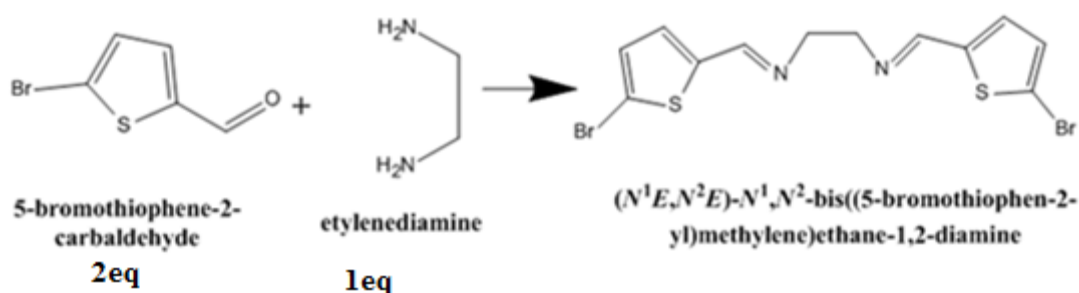
L₆ (N¹E,N²E)-N¹,N²-bis(2-chlorobenzylidene)ethane-1,2-diamine.

A 1:2 molar ratio ethanolic solution of ethylenediamine and the corresponding aldehyde were mixed together, where ethylenediamine

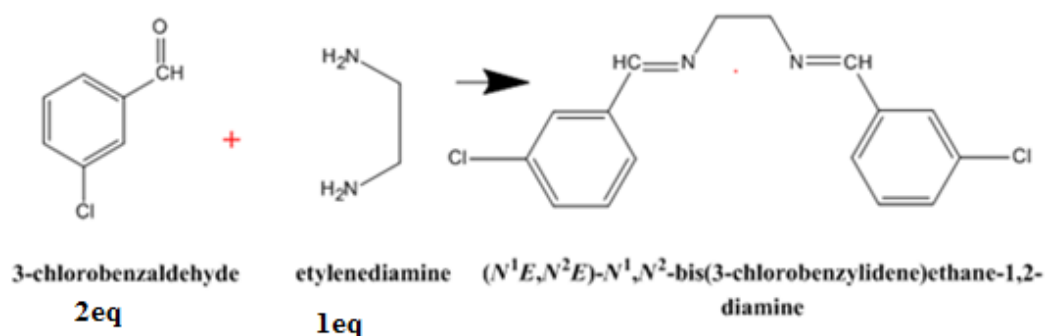
was dissolved in ethanol (10 mL) and the mixture was stirred and heated gently (50 °C) for 10 min, after which a solution of aldehyde in ethanol (5 mL) was added dropwise. The reaction mixture was refluxed for five hours with constant stirring, the reaction progress was monitored by thin-layer chromatography. The resulting mixture was concentrated in *vacuo* with constant stirring. Upon completion of the reaction, the mixture was cooled at room temperature and the solid obtained was filtered and washed with n-hexane. Then the solid product was dissolved in 25mL CH₂Cl₂, and 25 mL of distilled water were added with shaking in separatory funnel. This results in two layers, the organic layer was separated and 2.0g anhydrous of MgSO₄ was added to this organic layer for drying, the purified ligand left at room temperature to remove the solvent, then the solid product was recrystallized from ethanol (95%). The structure of ligands L₄, L₅, and L₆ are given in **Scheme 2.4**, **Scheme 2.5**, and **Scheme 2.6** respectively.



Scheme 2.4: The chemical reaction of Schiff's base ligand (L₄).



Scheme 2.5: The chemical reaction of Schiff's base ligand (L₅).



Scheme 2.6: The chemical reaction of Schiff's base ligand (L₆)

2.3.4 General procedure for synthesis the Copper (II) and Cadmium(II) complexes

2.3.4.1 General procedure for synthesis the Copper (II) complexes

A solution of copper bromide dihydrate dissolved in (10 mL) of absolute ethanol was added to solution of the corresponding ligand dissolved in (15 mL) of absolute ethanol. The mixture was refluxed with stirring for four hours until the color appear, the reaction mixture was cooled and the solvent was removed in *vacuo*. The obtained solid was washed several

times with diethyl ether and recrystallized from hot ethanol then left at room temperature.

2.3.4.2 General procedure to synthesis the Cadmium(II) complexes

A solution of cadmium chloride dihydrate dissolved in (10 mL) of absolute ethanol was added to solution of the corresponding ligand dissolved in (15 mL) of absolute methanol. The mixture was refluxed with stirring for ten hours, the reaction mixture was cooled and the solvent was removed in *vacuo*. The obtained solid was washed several times with diethyl ether and recrystallized from hot methanol then left at room temperature.

Chapter Three

Results and Discussion

3.1 Physical data of the prepared Ligands

All the physical data of the prepared ligands L₁ -L₆ were listed in **Table**

3.1.

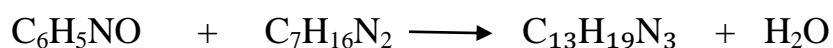
Table 3.1 : Physical and Elemental analysis of the Ligands.

Compound	Molecular Formula	Colour	Yield%	M.P	M wt. g/mol	Elemental analysis (found)					
						Elemental analysis (calculated)					
						%C	%H	%N	%Cl	%Br	%S
L₁	C ₁₃ H ₁₉ N ₃	golden brown	75.5%	L	217.3	71.47	8.99	19.54	-	-	-
						71.85	8.81	19.34			
L₂	C ₁₄ H ₁₉ BrN ₂	pale yellow	80.5%	L	295.22	57.22	6.04	9.55	-	27.19	-
						56.96	6.49	9.49		27.07	
L₃	C ₂₀ H ₂₀ Cl ₂ N ₂	colorless	85.0%	96	359.29	66.98	5.74	8.22	19.06	-	-
						66.86	5.61	7.80	19.73		
L₄	C ₁₆ H ₁₄ Br ₂ N ₂	hay colour	80.3%	85.5	394.10	48.38	3.41	7.63		40.36	-
						48.76	3.85	7.11	-	40.55	
L₅	C ₁₂ H ₁₀ Br ₂ N ₂ S ₂	colorless	75 %	105	406.16	35.68	2.36	6.35		40.11	15.5
						35.49	2.48	6.9	-	39.35	15.79
L₆	C ₁₆ H ₁₄ Cl ₂ N ₂	white	84.4%	92.5	305.20	63.32	4.85	9.01	22.82	-	-
						62.97	4.62	9.18	23.23		

3.2 Ligands Synthetic Investigations

3.2.1 Investigation about synthesis (L₁)

- i. [(E)-2-(piperidin-1-yl)-N-(pyridin-2-ylmethylene) ethanamine] was synthesized by condensation of 2-(piperidin-1-yl) ethanamine (0.5g, 3.9 mmol)with picolinaldehyde (0.42g, 3.9mmol) in ethanolic solution in 75.5% yield, as shown in **Scheme 3.1**. The structure was determined by IR, ¹H-NMR, and ¹³C-NMR spectroscopy.



Scheme 3.1: The chemical equation of Schiff's base ligand (L₁).

- ii. Oily golden brown product was collected, and washed the ligand several times with distilled water, n-hexane, where it is still in the oily product form.
- iii. L₁ chelating ligand, served as polydentate's chelating ligand towards CuBr₂ complex formations through lone pairs of electrons on three nitrogen atoms.
- iv. The formed ligand is stable in air and soluble in common organic solvents like chlorinated solvents, methanol and ethanol, and insoluble in water, n-hexane or ethers.

3.2.2 Investigation about synthesis L₂

[(E)-N-(3-bromobenzylidene)-2-(piperidin-1-yl)ethanamine]

was synthesized by condensation of 2-(piperidin-1-yl)ethanamine (0.5g, 3.9 mmol) with 3-bromobenzaldehyde (0.72, 3.9mmol) in ethanolic solution in 80.5% yield, as shown in **Scheme 3.2**. The structure was determined by IR, ¹H-NMR, and ¹³C-NMR spectroscopy.



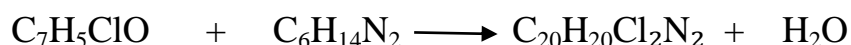
Scheme 3.2: The chemical equation of Schiff's base ligand (L₂).

- i. Oily pale yellow compound was collected and purified by washing with distilled water, n-hexane, then dissolving it in a small quantity of dichloromethane and left at room temperature to give a pure solid compound.
- ii. L₂ chelating ligand, served as polydentate's chelating ligand towards CdCl₂ and CuBr₂ complexes formation through lone pairs of electrons on two nitrogen atoms.
- iii. The formed ligand is stable in air and soluble in common organic solvents like chlorinated solvents, methanol and ethanol, and insoluble in water, n-hexane or ethers.

3.2.3 Investigation about synthesis L₃

- i. [(N¹E,N²E)-N¹,N²-bis(2-chlorobenzylidene)cyclohexane-1,2-diamine] was synthesized by condensation of (R,R)-1,2-

diaminocyclohexane (0.5g, 4.38mmol) with 2-chlorobenzaldehyde (0.6g, 4.38mmol) in ethanolic solution in 85.0% yield, as shown in **Scheme 3.3**. The structure was determined by IR, ¹H-NMR, and ¹³C-NMR spectroscopy.

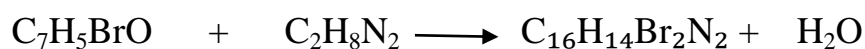


Scheme 3.3: The chemical equation of Schiff's base ligand (L₃).

- ii. The compound was collected and purified by washing with distilled water, n-hexane, then dissolving it in a small quantity of dichloromethane and left at room temperature to give a pure solid compound, then recrystallized from ethanol (95%) to produce colorless pure crystal for single-crystal X-ray diffraction analysis.
- iii. This compound is racemic, in which the cyclohexane ring adopts the expected chair conformation [37].
- iv. L₃ chelating ligand, served as polydentate's chelating ligand through lone pairs of electrons on two nitrogen atoms.
- v. The formed ligand is stable in air and soluble in common organic solvents like chlorinated solvents, methanol and ethanol, and insoluble in water, n-hexane or ethers.

3.2.4 Investigation about synthesis L₄

- i. [(N¹E,N²E)-N¹,N²-bis(3-bromobenzylidene)ethane-1,2-diamine] was synthesized by condensation of ethylenediamine (0.3g, 5mmol) (1eq) with 3-bromobenzaldehyde (1.8g, 10mmol) (2eq) in ethanolic solution in 80.3% yield, as shown in **Scheme 3.4**. The structure was determined by IR, ¹H-NMR, and ¹³C-NMR spectroscopy.



Scheme 3.4: The chemical equation of Schiff's base ligand (L₄).

- i. The hay colored compound was collected and purified by washing with distilled water, n-hexane, then dissolving it in a small quantity of dichloromethane and left at room temperature to give a pure solid compound.
- ii. L₄ chelating ligand, having the symmetry in structure, served as polydentate's chelating ligand towards CuBr₂ complex formations through lone pairs of electrons on two nitrogen atoms.
- iii. The formed ligand is stable in air and soluble in common organic solvents like chlorinated solvents, methanol and ethanol, and insoluble in water, n-hexane or ethers.

3.2.5 Investigation about synthesis L₅

- i. [(N¹E,N²E)-N¹,N²-bis((5-bromothiophen-2-yl)methylene)ethane-1,2-diamine] was synthesized by condensation of ethylenediamine (0.3g, 5mmol) (1eq) with 5-bromothiophene-2-carbaldehyde (1.9g, 10mmol)

(2eq) in ethanolic solution in 88.2% yield, as shown in **Scheme 3.5**.

The structure was determined by IR, $^1\text{H-NMR}$, and $^{13}\text{C-NMR}$ spectroscopy.

- ii. The colorless compound was collected and purified by washing with distilled water, n-hexane, then dissolving it in a small quantity of dichloromethane and left at room temperature to give pure solid compound, then recrystallized from ethanol (95%) to produce colorless pure crystal for single-crystal X-ray diffraction analysis.



Scheme 3.5: Scheme 2.1: The chemical equation of Schiff's base ligand (L_5).

- iii. L_5 chelating ligand, having the symmetry in structure, served as polydentate's chelating ligand towards CdCl_2 and CuBr_2 complexes formation through lone pairs of electrons on two nitrogen atoms and lone pairs of electrons on two sulfur atoms.
- iv. The formed ligand is stable in air and soluble in common organic solvents like chlorinated solvents, methanol and ethanol, insoluble in water, n-hexane or ethers.

3.2.6 Investigation about synthesis L_6

- i. $[(\text{N}^1\text{E}, \text{N}^2\text{E})\text{-N}^1, \text{N}^2\text{-bis(2-chlorobenzylidene)ethane-1,2-diamine}]$ was synthesized by condensation of Etylenediamine (0.3g, 5mmole) with 3-chlorobenzaldehyde (1.4g, 10mmol)(2eq) in ethanolic

solution in 84.4 % yield, as shown in **Scheme 3.6**. The structure was determined by IR, $^1\text{H-NMR}$, and $^{13}\text{C-NMR}$ spectroscopy.



Scheme 3.6: The chemical equation of Schiff's base ligand (L_6).

- ii. White powder compound was collected and purified by washing with distilled water, n-hexane, then dissolving in a small quantity of dichloromethane and left at room temperature to give a pure solid compound.
- iii. L_6 chelating ligand, having the symmetry in structure, served as polydentate's chelating ligand towards CuBr_2 complex formations through lone pairs of electrons on two nitrogen atoms.
- iv. The formed ligand is stable in air and soluble in common organic solvents like chlorinated solvents, methanol and ethanol, and insoluble in water, n-hexane or ethers.

3.3 Complexes Synthetic Investigations

3.3.1 Copper Complexes synthesis

All of the copper (II) complexes were prepared by mixing an ethanolic solution of $\text{CuCl}_2 \cdot 2\text{H}_2\text{O}$ salt and an ethanolic solution of the corresponding ligand, with a ligand to metal molar ratio 1:1. The solid mass was collected, washed with diethyl ether and dried over anhydrous calcium chloride in a desiccator. All of the copper (II) complexes were dark green

and these complexes were determined by spectroscopic means IR and UV-Visible.

3.3.2 Cadmium Complexes synthesis

All of the cadmium(II) complexes were prepared by mixing a methanolic solution of $\text{CdCl}_2 \cdot 2\text{H}_2\text{O}$ salt and a methanolic solution of the corresponding ligand, with a ligand to metal molar ratio 1:1. The solid mass was collected, washed with diethyl ether and dried over anhydrous calcium chloride in a desiccator. All of the complexes of Cd(II) were colorless and these complexes were determined by spectroscopic means IR and UV-Visible.

3.4 Spectroscopic analysis

3.4.1 IR Spectra Investigations

The IR spectra of the ligands displayed more or less strong intensity bands in the $4,000 - 400 \text{ cm}^{-1}$ range.

The IR spectra of the corresponding ligands have been examined in comparison with the spectra of the starting materials (1° amine, and carbonyl compound).

The IR spectra of the desired ligands in particular show main three sets of characteristic absorptions, $\nu \text{ C=N}$, $\nu \text{ N-H}$, and $\nu \text{ C-H}$ aromatic.

The IR spectra of the ligands and their complexes were recorded by using ATR- Fourier transform infrared spectrophotometer (Necolet Is5 - Id3) at room temperature.

3.4.1.1 The general investigations about free ligands spectra :

- ✓ The vibration of carbonyl ν C=O in the spectra of aldehyde shifted to low frequency when the ligand formation, this indicate to the formation of azomethine group (C=N).
- ✓ The ν N-H in the primary amine spectra disappeared in the spectra of ligand.
- ✓ The ν C=C of aromatic system shifted to low frequency in the ligand spectra.
- ✓ The ν CH₂ shifted to low frequency in the ligands spectra.

All other functional groups vibrations are also mentioned.

3.4.1.2 The general investigations about metal complexes with ligand spectra :

- ✓ The shifting of the azomethine group ν C=N to the lower frequency in all the metal complexes when compared to free ligand, suggests the coordination of metal ion through nitrogen atom of azomethine group. It is expected that coordination of nitrogen to the metal atom would reduce the electron density in the azomethine link and thus lower the ν C=N absorption.
- ✓ The frequencies of ν C=C , ν CH₂, ν CH are also lowered.
- ✓ New appearances of ν M-N or ν M-S bond in the region (400- 600) cm⁻¹, where this appearance of ν M-N & ν M-S vibrations support the

involvement of N or S atoms in complexation with metal ions under investigation .

3.4.1.3 IR spectrum of L_1

- ❖ In the spectrum of Picolinaldehyde the major band at 1707.4cm^{-1} is related to carbonyl vibration $\nu\text{ C=O}$, and we observe a small peak at 3414cm^{-1} as an overtone the C=O vibration; a frequency of about twice that of $\nu\text{ C=O}$ vibration.
- ✓ The aromatic (C-H) vibration appear at 3055.3 cm^{-1} .
- ✓ Aldehyde (C-H) vibration appear at 2821.1cm^{-1} .
- ✓ 1583.7cm^{-1} indicate to ring (C=C) vibration.
- ❖ In the spectrum of 2-(piperidin-1-yl)ethanamine, the major peak appears 3266.2 cm^{-1} which is related to N-H bond vibration, and $2934, 2802\text{cm}^{-1}$ are related to aliphatic $\nu\text{ C-H}$ bond.
- ❖ In the spectrum of L_1 , we observe a major peak at 1647.9 cm^{-1} which is related to azomethine group C=N, and the peak of N-H bond disappeared [39,40]. And the broad band at 3321.5 cm^{-1} indicates presence of water molecule, as shown in **Figure 3.1**.

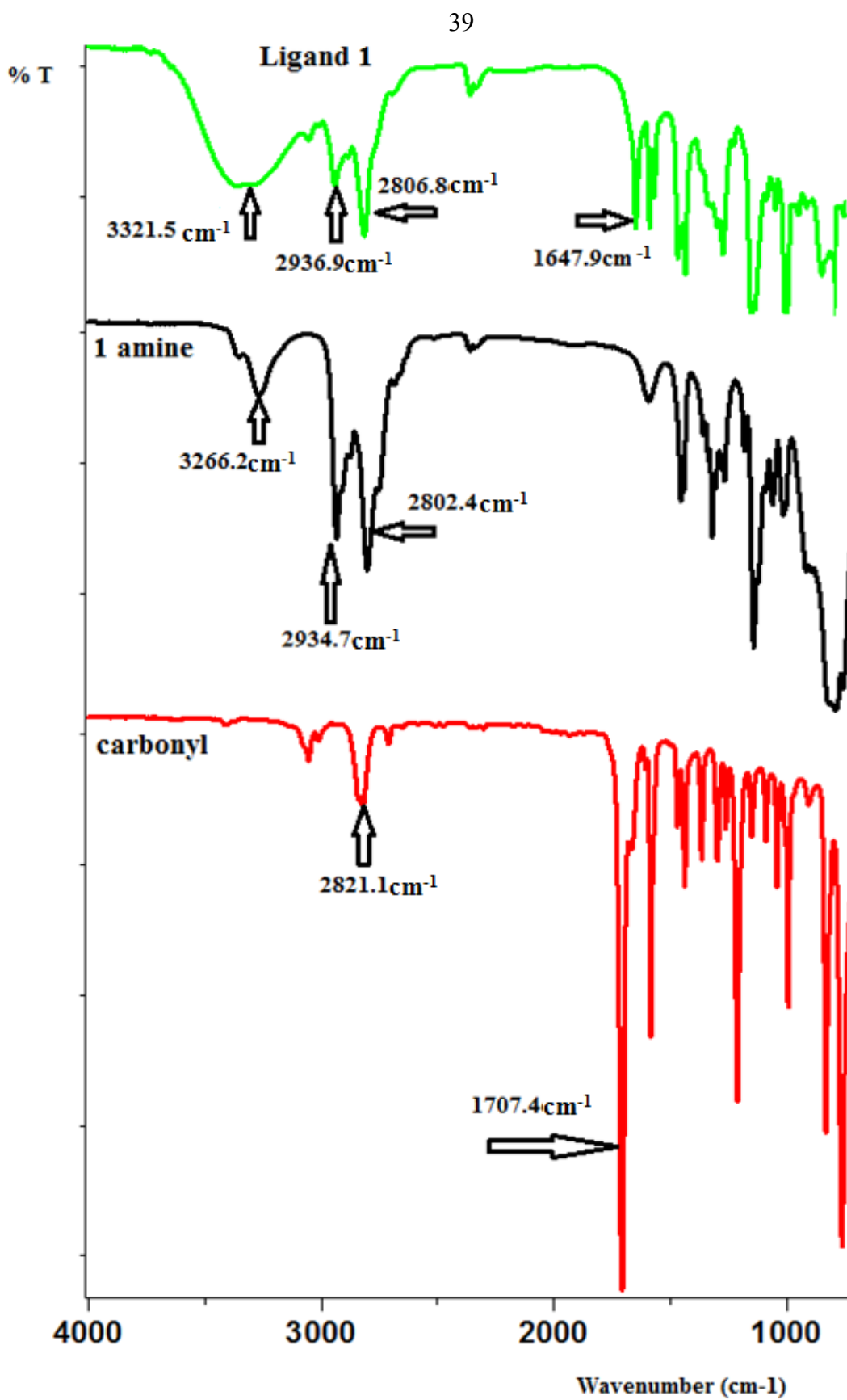


Figure 3.1 : IR spectrum of L₁

3.4.1.4 IR spectra of L_2

- ❖ In the spectrum of 3-bromobenzaldehyde, the major band appears at 1690.8 cm^{-1} that is related to carbonyl vibration $\nu\text{ C=O}$ (the low value is due to conjugation of C=O with the aromatic ring, where is the normal aldehyde appears at 1710 cm^{-1}) , we observe a small peak at 3381 cm^{-1} as an overtone of the C=O vibration; a frequency of about twice that of $\nu\text{ C=O}$ vibration.
- ✓ The aromatic (C-H) vibration appear at 3062.4 cm^{-1} .
- ✓ Aldehyde (C-H) vibration appear at $2828, 2729\text{ cm}^{-1}$.
- ✓ 1570.3 cm^{-1} indicate to ring (C=C) vibration.
- ❖ In the spectrum of 2-(piperidine-1-yl)ethanamine a major peak appears at 3265.8 cm^{-1} which is related to N-H band vibration. The bands at $2934, 2802\text{ cm}^{-1}$ are related to aliphatic $\nu\text{ C-H}$ bond.
- ❖ In the spectrum of L_2 , we observe a major peak at 1645 cm^{-1} that is related to azomethine group C=N , and the disappearance of N-H peak, as shown in **Figures 3.2, 3.3, and 3.4**.

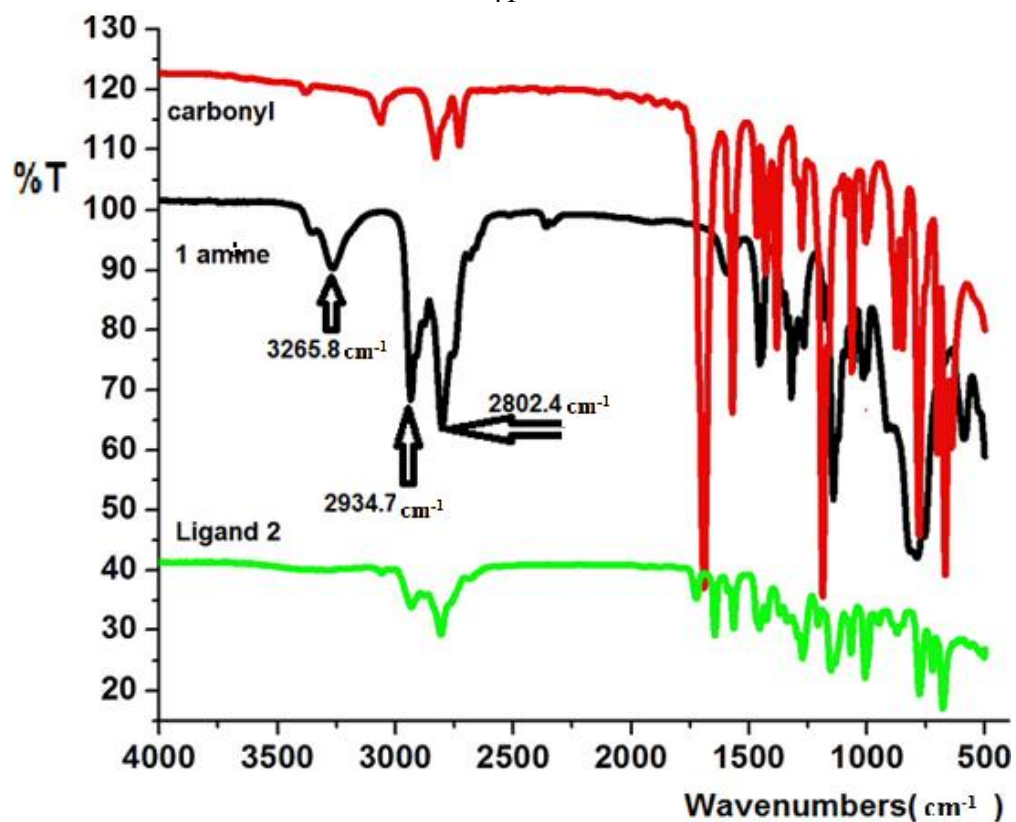


Figure 3.2 : IR spectrum of L₂

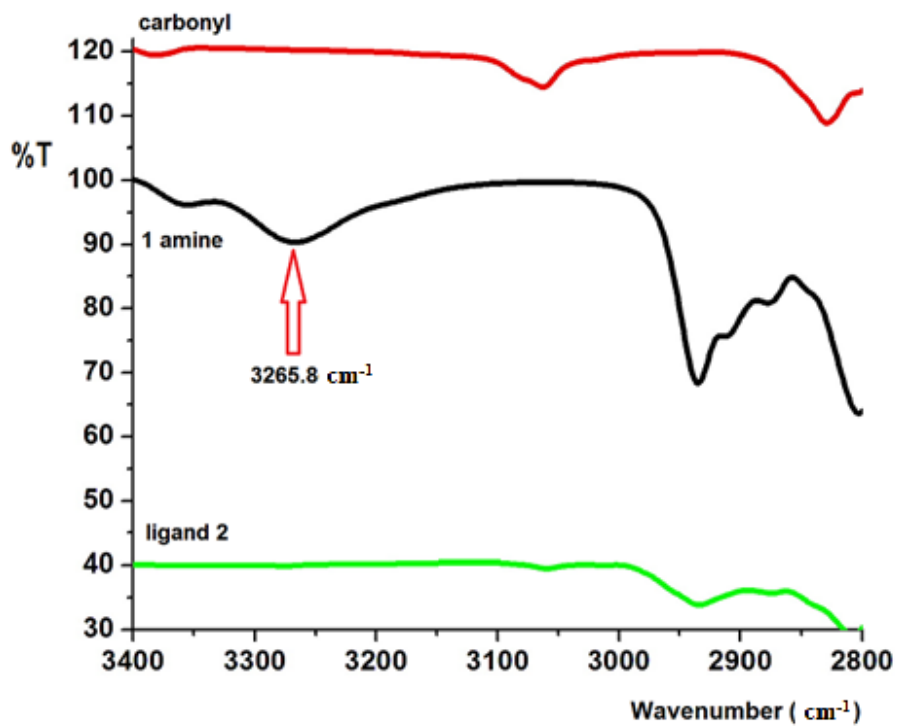


Figure 3.3 : IR spectrum of L₂, the region (2800-3400) cm⁻¹

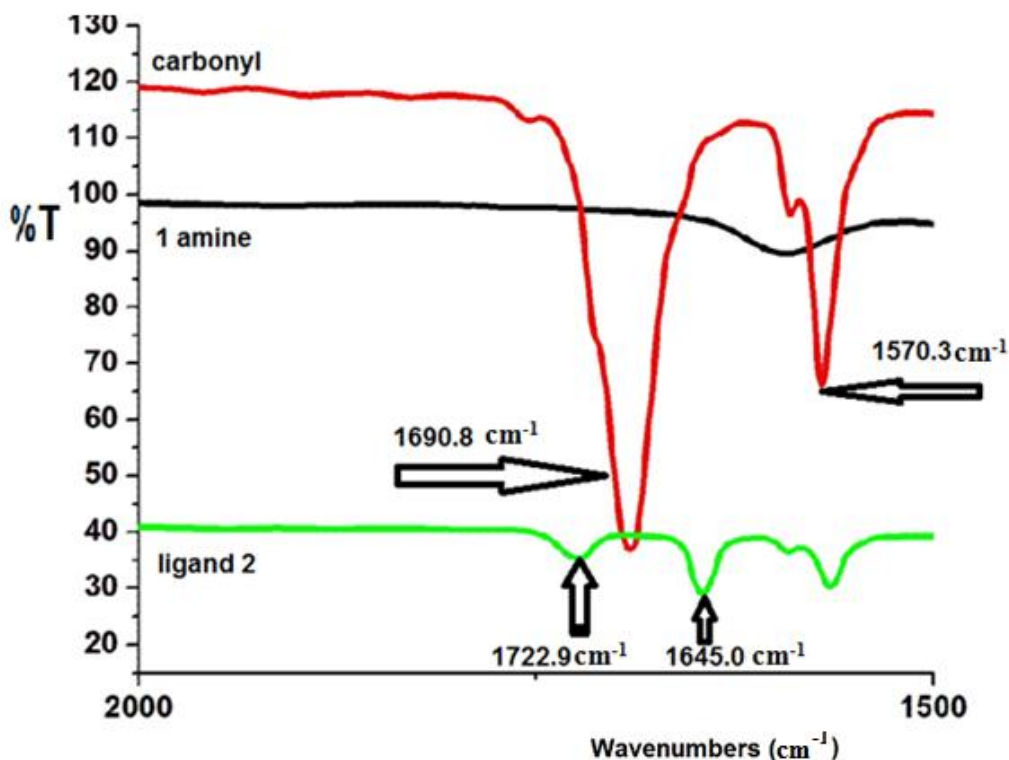


Figure 3.4 : IR spectrum of L₂, the region (1500-2000) cm⁻¹

3.4.1.5 IR spectrum of L₃

- ❖ In the spectrum of 2-chlorobenzaldehyde the major band at 1695.4 cm⁻¹ for carbonyl vibration ν C=O (the low value is due to conjugation of C=O with the aromatic ring, where is the normal aldehyde appears at 1710 cm⁻¹).
- ✓ The aromatic (C-H) vibration appear at 3066.9 cm⁻¹.
- ✓ Aldehyde (C-H) vibration appear at 2833 cm⁻¹ and 2729 cm⁻¹.
- ✓ 1572.2 cm⁻¹ is related to ring (C=C) vibration.
- ❖ In the spectrum of (R,R)-1,2-Diaminocyclohexane, the appearance of a major peak at 3280.9 cm⁻¹ indicates the presence N-H bond. Two peaks at 2919, 2852 cm⁻¹ respectively are related to C-H bond. The

absorption band at 3357.2 cm^{-1} indicates the presence of water molecule.

- ❖ In the spectrum of L_3 , we observe a major peak at 1654.2 cm^{-1} indicates to azomethine group $\nu\text{ C=N}$. and the disappearance of N-H peak, as shown in **Figure (3.5)**.

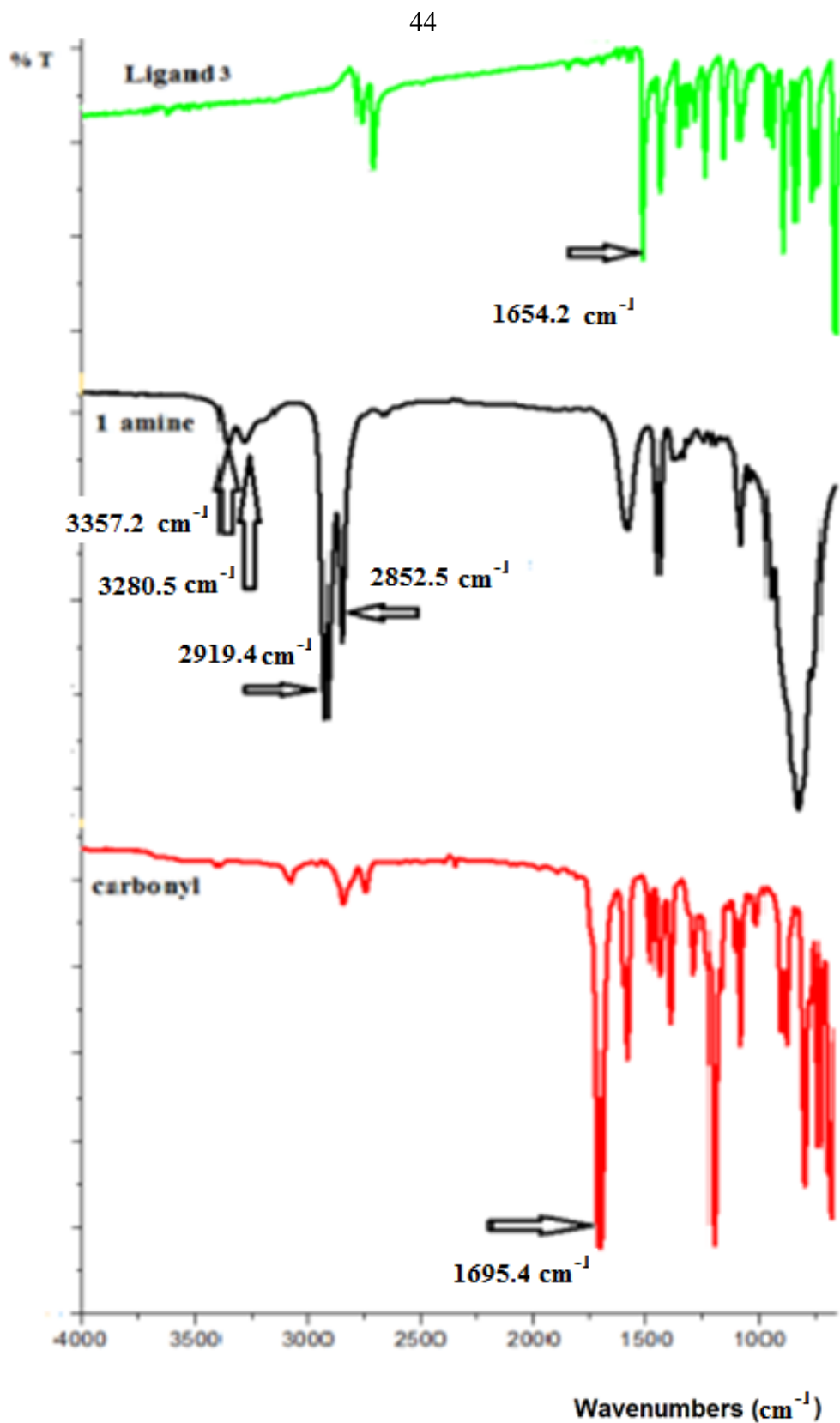


Figure 3.5 : IR spectrum of L_3

3.4.1.6 IR spectra of L₄

- ❖ In the spectrum of 3-bromobenzaldehyde, the major band at 1690.8 cm⁻¹ for carbonyl vibration ν C=O (the low value is due to conjugation of C=O with the aromatic ring, where is the normal aldehyde appears at 1710 cm⁻¹).
- ✓ The aromatic (C-H) vibration appear at 3062.4 cm⁻¹.
- ✓ Aldehyde (C-H) vibration at 2828, 2729 cm⁻¹.
- ✓ 1570.3 cm⁻¹ refers to ring (C=C) vibration.
- ❖ In the spectrum of ethylenediamine, a major peak that appears at 3280.9 cm⁻¹ is related to N-H bond vibration. Two peaks appear at 2920, 2849cm⁻¹ respectively are related C-H vibration. The band that appears at 3356.6 cm⁻¹ indicates the presence of water molecules.
- ❖ In the spectrum of L₄, we observe a major peak at 1640.6 cm⁻¹ that is related to azomethine group ν C=N, and the disappearance of N-H peak as shown in **Figures 3.6, 3.7, and 3.8.**

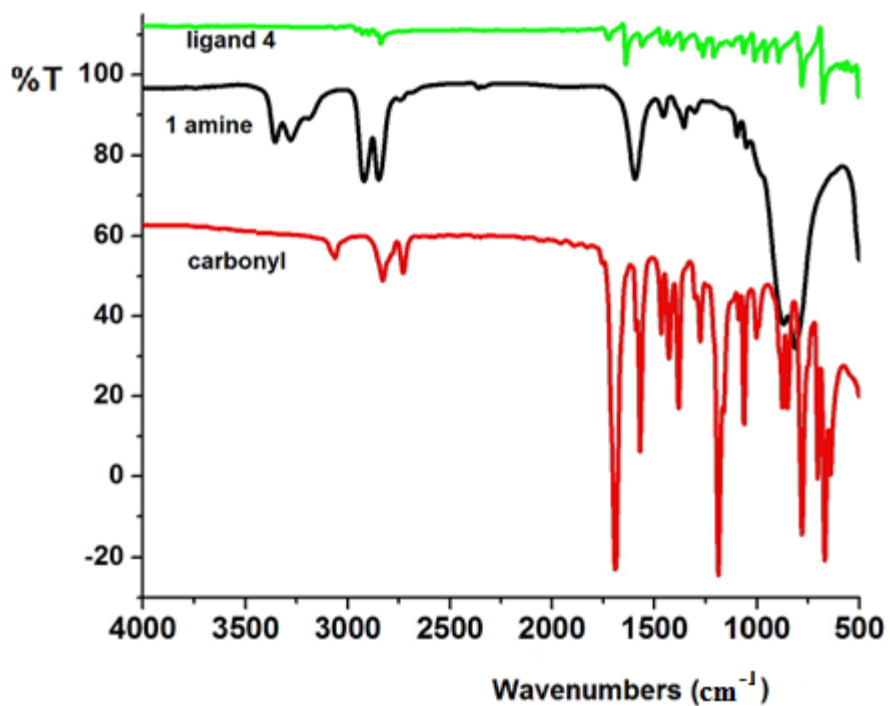


Figure 3.6 : IR spectrum of L₄

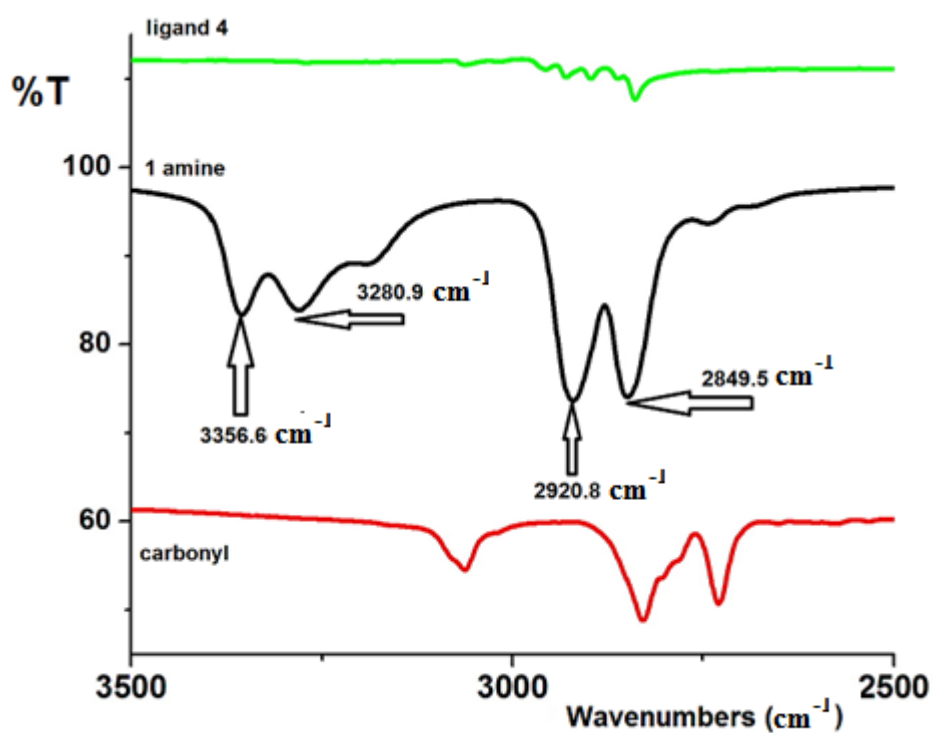


Figure 3.7 : IR spectrum of L₄, the region (2500-3500) cm⁻¹

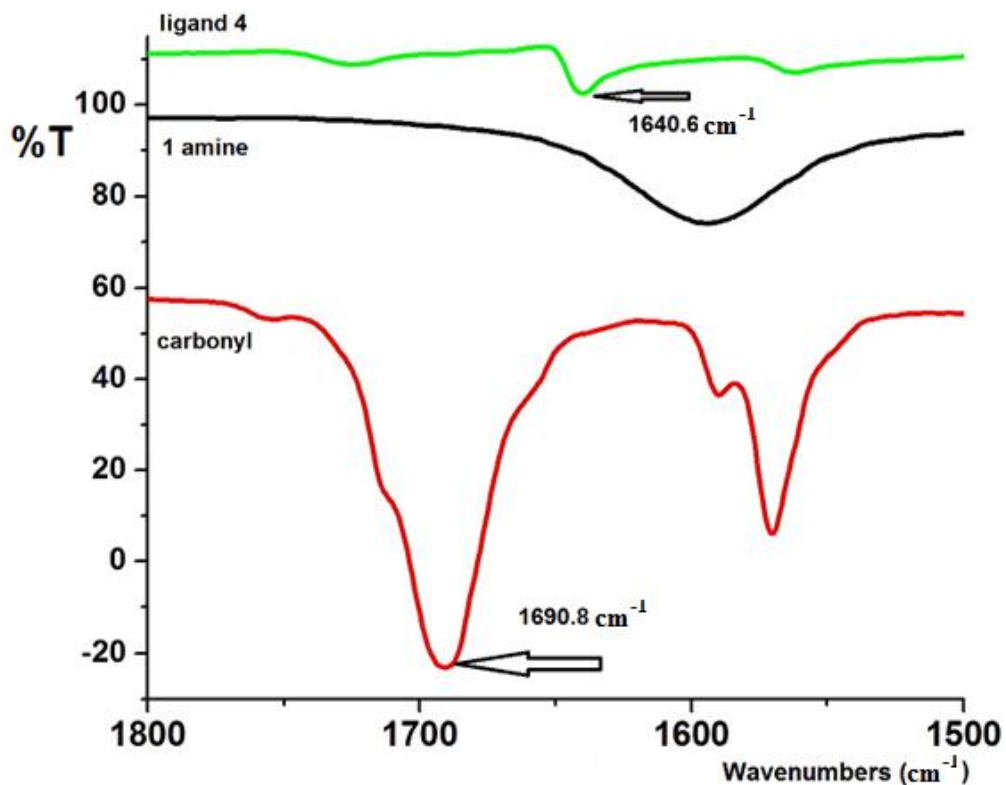


Figure 3.8 : IR spectrum of L_4 , the region ($1500-1800\text{ cm}^{-1}$)

3.4.1.7 IR spectrum of L_5

❖ In the spectrum of 5-bromothiophene-2-carbaldehyde the major band at 1657.8 cm^{-1} for carbonyl bond $\nu\text{ C=O}$ (the normal carbonyl appear at 1710 cm^{-1} , due to conjugation the band appear at the lower frequency than normal).

- ✓ The aromatic C-H vibration appear at 3094.4 cm^{-1} .
- ✓ Aldehyde C-H vibration appear at 2830 cm^{-1} , 2777 cm^{-1} .
- ✓ 1522.4 cm^{-1} is related to ring (C=C) vibration.

- ❖ In the spectrum of ethylenediamine a major peak at 3280.9 cm^{-1} indicate to N-H vibration. Two peaks at $2920, 2849\text{ cm}^{-1}$ are related to C-H vibration. The absorption band at 3356.6 cm^{-1} indicates the presence of water molecules as shown in **Figure 3.9**.
- ❖ In the spectrum of L_5 , we observe a major peak at 1628 cm^{-1} which is related to azomethine group C=N, and the disappearance of N-H peak as shown in **Figure 3.9**.

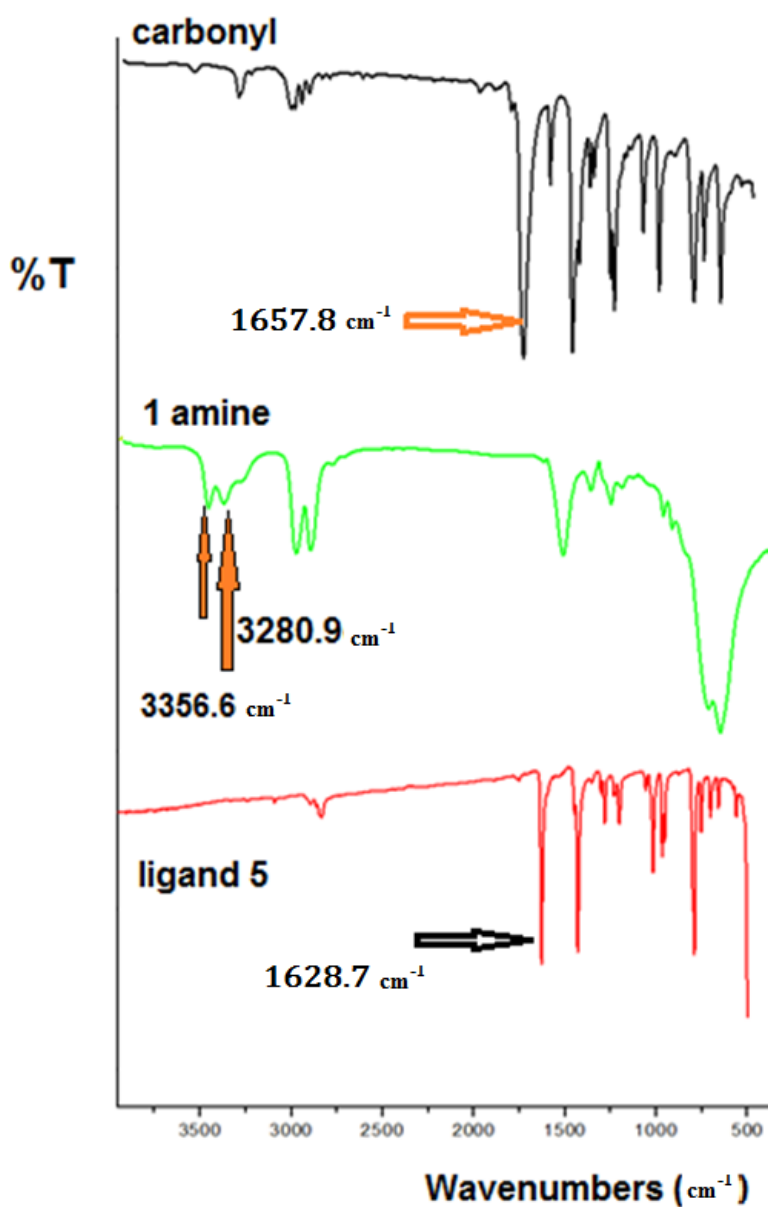


Figure 3.9 : IR spectrum of L_5

3.4.1.8 IR spectrum of L₆

- ❖ In the spectrum of 3-chlorobenzaldehyde a major band appears at 1694.4 cm^{-1} that is related to carbonyl vibration $\nu\text{ C=O}$ (the low value is due to conjugation of C=O with the aromatic ring, where is the normal aldehyde appears at 1710 cm^{-1}), we also observe a small peak at 3392 cm^{-1} as an overtone of the C=O vibration; a frequency of about twice that of $\nu\text{ C=O}$ vibration..
- ✓ The aromatic C-H vibration appear at 3065.9 cm^{-1} .
- ✓ Aldehyde C-H vibration appear at 2832 cm^{-1} , 2728 cm^{-1} .
- ✓ Two peaks appear at 1591.3 , 1572.1 cm^{-1} are related to ring (C=C) bond.
- ❖ In the spectrum of ethylenediamine a major peak appears at 3280.9 cm^{-1} that is related to $\nu\text{ N-H}$ vibration. The bands at 2920 , 2849 cm^{-1} are related to C-H vibration. And 3356.6 cm^{-1} indicates the presence of water molecules.
- ❖ In the spectrum of L₆, we observed a major peak at 1648.8 cm^{-1} that is related to azomethine group C=N, and the disappearance of N-H peak as shown in **Figure 3.10**.

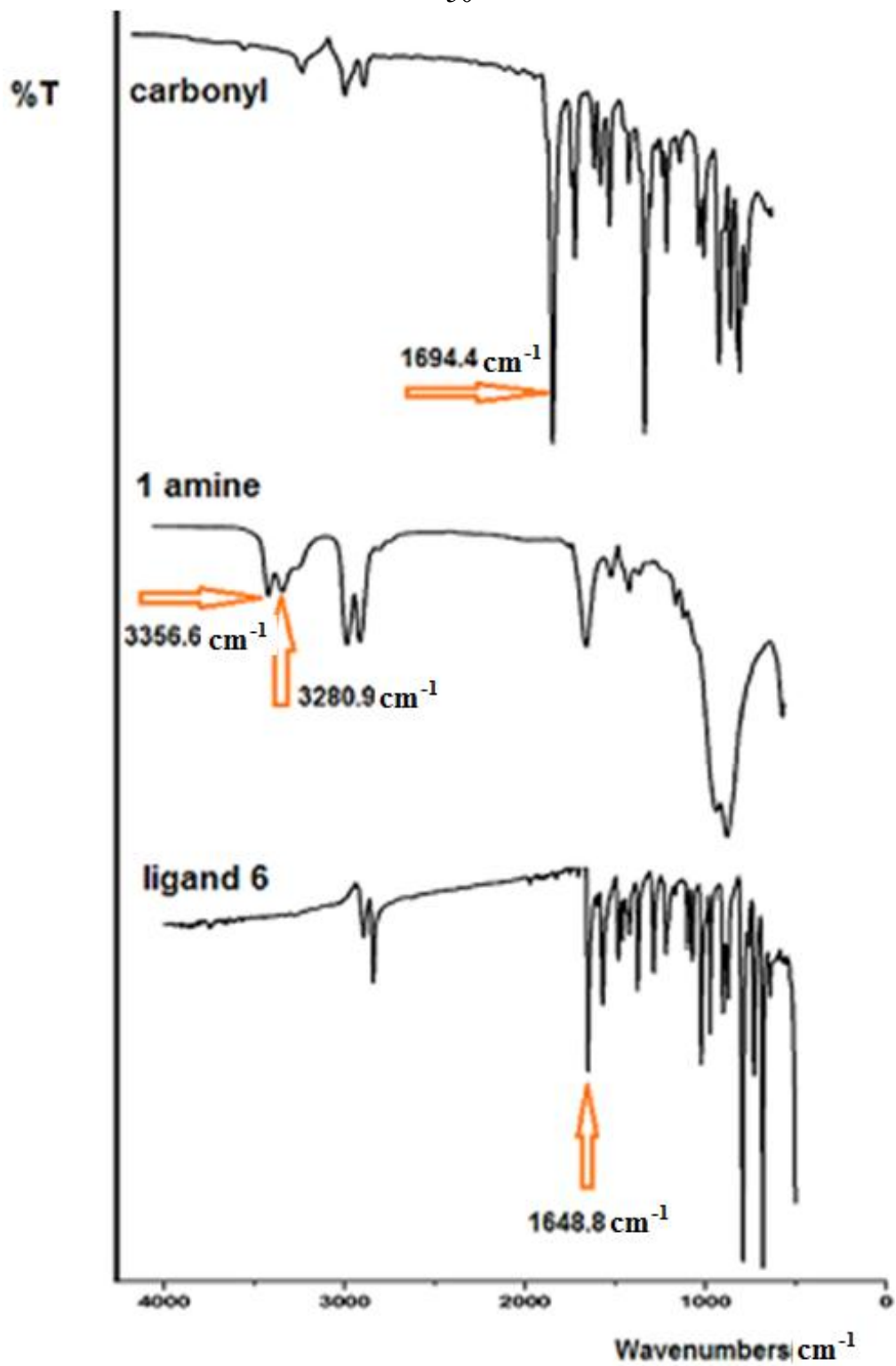


Figure 3.10 : IR spectrum of L₆

3.4.2 UV-VISIBLE Spectra Investigations

The rise of the electronic absorption bands in the UV/Visible spectra of the complexes are resulted from the electronic transitions between the energy levels.

The electronic absorption spectral data is very helpful in the explanation of ligands and the metal complexes. The Schiff base ligand shows the absorption on π - π^* and n - π^* transitions, which give bands at (200 nm- 360 nm). For Cu(II) complex, the spectra show bands at (400 nm- 800 nm), and for Cd(II) complex, the spectra show bands at (200nm- 300nm), where the electronic spectra of the Cadmium ion complexes had shown no electronic transfer within the $d \rightarrow d$ orbital as the 3d has 10 electrons .

The structure around the central transition metal can be estimated depending on their electronic transfer. So in LCuBr_2 complexes five coordination number through N or S atoms electron donors in the backbone of the ligand, expect to control the structural formula of two expected structures square pyramid or trigonal bipyramidal structure. In LCdCl_2 complexes only tetrahedral structure are expected.

The electronic absorption spectrum of the designed ligand and their complexes was carried out in (95% ethanol) at room temperature.

3.4.2.1 UV-Visible spectrum of L_2

The visible spectrum of the Cu(II) complex with L_2 was obtained at concentration (10^{-4} M) with the maximum absorption at 740 nm. It can be

assigned to (d to d) electron transition or LMCT [42], and the ligand exhibit no signal in the visible region as shown in **Figure 3.11**.

The appearance of λ_{\max} at 740 nm by addition L_2 to $CuBr_2$ confirmed the five coordination complexes formation as shown in **Chart 3.1**.

The changes in the solubility and color (by eyes), confirmed a non cationic formation of such complex.

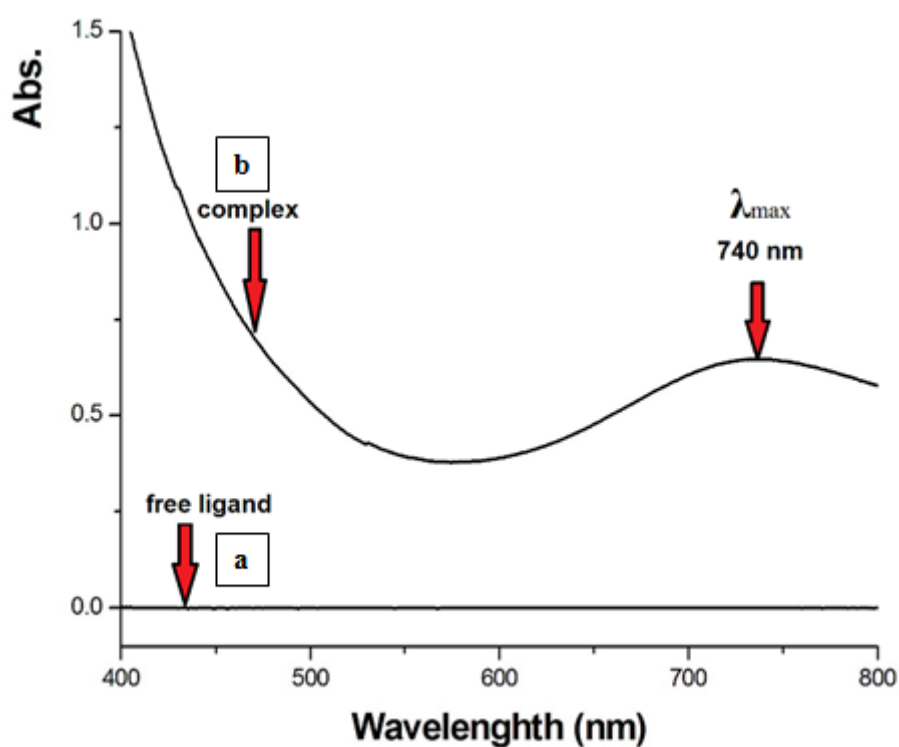


Figure 3.11: UV-Visible spectrum of L_2 (a), and L_2CuBr_2 (b).

In the UV region, the ligand that displayed transition at 215 nm may be assigned for π to π^* aromatic rings transitions. And the absorption band at 250 nm may be assigned to the $n-\pi^*$ electronic transition associated with the C=N linkages as shown in **Figure 3.12**.

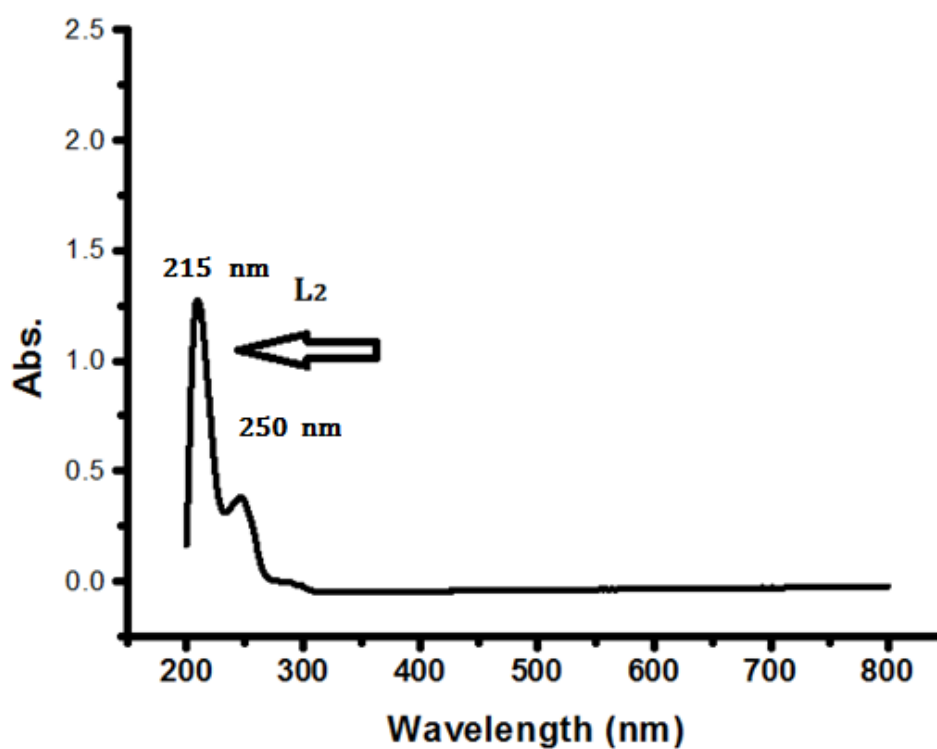


Figure 3.12: UV-Visible spectrum of L₂

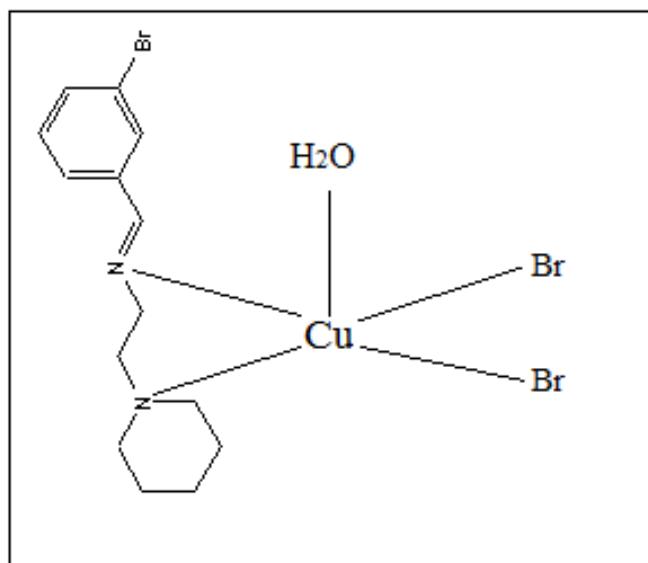


Chart 3.1 : Expected formula of L_2CuBr_2 depending on UV-Visible spectra

3.4.2.2 UV-Visible spectra of L_4

3.4.2.2.1 UV-Visible spectrum of Free L_4 and its complex with $CuBr_2$

In the UV region, the ligand that displayed transition at 210 nm may be assigned for π to π^* aromatic rings transitions. And the absorption band at 248 nm may be assigned to the $n-\pi^*$ electronic transition associated with the C=N linkages as shown in **Figure 3.13**.

The ligand displayed typical ligand-centered $\pi-\pi^*$ transitions at 210 nm and 248 nm for $n-\pi^*$ respectively. Upon coordination with metal ions, there are minor changes of these bands. The visible spectrum of the desired complex was obtained at higher concentration ($10^{-4}M$) with the maximum absorption at 570 nm, it can be assigned to d to d electron transition and the maximum absorption at 380 nm was assigned to LMCT, as shown in **Figure 3.13**.

The appearance of λ_{\max} at 570 nm by addition of L_4 to $CuBr_2$ confirmed the five coordination complexes formation as shown in **Chart 3.2**.

The changes in the solubility and color (by eyes), confirmed a non cationic formation of such complex.

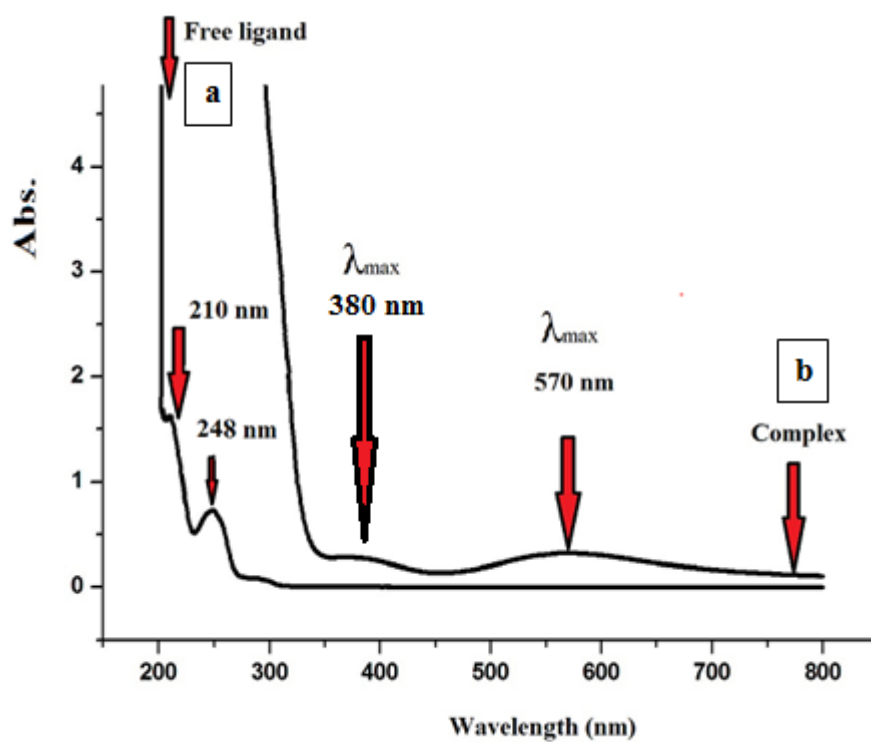


Figure 3.13: UV-Visible spectrum of the L_4 (a), L_4CuBr_2 (b)

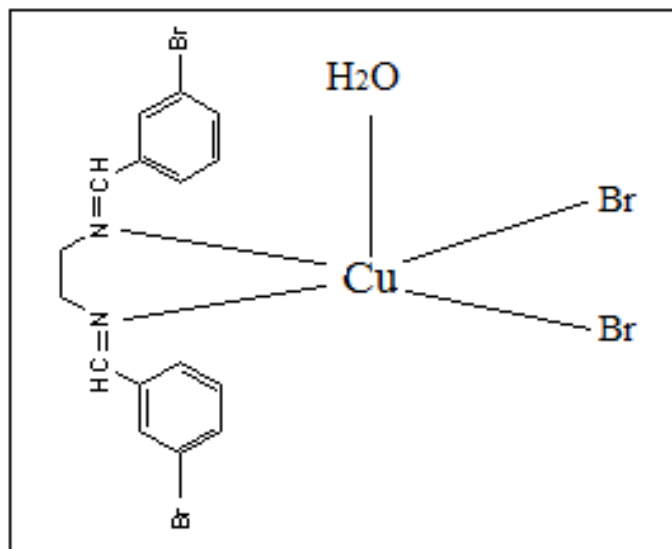


Chart 3.2 : Expected formula of L_4CuBr_2 depending on UV-Visible spectra

3.4.2.2.2 UV-Visible spectrum of Free L_4 and its complex with $CdCl_2$

When preparing L_4CdCl_2 complex, no significant change in UV-Vis behaves for $Cd(II)$ complexes (no electronic transfer within the $d \rightarrow d$ orbital as the 3d has 10 electrons).

In the UV region, the ligand displayed transition at 210 nm may be assigned for π to π^* aromatic rings transitions. The absorption band at 248 nm may be assigned to the $n-\pi^*$ electronic transition associated with the C=N linkages as shown in **Figure 3.14**.

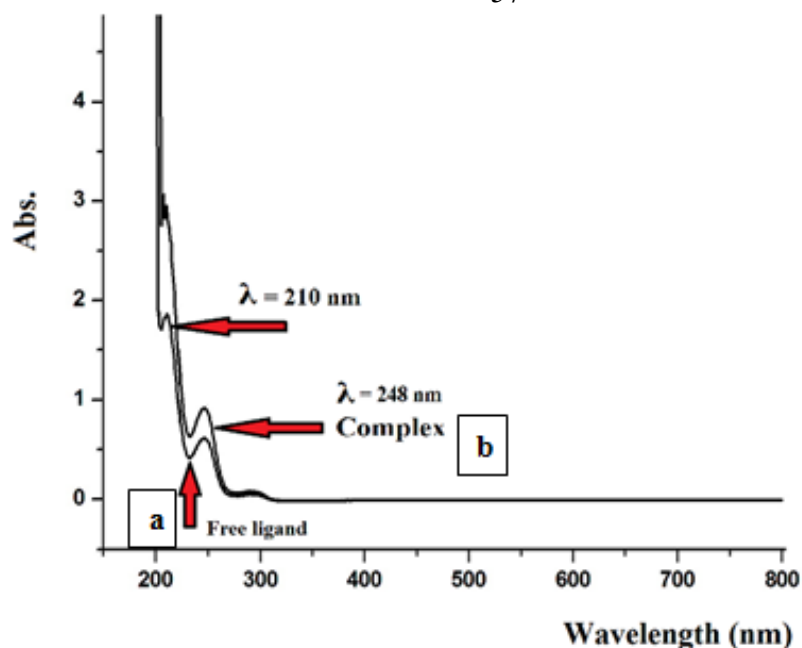


Figure 3.14: UV-Visible spectrum of L_4 (a), and $L_4\text{CdCl}_2$ (b).

3.4.2.3 UV-Visible spectra of L_5

3.4.2.3.1 UV-Visible spectrum of Free ligand and L_5 with CuBr_2

In the UV region, the ligand displayed $\pi-\pi^*$ transition at high wavelength 295nm due to delocalization of the electrons on ligand, while the other bidentate show expected electron transfer by 70-90 nm lower.

Upon coordination with metal ions, there are minor changes of these bands. The visible spectrum of the desired complex was obtained at higher concentration (10^{-4} M) with the maximum absorption above 800 nm due to delocalization of electrons on ligand where the ligand act as tetradentate chelating ligand with metal ion through two nitrogen and two sulfur atoms, as shown in **Figure 3.15**.

L_5 with four donor atoms (2N and 2S) is tetradentate ligand so it has special UV-VIS absorbance behavior. Due to the tetradentate of this ligand the expected d-d electron transfer was shifted to higher wavelength > 800 nm and this is due to the coordination of 2N and 2S to the Cu center as shown in **Chart 3.3**.

In this complex, the dicationic complex formation was confirmed by UV-VIS and water solubility formation.

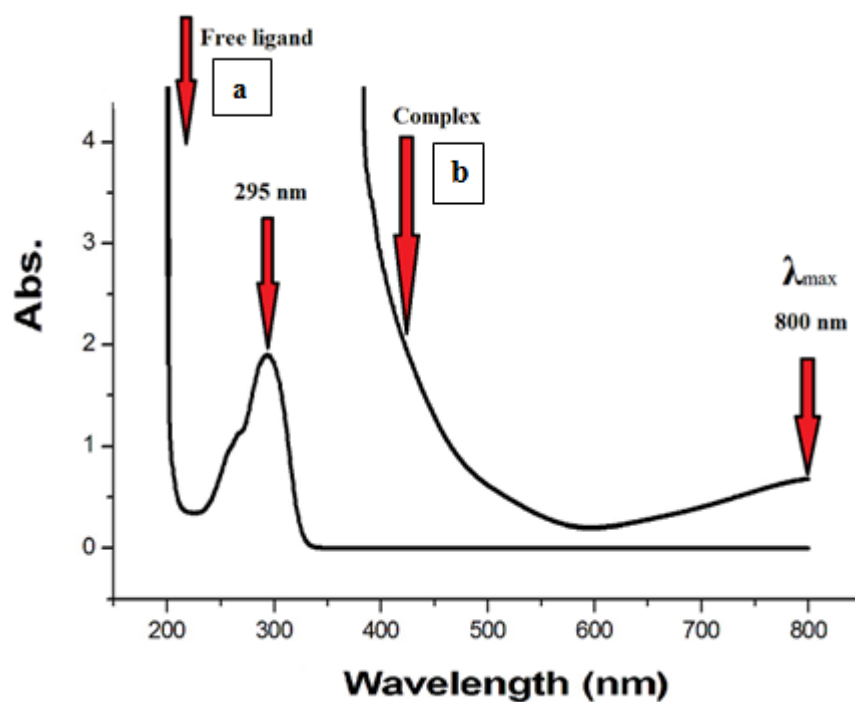


Figure 3.15: UV-Visible spectrum of L_5 (a), L_5CuBr_2 (b)

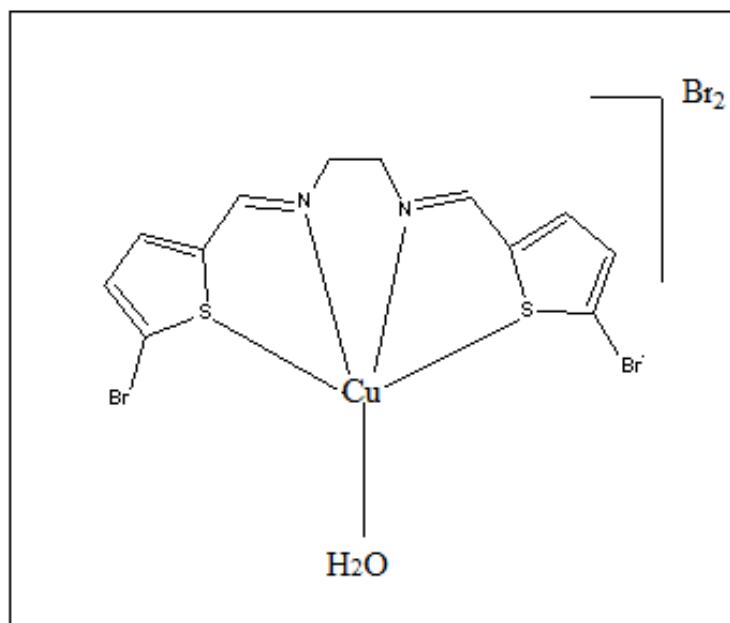


Chart 3.3 : Expected formula of L_5CuBr_2 depending on UV-Visible spectra

3.4.2.3.2 UV-Visible spectrum of Free ligand and L_5 with $CdCl_2$

When preparing L_5CdCl_2 complex, no significant change in UV-Vis behaves for Cd(II) complexes (no electronic transfer within the $d \rightarrow d$ orbital as the 3d has 10 electrons).

In the UV region, the ligand displayed $\pi-\pi^*$ transition at higher wavelength (295nm) due to delocalization of electron in the ligand while the other bidentate show expected electron transfer by 70-90 nm lower, as shown in **Figure 3.16.**

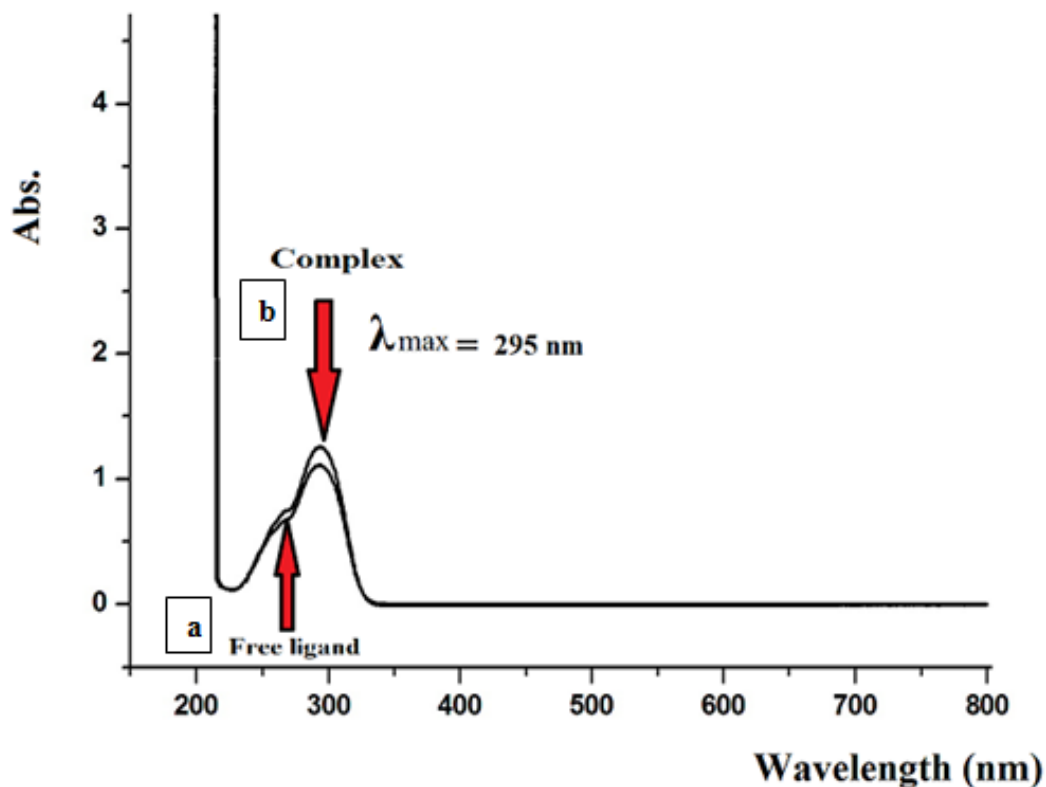


Figure 3.16: UV-Visible spectrum of L_5 (a), L_5CdCl_2 (b).

3.4.2.4 UV-Visible spectrum of L_6

In the UV region, the ligand displayed typical ligand-centered $\pi-\pi^*$ transition at 250 nm. Upon coordination with metal ions, there are minor changes of these bands. The visible spectrum of the desired complex L_6CuBr_2 was obtained at higher concentration (10^{-4} M) with the maximum absorption at 600 nm that can be assigned MLCT, as shown in **Figure 3.17**.

The appearance λ_{max} at 600 nm by addition L_6 to $CuBr_2$ confirm the five coordination complexes formation.

The changes in the solubility and color (by eyes), confirmed a non cationic formation of such complexes.

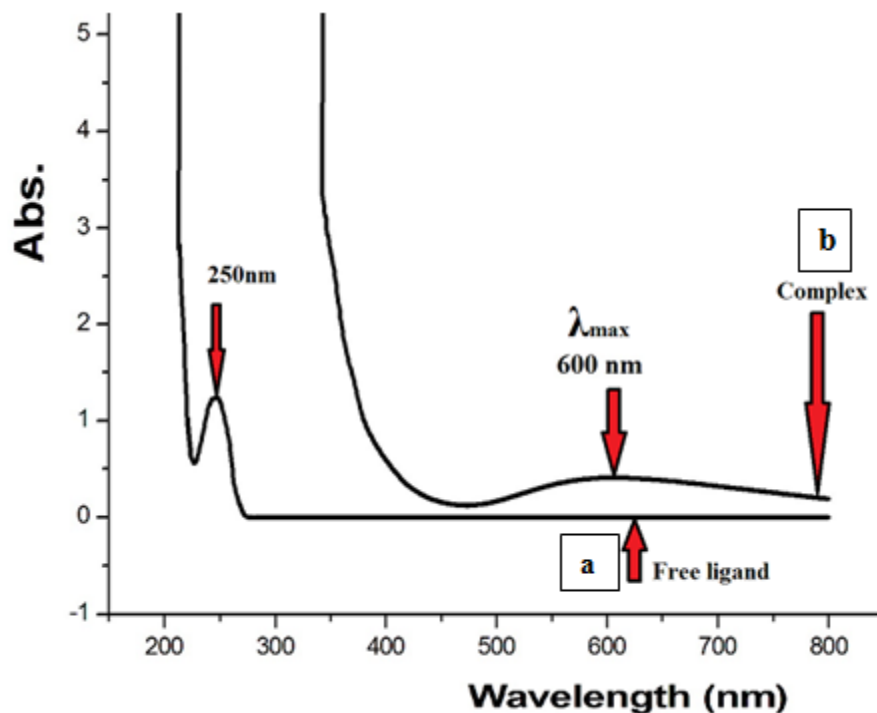


Figure 3.17: UV-Visible spectrum of L_6 (a), L_6CuBr_2 (b).

3.4.3 1H - NMR investigations of Schiff's bases L_1 - L_6

The 1H - NMR spectra of free ligands were recorded at room temperature by using $CDCl_3$ as a solvent, where these spectra are listed below.

In general the ligand revealed three types of 1H - NMR, aliphatic regions in 2-3.5 ppm, the phenylic protons in 7-8 ppm and aldehyde proton in 8-12 ppm.

3.4.3.1 1H - NMR spectra of L_1

The 1H -NMR spectrum **Figure (3.18)** of the Schiff base (1) showed that the signals in 3.747-3.868 ppm are related to methylene protons in two different environments.

The signals in 2.947-2.450 ppm are related to (h,i and j) protons of the piperidine ring. The (D-X) exchange between imine -CH=N proton and deuterium of chloroform gives the broad peak at 5.009 ppm .

The signal at 8.59 ppm was assigned to the proton of imine -CH=N group.

Signals in the region 7.578 -8.35 ppm were related to the aromatic protons (b, c, d and e).

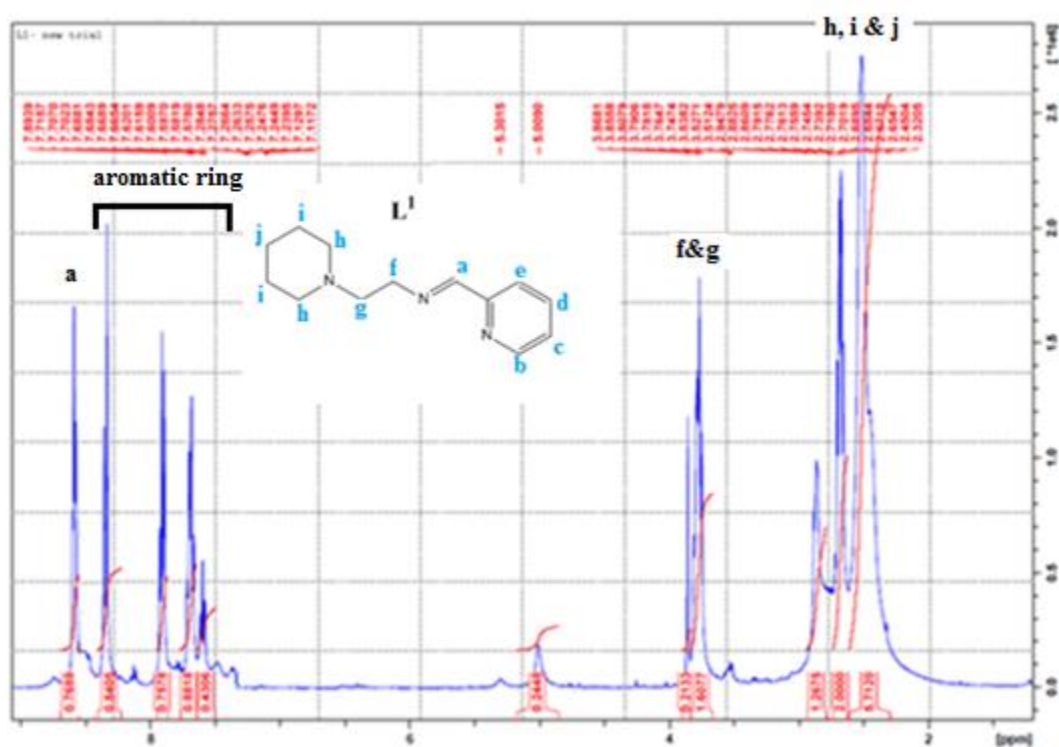


Figure 3.18 : ¹H-NMR spectrum of L₁

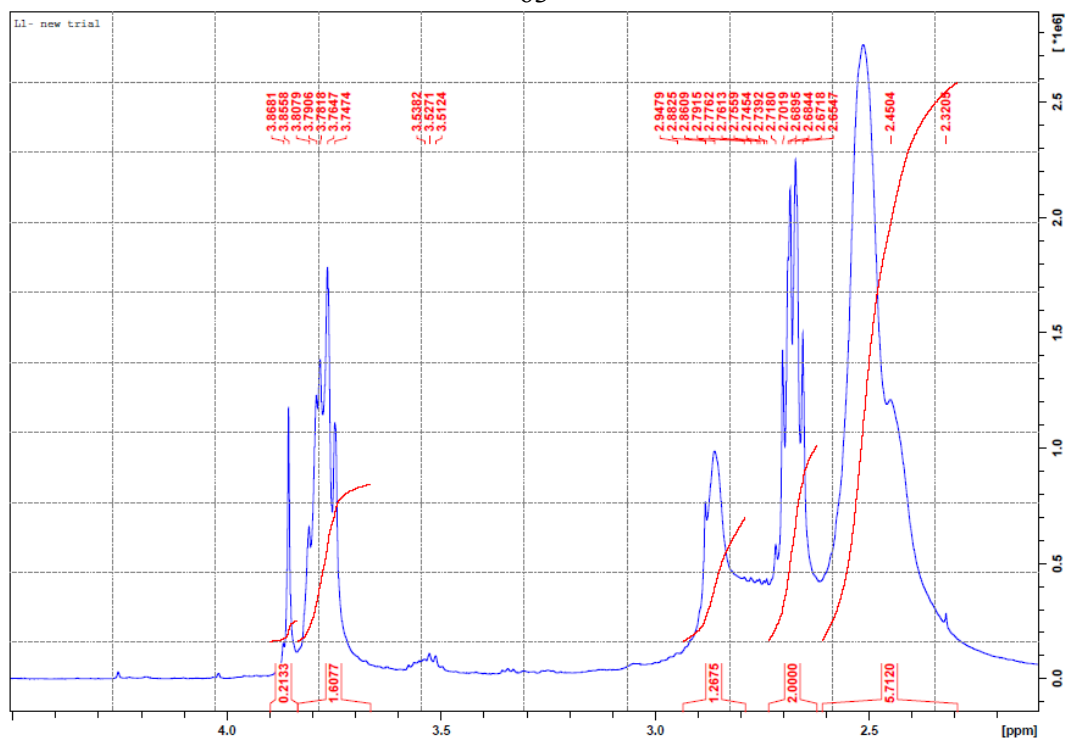


Figure 3.19 : ^1H -NMR spectrum of L_1 , the region (2-4.5)ppm.

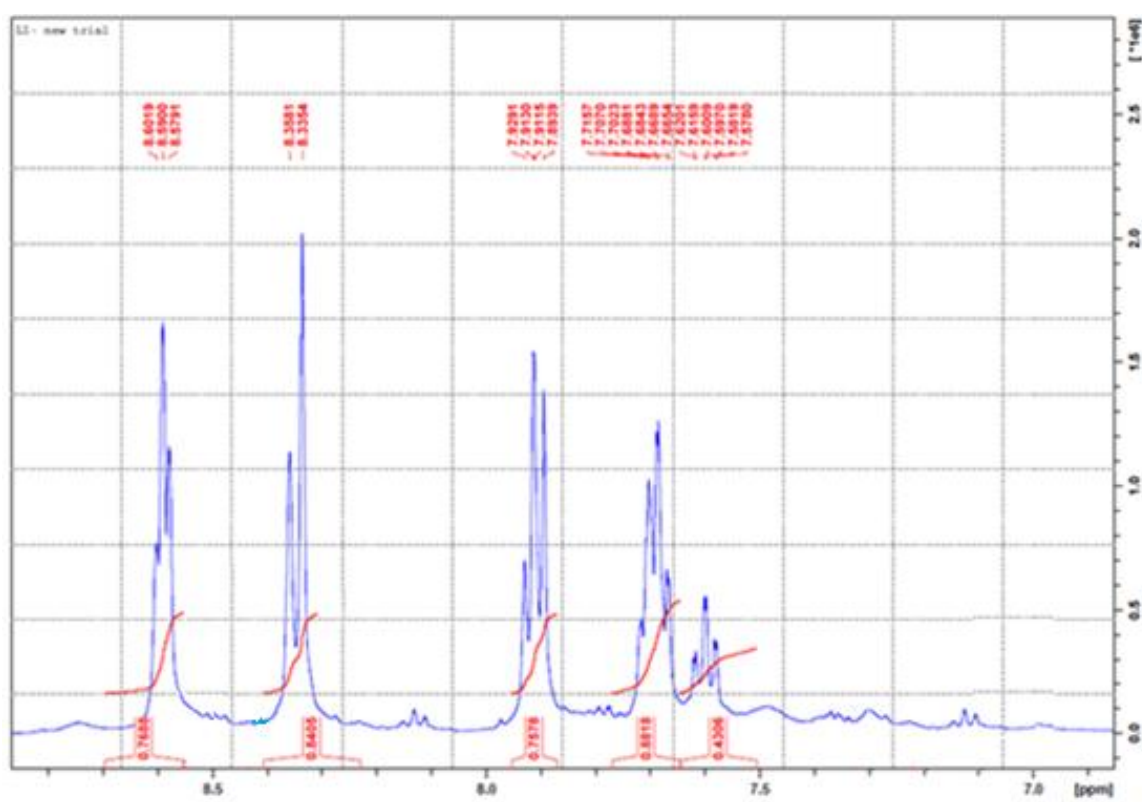


Figure 3.20 : ^1H -NMR spectrum of L_1 , the region (7-9)ppm.

3.4.3.2 $^1\text{H-NMR}$ spectrum of L_2

The $^1\text{H-NMR}$ spectrum **Figure (3.21)** of the Schiff's base (2) showed that: The signals at 2.791-1.200 ppm are related to (h,i and j) protons of the piperidine ring.

The signals in 3.623-3.785 ppm were related to methylene protons in two different environments.

The (D-X) exchange between imine $-\text{CH}=\text{N}$ proton and deuterium of chloroform gives the signal at 5.29 ppm.

Multiplet Signals in the region 7.608-7.894 ppm were related to the aromatic protons (b, c, d, and e).

The signal at 8.223 ppm was related to the proton of imine $-\text{CH}=\text{N}$ group.

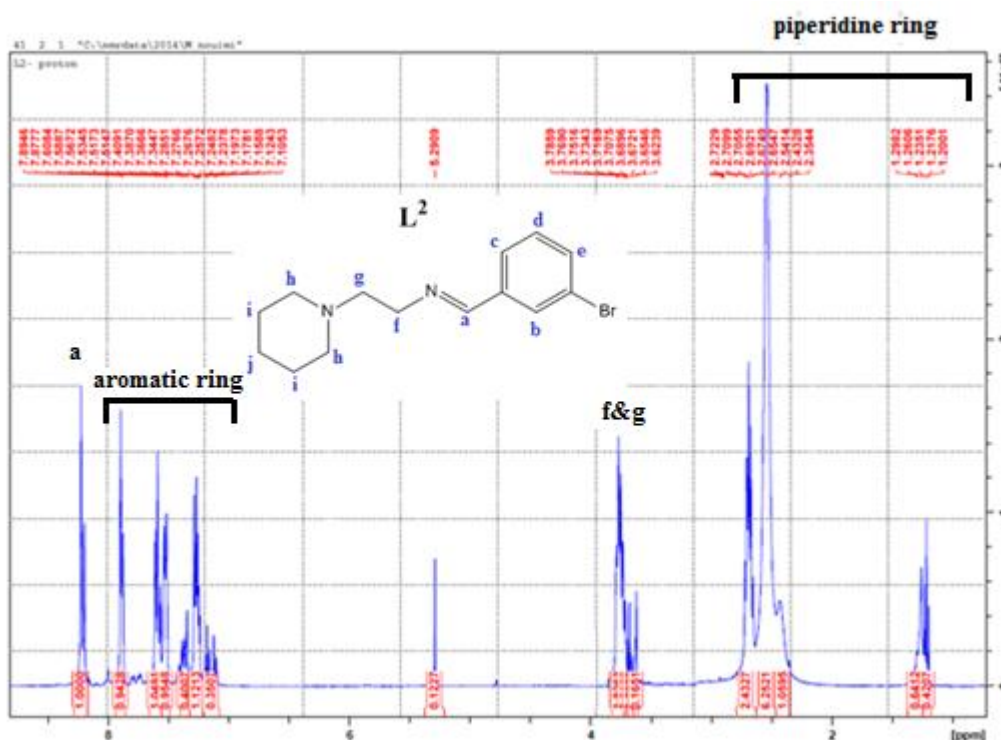


Figure 3.21 : $^1\text{H-NMR}$ spectrum of L_2

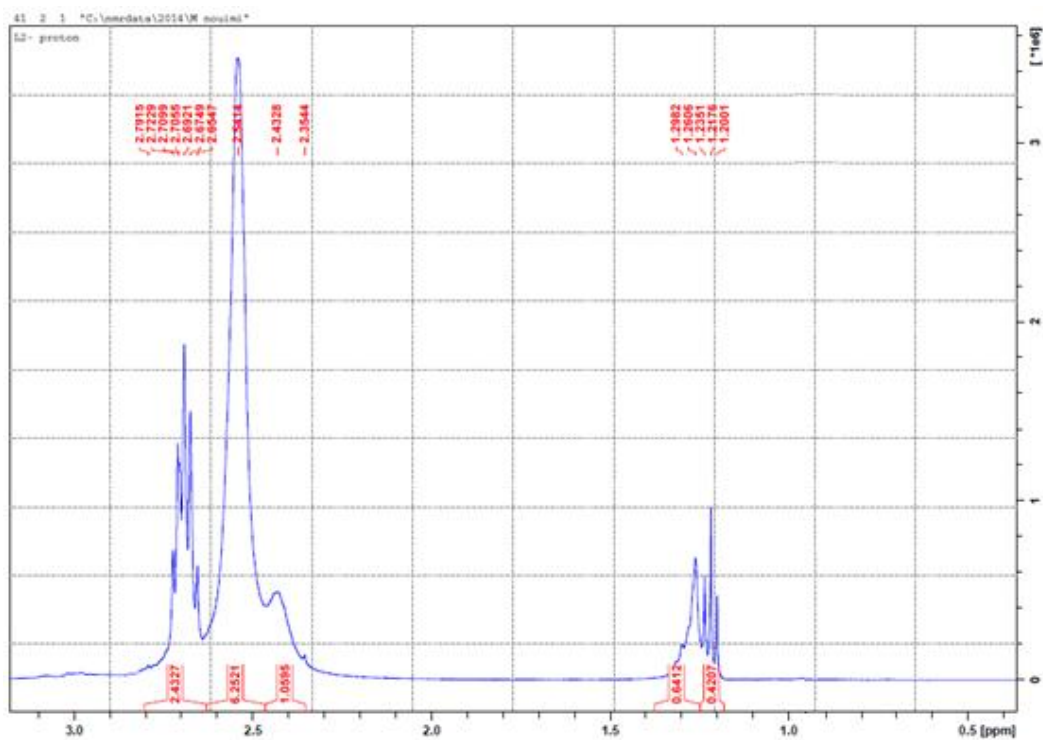


Figure 3.22 : ^1H -NMR spectrum of L_2 , the region (0-3)ppm.

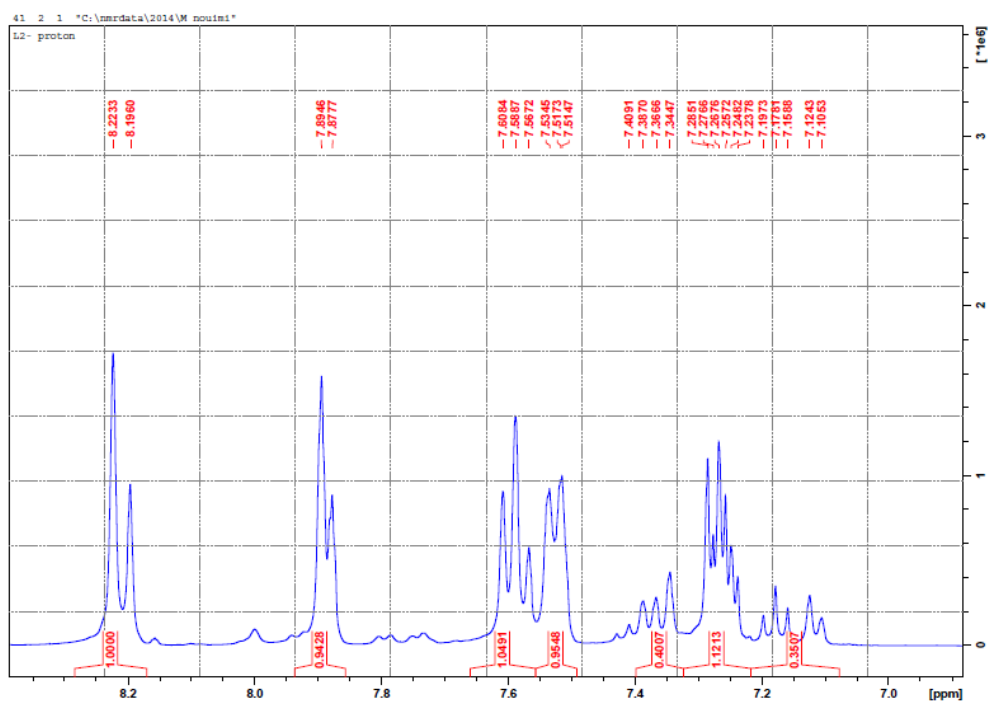


Figure 3.23 : ^1H -NMR spectrum of L_2 , the region (7-8.3)ppm

3.4.3.3 $^1\text{H-NMR}$ spectrum of L_3

The $^1\text{H-NMR}$ spectrum **Figure (3.24)** of the Schiff's base (3) where L_3 is symmetrical compound having the plane of symmetry.

The signal at 1.477 ppm was assigned to protons of methane proton *b*, 1.88ppm for methylene protons *c* and 3.4ppm for methylene protons *d*.

The signals in 7.181-7.911 ppm were assigned to the aromatic protons (*e*, *f*, *g*, and *h*). The signal at 8.632 ppm was assigned to the proton of imine - $\text{CH}=\text{N}$ group.

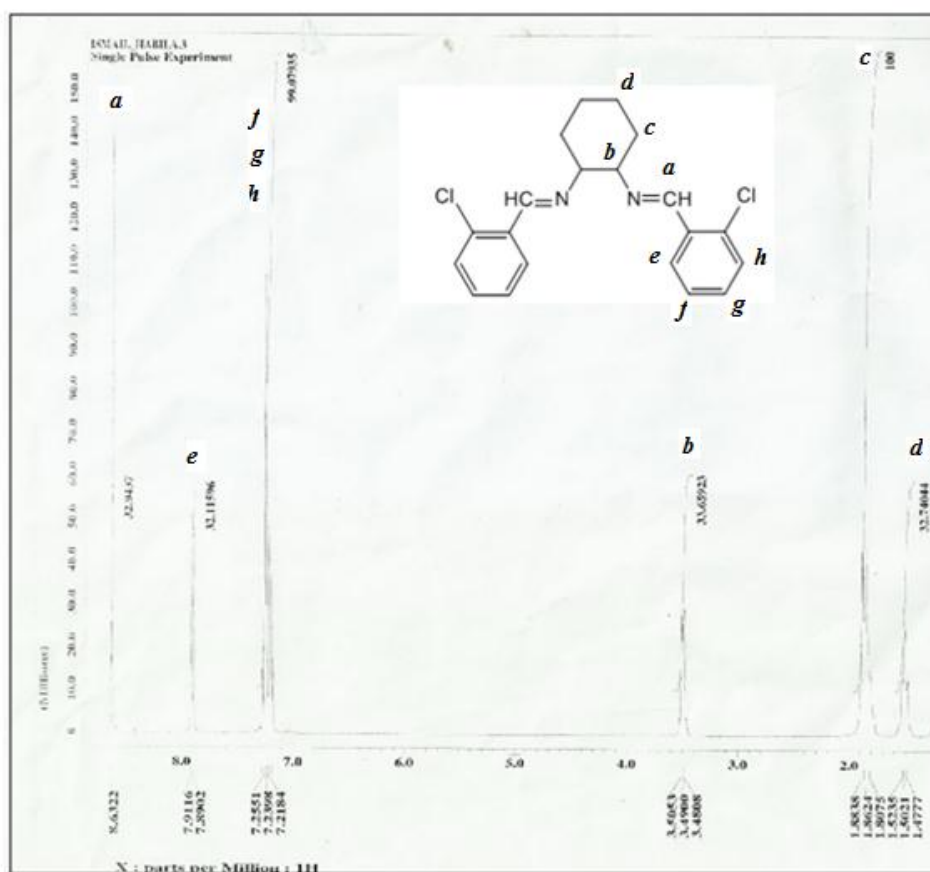


Figure 3.24 : $^1\text{H-NMR}$ spectrum of L_3

3.4.3.4 $^1\text{H-NMR}$ spectra of L_4

The $^1\text{H-NMR}$ spectrum **Figure (3.25)** of the Schiff's base (4) where L_4 is symmetrical compound having the plane of symmetry.

The signal at 3.089 ppm was assigned to methylene protons a. Signals in the region 7.253-7.904-ppm were assigned to the aromatic protons (c, d, e and f).

The signal at 8.229 ppm was assigned to the proton of imine $-\text{CH}=\text{N}$ group.

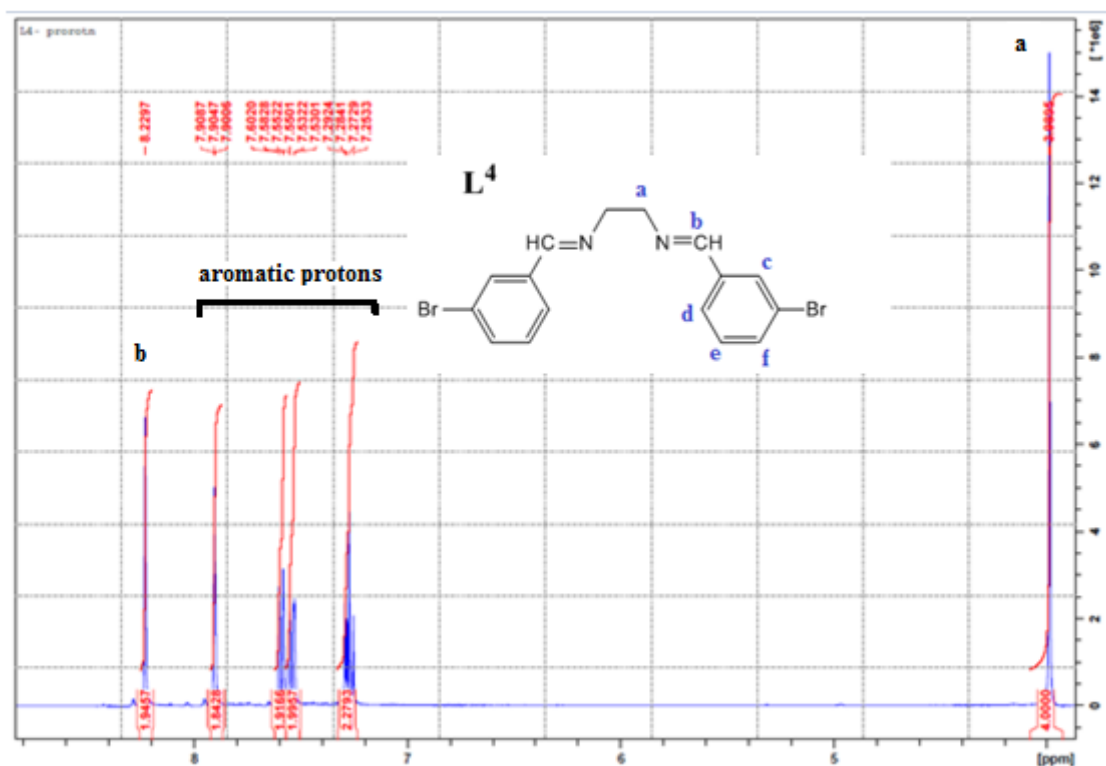


Figure 3.25 : $^1\text{H-NMR}$ spectrum of L_4

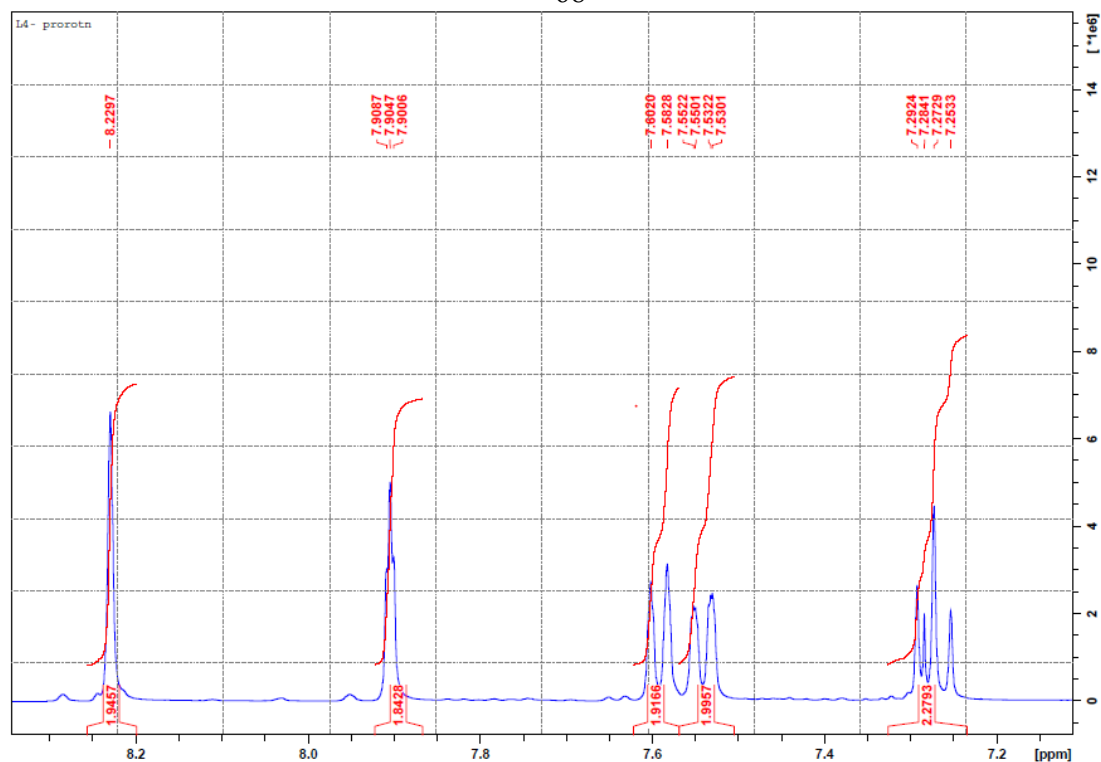


Figure 3.26 : ^1H -NMR spectrum of L_4 , the region (7-8.3) ppm

3.4.3.5 ^1H -NMR spectrum of L_5

The ^1H -NMR spectrum **Figure (3.27)** of the Schiff's base (5), where L_5 is symmetrical compound having the plane of symmetry.

The signal at 3.9 ppm was assigned to protons of methylene proton a. The signals at 6.99 ppm were assigned to the aromatic protons (c and d). And the signal at 8.198 ppm was assigned to the proton of imine $-\text{CH}=\text{N}$ group.

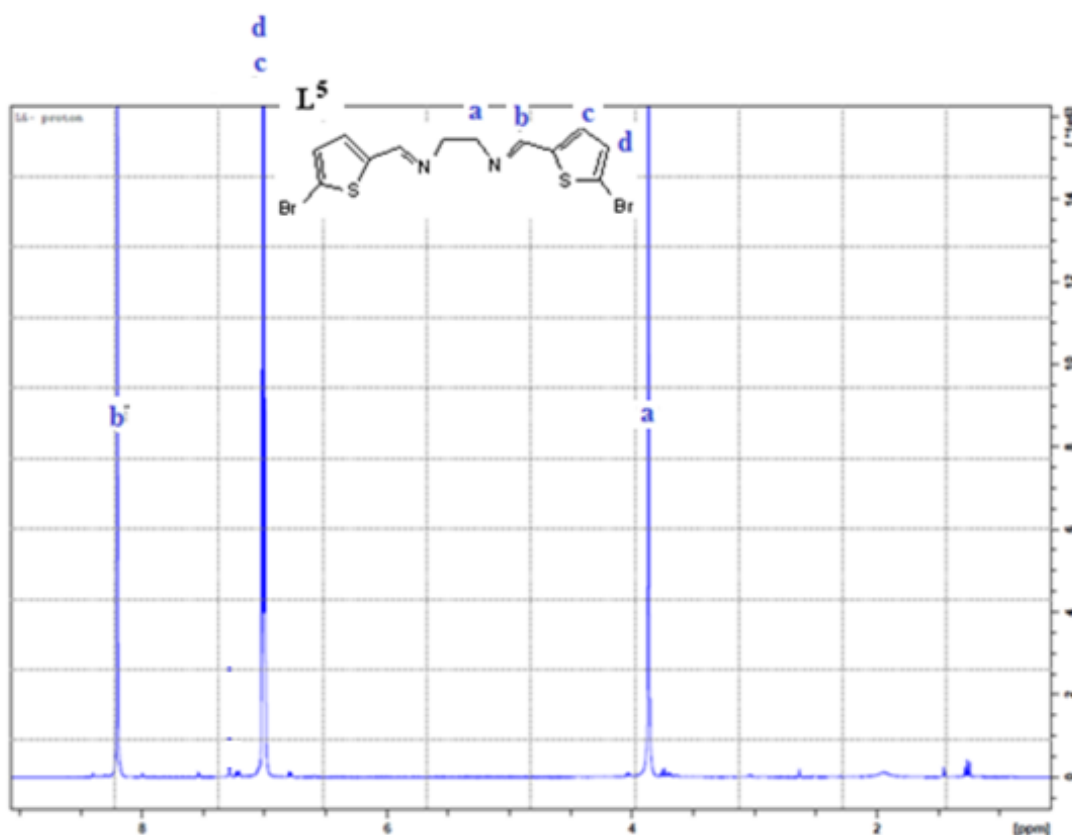


Figure 3.27 : ¹H-NMR spectrum of L₅

3.4.3.6 ¹H-NMR spectrum of L₆

The ¹H-NMR spectrum **Figure (3.28)** of the Schiff's base (6) where L₆ is symmetrical compound having the plane of symmetry.

The signal at 3.995 ppm was assigned to protons of methylene proton a. The signals in the region 7.753-7.284 ppm were assigned to the aromatic protons (c and d). The signal at 8.251 ppm was assigned to the proton of imine -CH=N group.

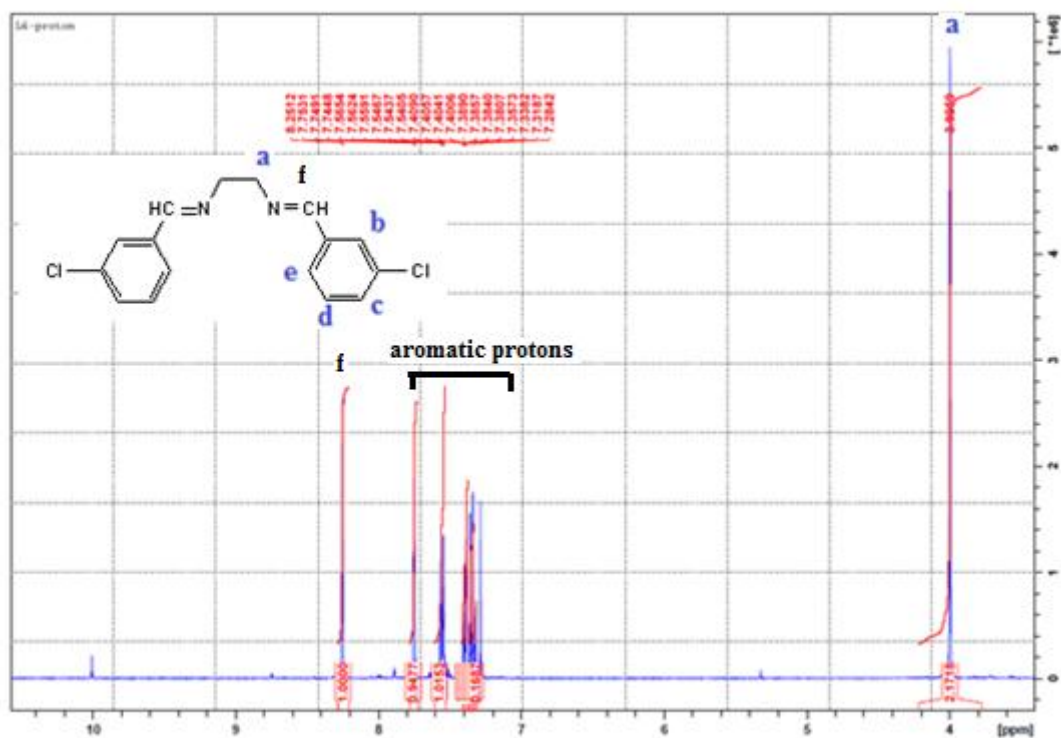


Figure 3.28 : ^1H -NMR spectrum of L_6

3.4.4 ^{13}C -NMR investigation

The ^{13}C -NMR spectra of the designed ligands L_1 - L_6 have been recorded in CDCl_3 solution at room temperature, the spectral data confirms the ^1H -NMR spectral results. In all ^{13}C -NMR spectra, the number of signals corresponds to the number of magnetically non-equivalent carbon atoms in the ligand.

In ^{13}C -NMR spectra the state of hybridization is the dominating factor determining the chemical shift of a carbon atom sp^3 -hybrid carbon atoms absorb up field while sp^2 carbon atoms absorb at lower field strength i.e. $\text{sp}^3 > \text{sp} > \text{sp}^2$.

3.4.4.1 ^{13}C -NMR spectrum of L_1

The azomethine carbon atom of the ligand appeared at 162.7 ppm. The aromatic ring carbon atoms appeared in the (121.3–154.3) ppm range where the signal at 154.3ppm indicates to quaternary carbon a .

The signals at 88.9 and 51.3 ppm are related to the carbons of ethylene - $\text{CH}_2\text{-CH}_2\text{-}$ group g&h respectively. The signals 45.8, 53.7 and 58.8 ppm are related to the carbons of piperidine ring i, j, and k respectively, as shown in **Figure 3.29**.

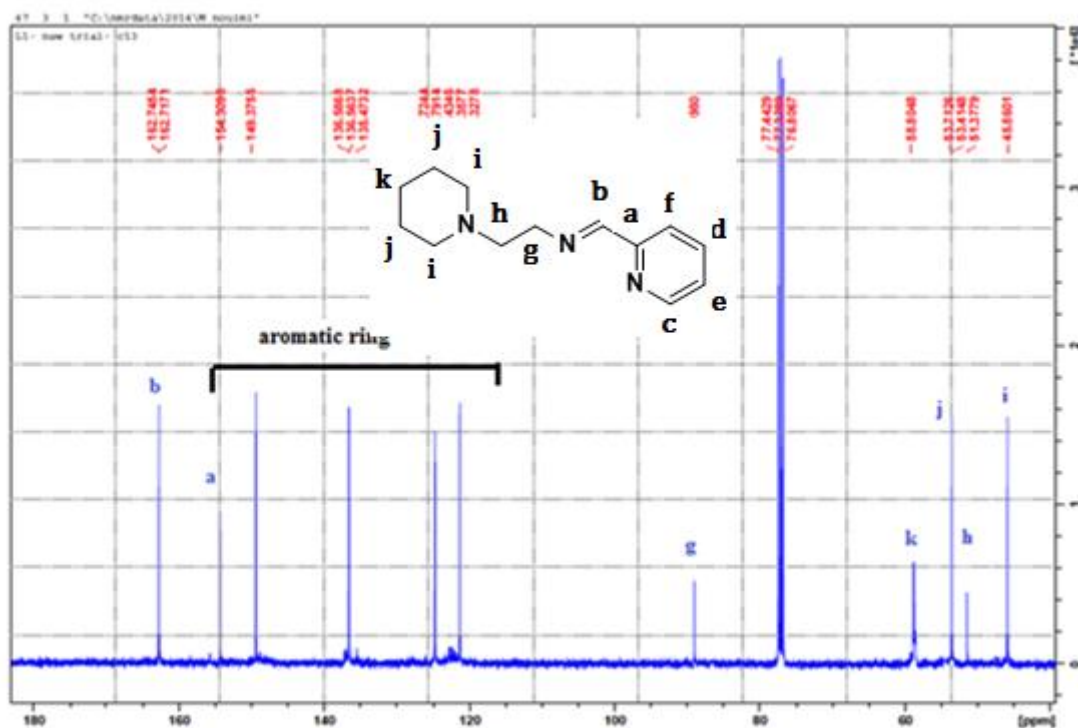


Figure 3.29 : ^{13}C -NMR spectrum of L_1

3.4.4.2 ^{13}C -NMR spectra of L_2

The azomethine carbon atom of the ligand appeared at 190.7 ppm. The aromatic ring carbon atoms appeared in the (127.3-138.1) ppm range where the peak at 131.2 ppm is related to quaternary carbon b. The signals at 87.8 and 53.7 ppm are related to the carbons of ethylene $-\text{CH}_2-\text{CH}_2-$ group j&h respectively. The signals 46.0, 54.7 and 58.9 ppm are related to the carbons of piperidine ring I, k, and l respectively, as shown in **Figure 3.30**.

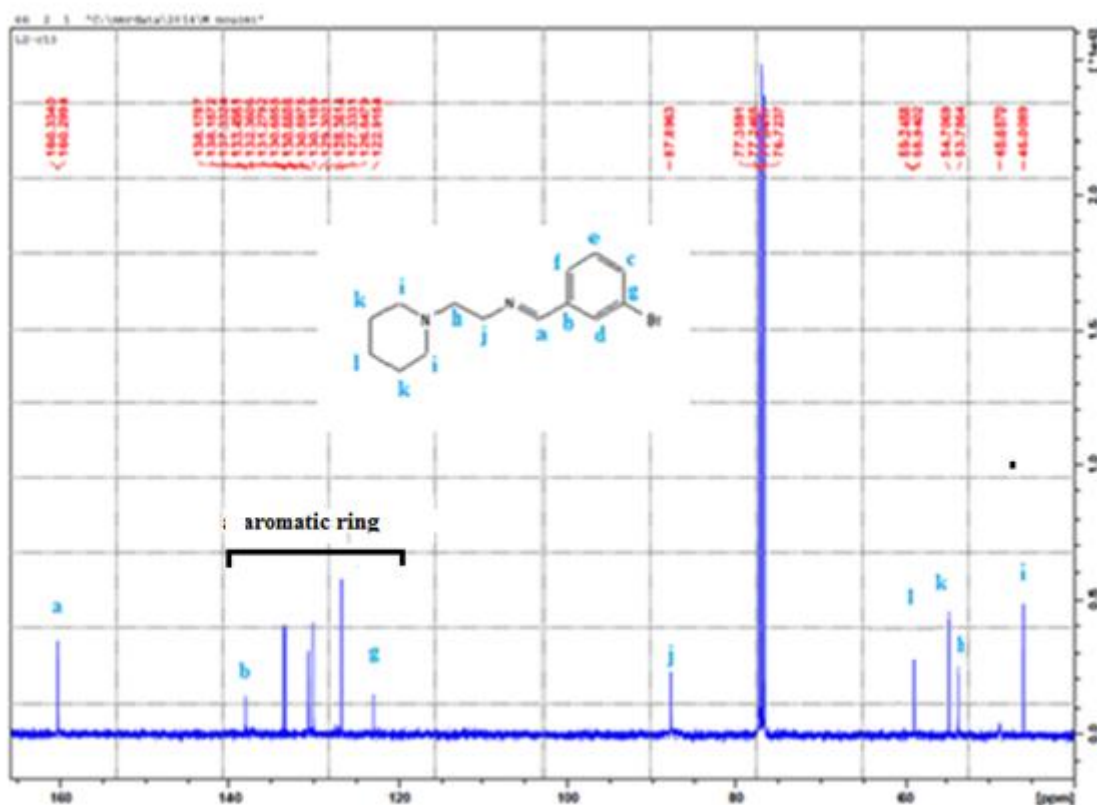


Figure 3.30 : ^{13}C -NMR spectrum of L_2

3.4.4.3 ^{13}C -NMR spectrum of L_3

The signal of azomethine carbon atom of the ligand appeared at 158 ppm. The aromatic ring carbon atoms appeared in the (128.5–134.9) ppm range. The signals at 32.9 & 24.4 ppm are related to the carbons c&d respectively. The signal at 73.9 ppm is related to carbon b, as shown in **Figure3.31**.

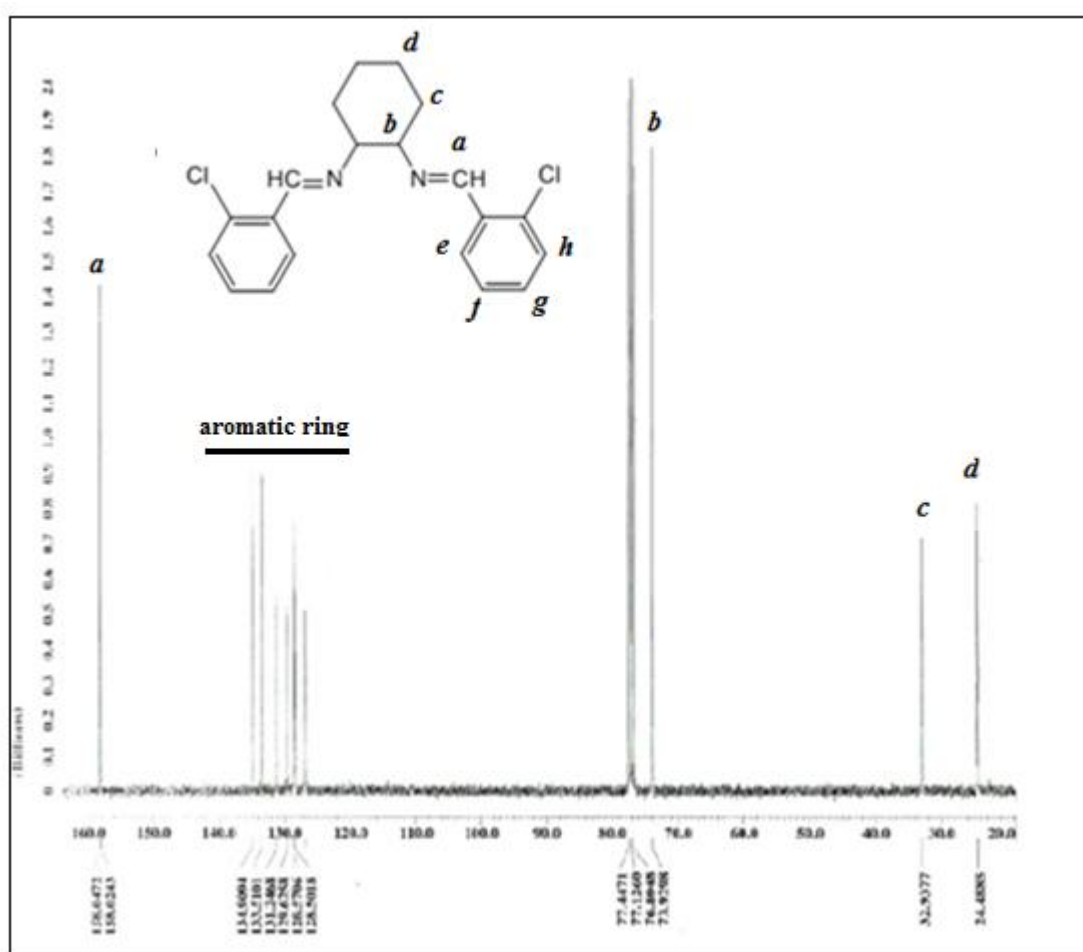


Figure 3.31 : ^{13}C -NMR spectrum of L_3

3.4.4.4 ^{13}C -NMR spectrum of L_4

This ligand is having a plane of symmetry. The signal of the azomethine carbon atom of the ligand appeared at 161.1 ppm. The aromatic ring carbon atoms are appeared in the (122.9-138.0) ppm range, where the signal at 138 ppm is related to quaternary carbon g, and another quaternary carbon at 122.9 ppm is related to carbon b. The signal at 61.3 ppm is related to the methylene carbon h, as shown in **Figure 3.32**.

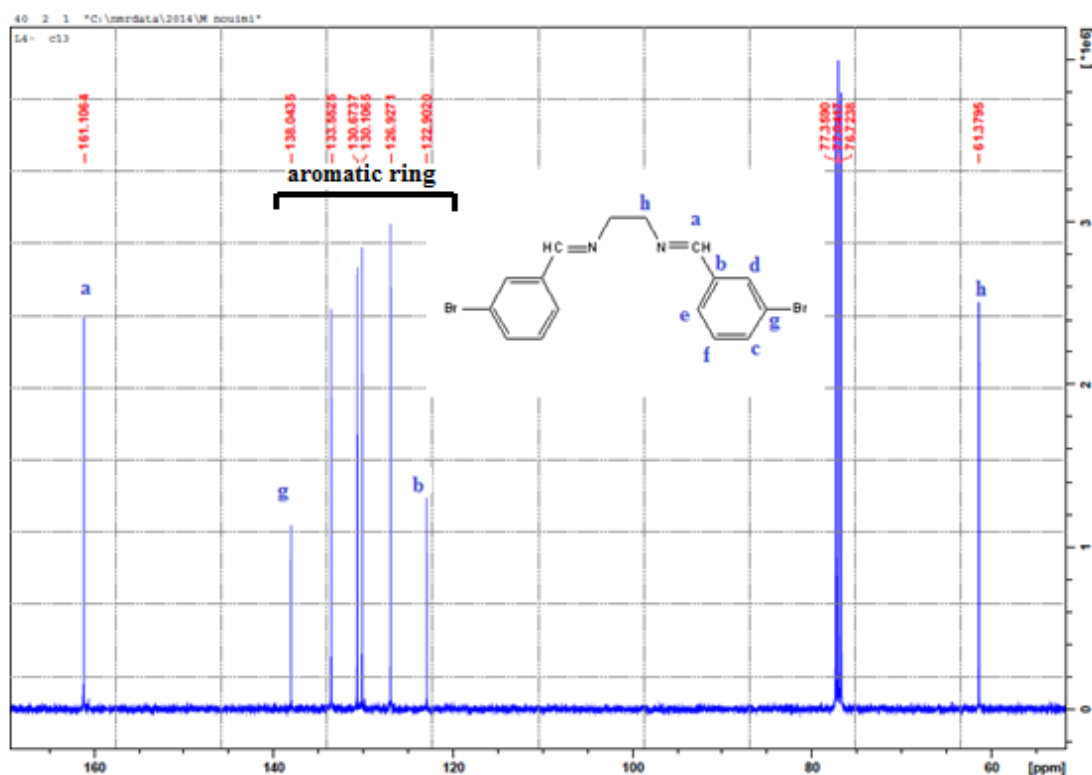


Figure 3.32 : ^{13}C -NMR spectrum of L_4

3.4.4.5 ^{13}C -NMR spectrum of L_5

This ligand is having a plane of symmetry. The signal of the azomethine carbon atom of the ligand appeared at 155.2 ppm. The aromatic ring carbon atoms appeared in the (116.9-143.9) ppm range.

There are two signals that are related to quaternary carbons at 143.9 ppm and 116.9 ppm for C(e)&C(b) respectively .

The signal at 60.6 ppm is related to the methylene carbon f, as shown in **Figure 3.33**.

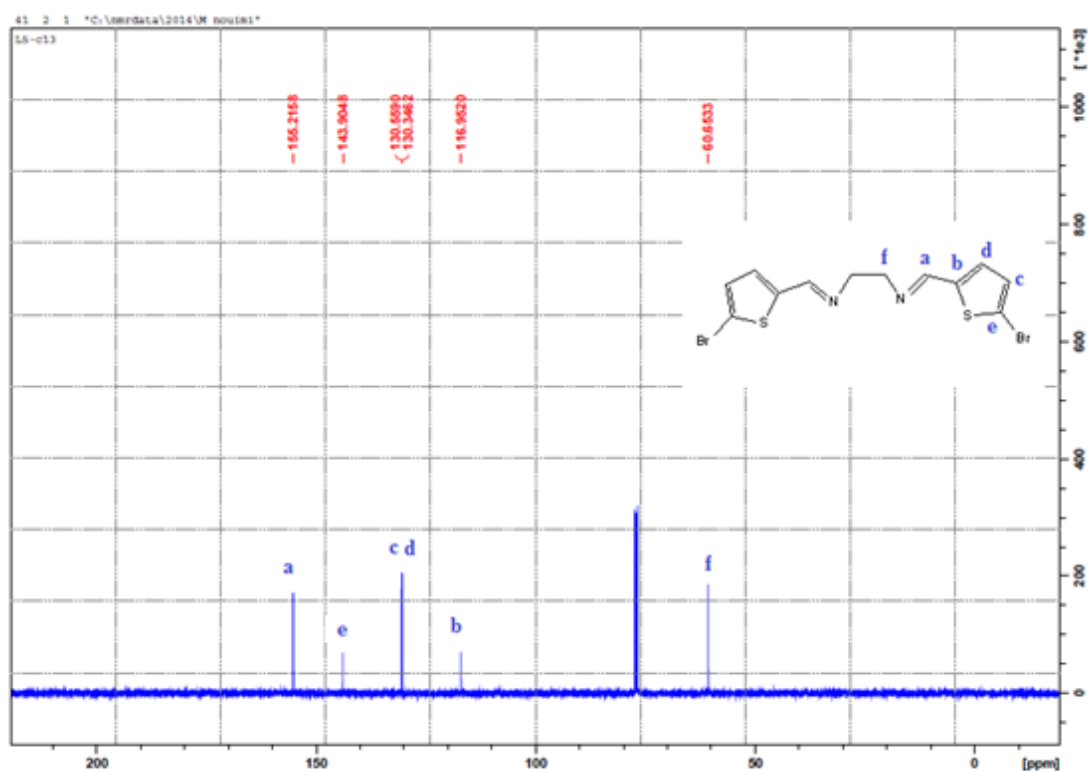


Figure 3.33 : ^{13}C -NMR spectrum of L_5

3.4.4.6 ^{13}C -NMR spectrum of L_6

This ligand is having a plane of symmetry. The signal of the azomethine carbon appeared at 161.2 ppm. The aromatic ring carbon atoms appeared in the (126.4-137.8) ppm range .

There are two signals that are related to quaternary carbons at 137.8 ppm and 134.7 ppm for C(c) & C(b) respectively .

The signal at 61.3 ppm is related to the methylene carbon (h), as shown in

Figure 3.34.

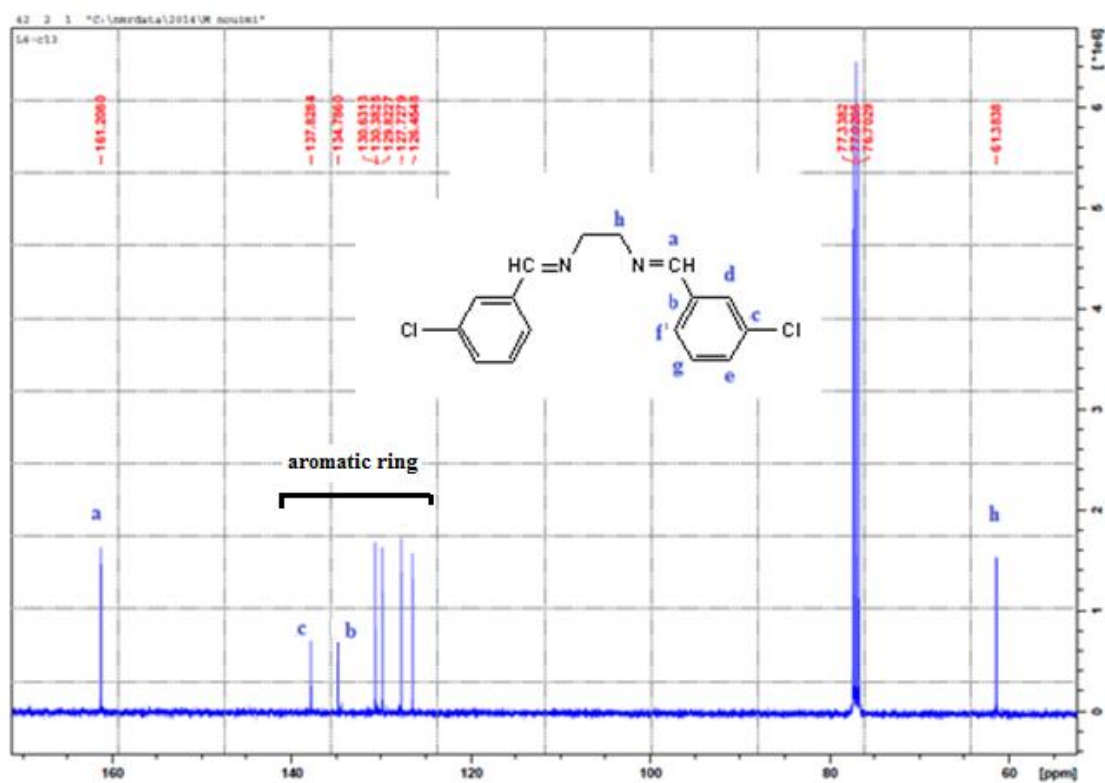


Figure 3.34 : ^{13}C -NMR spectrum of L_6

3.5 Thermogravimetric analyses of L_4 and their $CuBr_2$ and $CdCl_2$ complexes

The thermal stabilities of the complexes were investigated by TG/DTA. The TGA curves were obtained at a heating rate of $10\text{ }^\circ\text{C min}^{-1}$ in air atmosphere. The temperature range of 25-1000 $^\circ\text{C}$, for the free ligand (L_4), Cadmium Chloride with ligand (L_4) and the Copper Bromide complex with ligand (L_4). The thermogravimetric analyses of these complexes revealed the occurrence of three consecutive processes, namely dehydration, ligand pyrolysis and inorganic residue formation. The desired Cu(II) complexes showed similar thermogravimetric behavior, the TG/DTA spectra of $[L_4CuBr_2]$ illustrated mainly the expected three steps of weight loss. First step was losing uncoordinated water molecule at endothermic sign of DTA at $92\text{ }^\circ\text{C}$. The second decomposition stage from $220\text{ }^\circ\text{C}$ and end at $370\text{ }^\circ\text{C}$ losing around 40% of weight, diamine lose with two DTA exothermic signs at 250 and $480\text{ }^\circ\text{C}$ with expected final product of this step is $CuBr_2$. The third step starts from $370\text{ }^\circ\text{C}$ and end at $580\text{ }^\circ\text{C}$ which lead to the removal of bromide ions of $CuBr_2$ to form copper oxide (CuO) final product with sharp weight loss. The final residue was analyzed by IR spectra and identified as copper oxide (CuO , 22%), as shown in **Figure 3.35**.

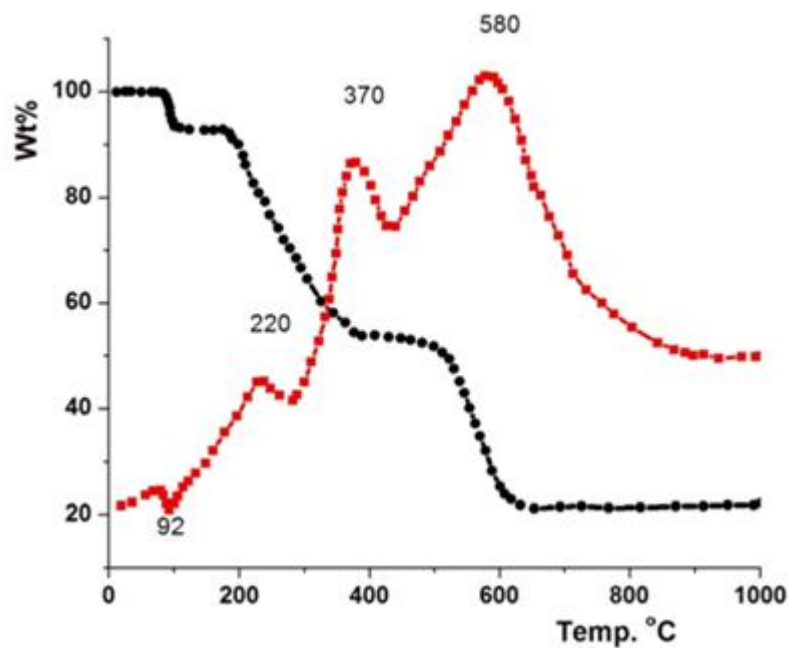


Figure 3.35: TG/DTA thermal curve of solid (L_4CuBr_2) complex

The TG/DTA data (**Figure 3.35**) support our expected complex structure formula as shown in **Chart 3.4**.

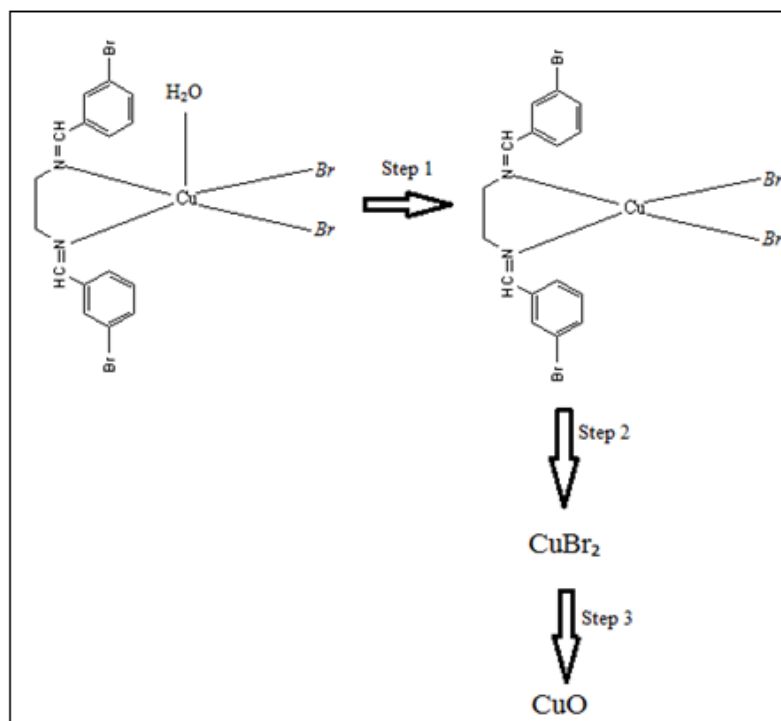


Chart 3.4: Decomposition steps of L_4CuBr_2

The TG/DTA spectrum of free ligand (L_4) illustrated mainly the expected one step of weight loss. In the spectrum (**Figure 3.36**), we observed no change from zero to 95 °C, which indicates that no water molecule coordinate to the ligand, and the decomposition of L_4 take place in one step with DTA exothermic step at 95 °C as below.

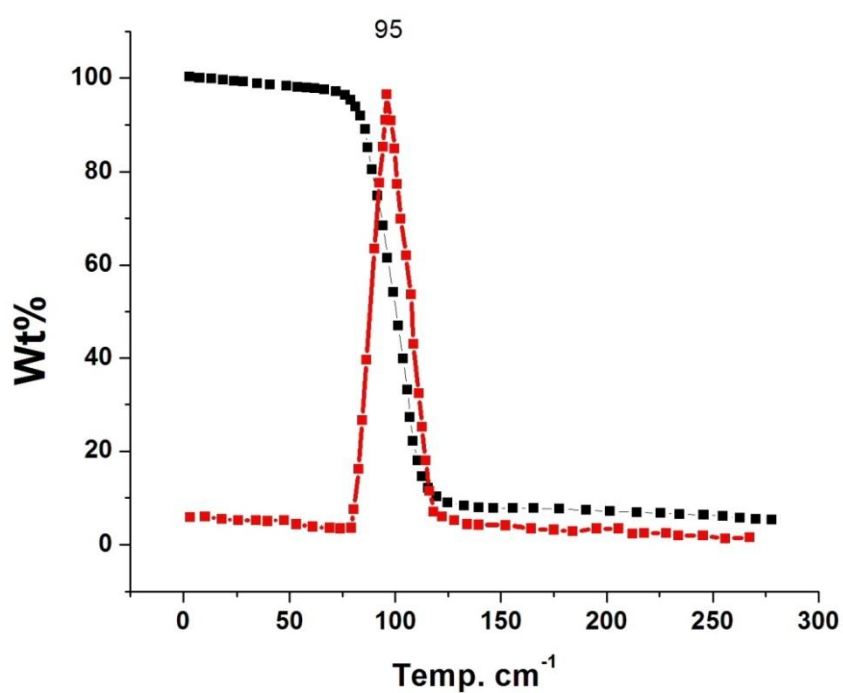


Figure 3.36: TG/DTA thermal curve of solid L_4 .

The TG/DTA spectrum of L_4CdCl_2 illustrated mainly the expected one step of weight loss. In the spectrum (**Figure 3.37**), we observed no change from zero to 250 °C, which indicates that no water molecule coordinate on the complex, and the decomposition of complex take place within (250-350) °C in one step as below, with one exothermic DTA value at 330 °C.

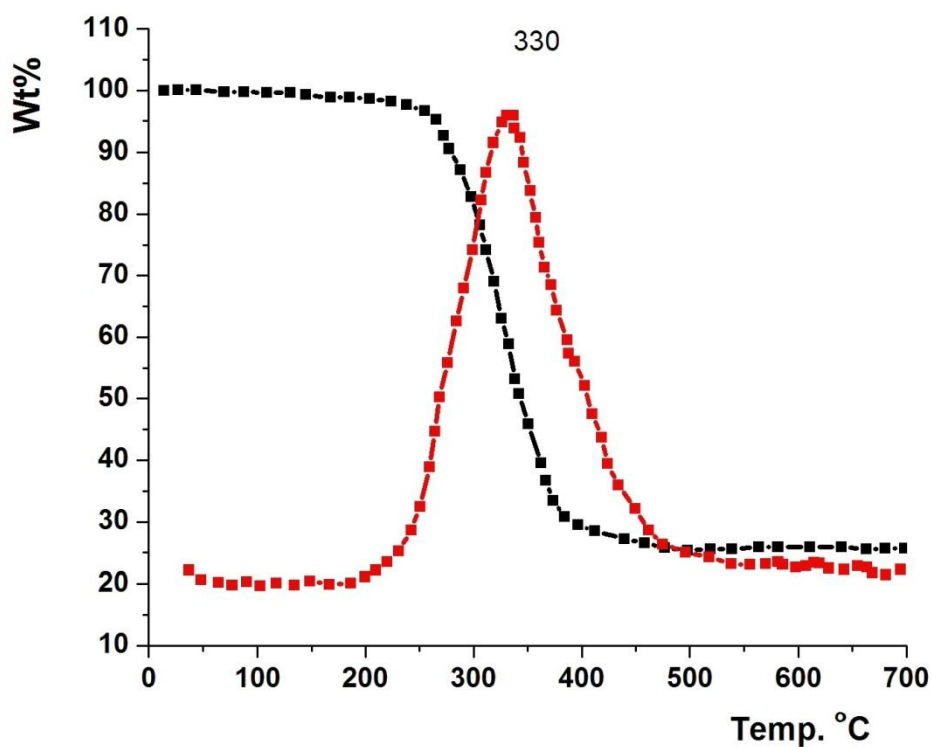
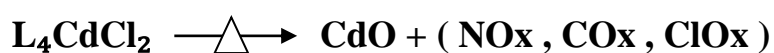


Figure 3.37: TG/DTA thermal curve of solid (L_4CdCl_2) complex.

3.6 Single-Crystal X-Ray Data collection

Single crystals of L_3 and L_5 were collected by evaporation from ethanol solution for couple of days then measured, unfortunately no complexes were collected as crystals.

3.6.1 X-Ray Crystal Structure of L_3

L_3 was solved in the monoclinic system with space group $P2_1/c$ with cell coordinates $a = 5.9029 (5) \text{ \AA}$, $b = 19.5613 (13) \text{ \AA}$, $c = 16.1662 (11) \text{ \AA}$,

$\beta = 93.493 (7)^\circ$, $V = 1863.2 (2) \text{ \AA}^3$, $Z = 4$, where slow evaporation of ethanol solution of pure L_3 yielded colorless crystals. A crystal of dimensions $0.30 \times 0.20 \times 0.15 \text{ mm}$ was selected for X-ray diffraction analysis (**Table 3.2**).

Data were collected on CrysAlis PRO (Agilent, 2011); cell refinement: CrysAlis PRO; data reduction: CrysAlis PRO; program(s) used to solve structure: SHELXS97 (Sheldrick, 2008); program(s) used to refine structure: SHELXL97 (Sheldrick, 2008); molecular graphics: ORTEPIII (Burnett & Johnson, 1996); software used to prepare material for publication: SHELXL97.

This compound is racemic, in which the cyclohexane ring adopts the expected chair conformation, with a dihedral angle of $62.52 (8)^\circ$ between the aromatic rings of the two 2-chlorophenyl substituent groups (**Fig. 3.38**). The structure of the chiral isomeric (1*R*,2*R*) 4-chlorophenyl analogue has

been reported (Arvinnezhad *et al.*, 2012). In the title compound, the conformation is stabilized by intramolecular C7—H...Cl1 and

C14—H...Cl2 interactions [3.066 (2) and 3.076 (3) Å, respectively] (Table 1). In the crystal there are weak intermolecular methine C—H...Cl interactions [C10—H...Cl1 [3.600 (3) Å] ($-x + 2, -y, -z$), C11—H...Cl1 [3.553 (3) Å] ($x - 1, y, z$) and C20—H...Cl2 [3.464 (3) Å] ($1 + x + 1, y, z$). Also present in the crystal are Cl...Cl contacts [Cl1...Cl1, 3.557 (3) Å ($-x + 1, -y, -z$)] and 3.891 (3) Å ($-x + 2, -y, -z$). (**Fig. 3.39**) [36].

Table 3.2. The crystal and experimental data of L₃

Crystal data

C₂₀H₂₀Cl₂N₂

$M_r = 359.28$

Monoclinic, $P2_1/n$

Hall symbol: $-P 2_1 n$

$a = 5.9029$ (5) Å

$b = 19.5613$ (13) Å

$c = 16.1662$ (11) Å

$\beta = 93.493$ (7)°

$V = 1863.2$ (2) Å³

$Z = 4$

$F(000) = 752$

$D_x = 1.281$ Mg m⁻³

Mo $K\alpha$ radiation, $\lambda = 0.71073$ Å

Cell parameters from 2442 reflections

$\theta = 3.1$ – 29.1 °

$\mu = 0.35$ mm⁻¹

$T = 293$ K

Block, colourless

$0.30 \times 0.20 \times 0.15$ mm

Data collection

Agilent Xcalibur Eos

diffractometer

Radiation source: Enhance (Mo) X-ray Source

Graphite monochromator

Detector resolution: 16.0534 pixels mm⁻¹

ω scans

Absorption correction: multi-scan

(*CrysAlis PRO*; Agilent, 2011)

$T_{\min} = 0.902$, $T_{\max} = 0.949$

7483 measured reflections

3273 independent reflections

2252 reflections with $I > 2\sigma(I)$

$R_{\text{int}} = 0.030$

$\theta_{\max} = 25.0$ °, $\theta_{\min} = 3.3$ °

$h = -7 \rightarrow 6$

$k = -23 \rightarrow 18$

$l = -19 \rightarrow 17$

Refinement

Refinement on F^2

Least-squares matrix: full

$R[F^2 > 2\sigma(F^2)] = 0.046$

$wR(F^2) = 0.106$

$S = 1.02$

3273 reflections

217 parameters

0 restraints

Primary atom site location: structure-invariant

direct methods

Secondary atom site location: difference Fourier map

Hydrogen site location: inferred from neighbouring sites

H-atom parameters constrained

$w = 1/[\sigma^2(F_o^2) + (0.0349P)^2 + 0.4202P]$

where $P = (F_o^2 + 2F_c^2)/3$

$(\Delta/\sigma)_{\max} < 0.001$

$\Delta\rho_{\max} = 0.28$ e Å⁻³

$\Delta\rho_{\min} = -0.20$ e Å⁻³

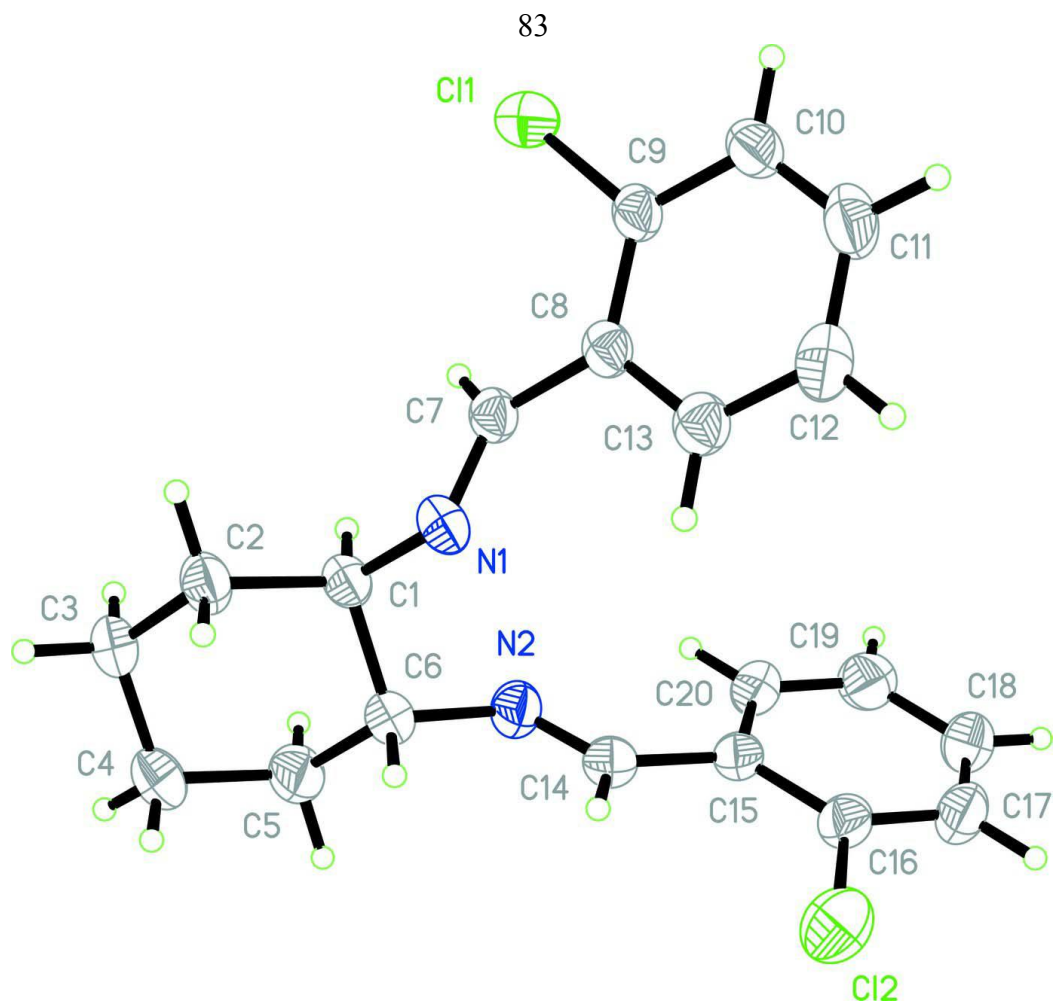


Figure 3.38: Molecular conformation and atom-numbering scheme for the L_3 . Displacement ellipsoids are drawn at the 30% probability level. H atoms are represented as small spheres of arbitrary radii.

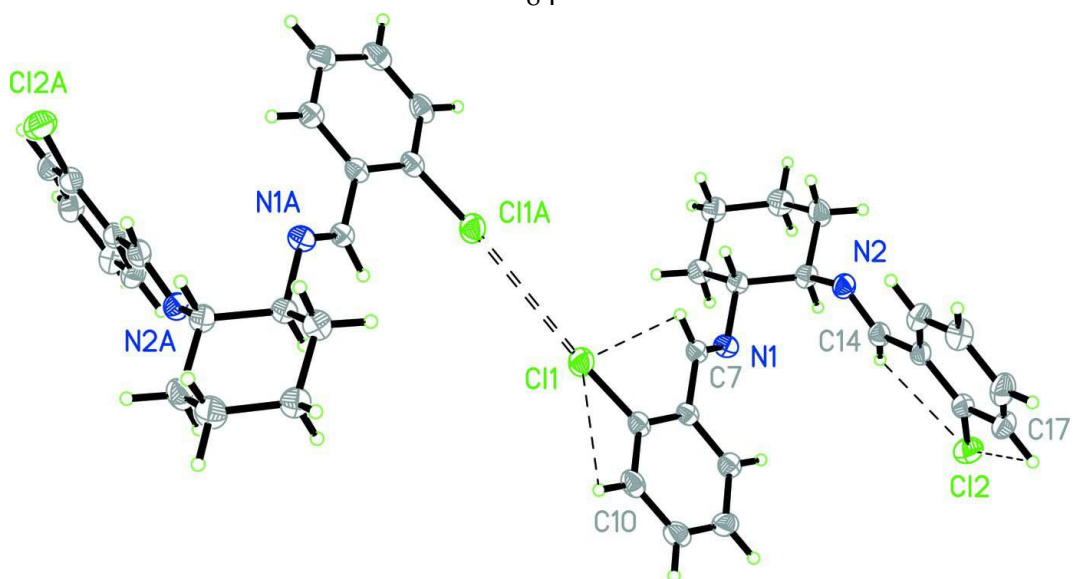


Figure 3.39: Molecular conformation showing intramolecular C7—H...Cl1, C10—H...Cl1, C14—H...Cl2 and C17—H...Cl2 contacts, as well as a short intermolecular Cl1...Cl1A contact. For symmetry code (A): $-x + 1, -y, -z$. for L_3

Table 3.3 Fractional atomic coordinates and isotropic or equivalent isotropic displacement parameters (A²)

	<i>x</i>	<i>y</i>	<i>z</i>	<i>U</i> _{iso} */ <i>U</i> _{eq}
C11	0.73684 (13)	0.05324 (3)	0.02770 (4)	0.0762 (2)
C12	1.12436 (13)	0.46542 (4)	0.17646 (5)	0.0914 (3)
N1	0.7836 (3)	0.26396 (10)	-0.03727 (11)	0.0555 (5)
C8	0.9564 (4)	0.17516 (12)	0.04725 (12)	0.0489 (6)
C1	0.5739 (4)	0.29405 (11)	-0.07382 (12)	0.0520 (6)
H1B	0.4442	0.2674	-0.0567	0.062*
C6	0.5559 (4)	0.36693 (12)	-0.04157 (13)	0.0583 (7)
H6A	0.6885	0.3932	-0.0568	0.070*
N2	0.5510 (4)	0.36480 (10)	0.04896 (11)	0.0613 (6)
C14	0.7170 (5)	0.39062 (12)	0.09007 (14)	0.0586 (6)
H14A	0.8318	0.4110	0.0617	0.070*
C7	0.7660 (4)	0.20790 (12)	-0.00033 (12)	0.0492 (6)
H7A	0.6258	0.1861	-0.0032	0.059*
C13	1.1395 (4)	0.21396 (13)	0.07903 (13)	0.0587 (6)
H13A	1.1465	0.2602	0.0661	0.070*
C15	0.7373 (4)	0.38992 (12)	0.18143 (14)	0.0550 (6)
C10	1.1237 (5)	0.07662 (14)	0.11857 (14)	0.0673 (8)
H10A	1.1179	0.0304	0.1317	0.081*
C9	0.9546 (4)	0.10611 (12)	0.06799 (12)	0.0540 (6)
C16	0.9153 (4)	0.42153 (12)	0.22641 (15)	0.0615 (7)
C20	0.5769 (5)	0.35715 (13)	0.22604 (15)	0.0669 (7)
H20A	0.4546	0.3359	0.1976	0.080*
C11	1.3010 (5)	0.11644 (17)	0.14930 (15)	0.0777 (9)
H11A	1.4156	0.0972	0.1838	0.093*
C17	0.9323 (5)	0.42009 (15)	0.31214 (17)	0.0756 (8)
H17A	1.0535	0.4415	0.3411	0.091*
C2	0.5740 (4)	0.29389 (13)	-0.16818 (13)	0.0634 (7)
H2B	0.7073	0.3178	-0.1853	0.076*
H2C	0.5804	0.2472	-0.1880	0.076*
C3	0.3615 (5)	0.32848 (13)	-0.20597 (14)	0.0679 (7)
H3A	0.3679	0.3298	-0.2658	0.081*
H3B	0.2292	0.3020	-0.1931	0.081*
C5	0.3413 (5)	0.40078 (14)	-0.07892 (15)	0.0783 (9)
H5A	0.3340	0.4476	-0.0594	0.094*
H5B	0.2093	0.3766	-0.0610	0.094*
C12	1.3100 (4)	0.18501 (17)	0.12915 (15)	0.0725 (8)
H12A	1.4315	0.2116	0.1495	0.087*
C19	0.5930 (5)	0.35511 (14)	0.31149 (17)	0.0783 (8)
H19A	0.4841	0.3322	0.3401	0.094*
C4	0.3382 (5)	0.40022 (14)	-0.17353 (16)	0.0825 (9)
H4A	0.1970	0.4199	-0.1962	0.099*
H4B	0.4620	0.4281	-0.1915	0.099*
C18	0.7716 (6)	0.38728 (15)	0.35396 (17)	0.0819 (9)
H18A	0.7825	0.3866	0.4116	0.098*

Table 3.4 Atomic displacement parameters \AA^2

	U^{11}	U^{22}	U^{33}	U^{12}	U^{13}	U^{23}
C11	0.0871 (5)	0.0566 (4)	0.0835 (5)	0.0021 (4)	-0.0058 (4)	0.0000 (3)
C12	0.0686 (5)	0.1026 (6)	0.1027 (6)	-0.0136 (4)	0.0018 (4)	-0.0098 (4)
N1	0.0581 (13)	0.0600 (13)	0.0482 (11)	0.0065 (10)	0.0025 (10)	0.0112 (9)
C8	0.0547 (15)	0.0576 (15)	0.0350 (11)	0.0102 (12)	0.0076 (10)	-0.0003 (10)
C1	0.0560 (15)	0.0538 (14)	0.0457 (12)	0.0028 (12)	0.0003 (11)	0.0077 (10)
C6	0.0690 (17)	0.0549 (15)	0.0499 (13)	0.0001 (13)	-0.0050 (12)	0.0039 (11)
N2	0.0686 (14)	0.0649 (13)	0.0497 (11)	0.0024 (11)	-0.0019 (10)	-0.0047 (9)
C14	0.0677 (17)	0.0493 (14)	0.0583 (15)	0.0044 (13)	0.0002 (13)	-0.0018 (11)
C7	0.0542 (14)	0.0543 (14)	0.0393 (11)	0.0055 (12)	0.0034 (10)	-0.0002 (11)
C13	0.0649 (17)	0.0636 (16)	0.0478 (13)	0.0032 (13)	0.0052 (12)	-0.0007 (11)
C15	0.0638 (16)	0.0454 (14)	0.0547 (14)	0.0065 (12)	-0.0065 (13)	-0.0056 (11)
C10	0.087 (2)	0.0641 (17)	0.0496 (14)	0.0270 (16)	-0.0021 (14)	-0.0012 (12)
C9	0.0653 (16)	0.0589 (15)	0.0376 (12)	0.0145 (13)	0.0024 (11)	-0.0025 (10)
C16	0.0647 (17)	0.0533 (15)	0.0656 (16)	0.0062 (13)	-0.0041 (13)	-0.0067 (12)
C20	0.0782 (19)	0.0636 (17)	0.0576 (16)	-0.0079 (15)	-0.0060 (14)	-0.0053 (12)
C11	0.081 (2)	0.097 (2)	0.0536 (15)	0.0358 (18)	-0.0137 (15)	-0.0084 (15)
C17	0.081 (2)	0.076 (2)	0.0680 (18)	0.0003 (17)	-0.0157 (16)	-0.0181 (15)
C2	0.0752 (18)	0.0686 (17)	0.0461 (13)	0.0056 (14)	0.0021 (13)	0.0066 (12)
C3	0.0817 (19)	0.0721 (18)	0.0481 (14)	0.0024 (15)	-0.0103 (13)	0.0079 (12)
C5	0.096 (2)	0.0648 (17)	0.0712 (18)	0.0260 (16)	-0.0146 (16)	-0.0042 (14)
C12	0.0621 (17)	0.098 (2)	0.0570 (16)	0.0101 (17)	-0.0040 (14)	-0.0143 (15)
C19	0.095 (2)	0.0727 (19)	0.0674 (18)	-0.0071 (17)	0.0074 (16)	0.0016 (14)
C4	0.100 (2)	0.0716 (19)	0.0717 (18)	0.0166 (17)	-0.0243 (17)	0.0146 (14)
C18	0.111 (3)	0.077 (2)	0.0552 (16)	0.0005 (19)	-0.0075 (18)	-0.0097 (14)

Table 3.5 Geometric parameters (Å, °)

C1—C9	1.745 (2)	C10—H10A	0.9300
C12—C16	1.742 (3)	C16—C17	1.384 (3)
N1—C7	1.256 (3)	C20—C19	1.379 (3)
N1—C1	1.462 (3)	C20—H20A	0.9300
C8—C9	1.392 (3)	C11—C12	1.382 (4)
C8—C13	1.393 (3)	C11—H11A	0.9300
C8—C7	1.469 (3)	C17—C18	1.359 (4)
C1—C6	1.524 (3)	C17—H17A	0.9300
C1—C2	1.525 (3)	C2—C3	1.520 (3)
C1—H1B	0.9800	C2—H2B	0.9700
C6—N2	1.466 (3)	C2—H2C	0.9700
C6—C5	1.522 (3)	C3—C4	1.507 (4)
C6—H6A	0.9800	C3—H3A	0.9700
N2—C14	1.256 (3)	C3—H3B	0.9700
C14—C15	1.475 (3)	C5—C4	1.529 (3)
C14—H14A	0.9300	C5—H5A	0.9700
C7—H7A	0.9300	C5—H5B	0.9700
C13—C12	1.375 (3)	C12—H12A	0.9300
C13—H13A	0.9300	C19—C18	1.375 (4)
C15—C20	1.383 (3)	C19—H19A	0.9300
C15—C16	1.386 (3)	C4—H4A	0.9700
C10—C11	1.373 (4)	C4—H4B	0.9700
C10—C9	1.378 (3)	C18—H18A	0.9300
C7—N1—C1	116.8 (2)	C15—C20—H20A	119.1
C9—C8—C13	117.2 (2)	C10—C11—C12	120.3 (2)
C9—C8—C7	122.2 (2)	C10—C11—H11A	119.9
C13—C8—C7	120.5 (2)	C12—C11—H11A	119.9
N1—C1—C6	108.26 (18)	C18—C17—C16	119.8 (3)

N1—C1—C2	110.58 (19)	C18—C17—H17A	120.1
C6—C1—C2	110.38 (18)	C16—C17—H17A	120.1
N1—C1—H1B	109.2	C3—C2—C1	110.5 (2)
C6—C1—H1B	109.2	C3—C2—H2B	109.5
C2—C1—H1B	109.2	C1—C2—H2B	109.5
N2—C6—C5	110.0 (2)	C3—C2—H2C	109.5
N2—C6—C1	108.72 (18)	C1—C2—H2C	109.5
C5—C6—C1	110.19 (19)	H2B—C2—H2C	108.1
N2—C6—H6A	109.3	C4—C3—C2	111.4 (2)
C5—C6—H6A	109.3	C4—C3—H3A	109.3
C1—C6—H6A	109.3	C2—C3—H3A	109.3
C14—N2—C6	117.0 (2)	C4—C3—H3B	109.3
N2—C14—C15	122.6 (3)	C2—C3—H3B	109.3
N2—C14—H14A	118.7	H3A—C3—H3B	108.0
C15—C14—H14A	118.7	C6—C5—C4	110.7 (2)
N1—C7—C8	123.1 (2)	C6—C5—H5A	109.5
N1—C7—H7A	118.4	C4—C5—H5A	109.5
C8—C7—H7A	118.4	C6—C5—H5B	109.5
C12—C13—C8	121.1 (3)	C4—C5—H5B	109.5
C12—C13—H13A	119.5	H5A—C5—H5B	108.1
C8—C13—H13A	119.5	C13—C12—C11	120.1 (3)
C20—C15—C16	117.0 (2)	C13—C12—H12A	119.9
C20—C15—C14	120.7 (2)	C11—C12—H12A	119.9
C16—C15—C14	122.3 (3)	C18—C19—C20	119.4 (3)
C11—C10—C9	119.1 (3)	C18—C19—H19A	120.3
C11—C10—H10A	120.5	C20—C19—H19A	120.3
C9—C10—H10A	120.5	C3—C4—C5	111.0 (2)
C10—C9—C8	122.2 (2)	C3—C4—H4A	109.4
C10—C9—C11	117.6 (2)	C5—C4—H4A	109.4
C8—C9—C11	120.09 (17)	C3—C4—H4B	109.4
C17—C16—C15	121.5 (3)	C5—C4—H4B	109.4
C17—C16—C12	117.6 (2)	H4A—C4—H4B	108.0
C15—C16—C12	120.8 (2)	C17—C18—C19	120.3 (3)
C19—C20—C15	121.9 (2)	C17—C18—H18A	119.8
C19—C20—H20A	119.1	C19—C18—H18A	119.8
C7—N1—C1—C6	126.4 (2)	C20—C15—C16—C17	0.3 (4)
C7—N1—C1—C2	-112.5 (2)	C14—C15—C16—C17	-179.7 (2)
N1—C1—C6—N2	-60.1 (3)	C20—C15—C16—C12	-178.99 (19)
C2—C1—C6—N2	178.69 (19)	C14—C15—C16—C12	1.0 (3)
N1—C1—C6—C5	179.2 (2)	C16—C15—C20—C19	-0.7 (4)
C2—C1—C6—C5	58.1 (3)	C14—C15—C20—C19	179.3 (2)
C5—C6—N2—C14	-125.3 (2)	C9—C10—C11—C12	-0.5 (4)
C1—C6—N2—C14	114.0 (2)	C15—C16—C17—C18	-0.2 (4)
C6—N2—C14—C15	-178.0 (2)	C12—C16—C17—C18	179.1 (2)
C1—N1—C7—C8	-173.03 (19)	N1—C1—C2—C3	-177.1 (2)
C9—C8—C7—N1	-161.7 (2)	C6—C1—C2—C3	-57.3 (3)
C13—C8—C7—N1	23.4 (3)	C1—C2—C3—C4	56.3 (3)

C7—C8—C13—C12	174.8 (2)	C1—C6—C5—C4	-57.3 (3)
N2—C14—C15—C20	3.3 (4)	C8—C13—C12—C11	-0.4 (4)
N2—C14—C15—C16	-176.7 (2)	C10—C11—C12—C13	0.9 (4)
C11—C10—C9—C8	-0.4 (4)	C15—C20—C19—C18	0.9 (4)
C11—C10—C9—C11	178.1 (2)	C2—C3—C4—C5	-55.8 (3)
C13—C8—C9—C10	0.8 (3)	C6—C5—C4—C3	56.3 (3)
C7—C8—C9—C10	-174.3 (2)	C16—C17—C18—C19	0.5 (4)
C13—C8—C9—C11	-177.66 (17)	C20—C19—C18—C17	-0.8 (4)
C7—C8—C9—C11	7.3 (3)		

Table 3.6: Hydrogen - Bond Geometry (\AA , $^\circ$)

$D-H\cdots A$	$D-H$	$H\cdots A$	$D\cdots A$	$D-H\cdots A$
C7—H7A—C11	0.93	2.72	3.066 (2)	103
C14—H14A—C12	0.93	2.68	3.076 (3)	107

3.6.2 X-Ray Crystal Structure of L_5

L_5 was solved in the monoclinic system with space group $P2_1/c$ with cell coordinates $a = 10.914(3) \text{ \AA}$, $b = 4.4864(18) \text{ \AA}$, $c = 30.692(9) \text{ \AA}$, $\alpha = 90^\circ$, $\beta = 91.264(13)^\circ$, $\gamma = 90^\circ$, $V = 1502.45 \text{ \AA}^3$, and $Z = 4$, where slow evaporation of ethanol solution of pure L_5 yielded colorless crystals.

A crystal of dimensions $0.54 \times 0.53 \times 0.30 \text{ mm}$ was selected for X-ray diffraction analysis. Data were collected on a Bruker APEX-II diffractometer equipped with CCD detector and graphite monochromatic Mo $K\alpha$ radiation ($\lambda = 0.71073 \text{ \AA}$) at 293°K . Cell refinement and data reduction were carried out by Bruker SAINT [47]. SHELXS-97 [48,49] was used to solve structure (**Table 3.7**). The final refinement was carried out by full-matrix least-squares techniques with anisotropic thermal data for nonhydrogen atoms on F^2 . All the hydrogen atoms were placed in calculated positions. The crystal structure of L_5 was finally refined with R factor of 4.43% for 4390 unique reflections. Molecules were found to be packed in crystal lattice through intermolecular hydrogen bonding .

Details of crystal data, data collection and refinement are given below.

Table 3.7 Crystal data and structure refinement for L₅.

<i>Parameters</i>	
Empirical formula	C ₁₂ H ₁₀ Br ₂ N ₂ S ₂
Formula weight	406.16
Temperature	293 °K
Wave length	0.71073 Å
Crystal system,	monoclinic,
space group	P2 ₁ /c
Unit cell dimensions	a = 10.914(3) Å b = 4.4864(18) Å c = 30.692(9) Å alpha = 90 ° beta = 91.264(13) ° gamma = 90 °
Volume	1502.45 (17) Å ³
Z	4
Calculated density	1.294 Mg/m ³
Absorption coefficient	0.241 mm ⁻¹
F(000)	512
Crystal size	0.54 × 0.53 × 0.30
Theta range for data collection	1.57° to 25.50°.
Limiting indices	-11 ≤ h ≤ 12, -12 ≤ k ≤ 11, -14 ≤ l ≤ 16
Reflections collected / unique	7454 / 4390 [R(int) = 0.0182]
Completeness to theta	25.50-94.4 %
Absorption correction	Semi-empirical from equivalents
Max. and min. transmission	0.9647 and 0.9161
Refinement method	Full-matrix least-squares on F ²
Data / restraints / parameters	4390 / 0 / 311
Goodness-of-fit on F ²	1.038
Final R indices [I > 2σ(I)]	R1 = 0.0443, wR2 = 0.1124
R indices (all data)	R1 = 0.0573, wR2 = 0.1222
Largest diff. peak and hole	0.232 and -0.172 e.Å ⁻³

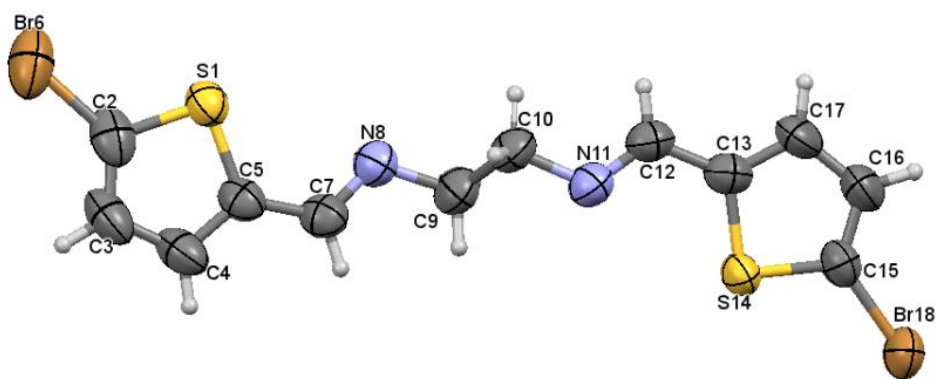
Table 3.8. Selected geometric parameters (\AA^2 °) for L_5 .

Br1—C11	1.871(6)	N2—C7	1.254(8)
Br2—C12	1.874(7)	C1—C2	1.38(1)
S1—C3	1.718(6)	C1—C11	1.337(9)
S1—C11	1.720(6)	C2—C3	1.37(1)
S2—C8	1.730(6)	C3—C4	1.444(9)
S2—C12	1.719(7)	C5—C6	1.50(1)
N1—C4	1.250(8)	C7—C8	1.425(9)
N1—C5	1.455(9)	C8—C9	1.368(9)
N2—C6	1.463(8)	C9—C10	1.38(1)
S1—C11—C1	112.1(5)	C5—C6—N2	112.3(6)
S1—C3—C2	109.8(5)	C6—N2—C7	117.1(6)
C11—C1—C2	112.4(7)	N2—C7—C8	124.1(6)
C1—C2—C3	114.4(7)	C7—C8—S2	121.4(5)
S1—C11—Br1	119.6(3)	C8—S2—C12	91.2(3)
S1—C3—C4	120.0(5)	S2—C12—Br2	119.4(4)
C3—C4—N1	121.2(6)	S2—C12—C10	112.1(6)
C4—N1—C5	119.9(6)	C12—C10—C9	111.9(7)
N1—C5—C6	109.5(6)	C10—C9—C8	114.8(6)
S1—C3—C4—N1	-4.7(9)	N2—C7—C8—C9	-179.7(7)
C3—C4—N1—C5	-180.0(6)	S1—C11—C1—C2	-0.3(9)
C4—N1—C5—C6	-131.9(6)	C11—1—C2—3	0(1)
C5—C6—N2—C7	127.2(6)	C1—C2—C3—S1	-0.0(9)
H6—N2—C7—C8	148.2	S2—C12—C10—C9	0.2(8)
N2—C7—C8—S2	3.1(9)	C12—C10—C9—C8	-0.4(9)

Table 3.9: Hydrogen bonding data for L₅.

D	H	A	D-H	H...A	D...A	D-H...A
C21	H21A	O1 ^a	0.9300	2.5500	3.390(3)	150.00
C22	H22A	O1 ^a	0.9600	2.4000	3.299(3)	155.00
C27	H27A	O2 ^b	0.9600	2.3900	3.232(3)	146.00

Symmetry codes: ^a1-x,-y,-z, ^b2-x,1-y,2-z

**Figure 3.40:** The ORTEP diagram of the final X-ray model of L₅.

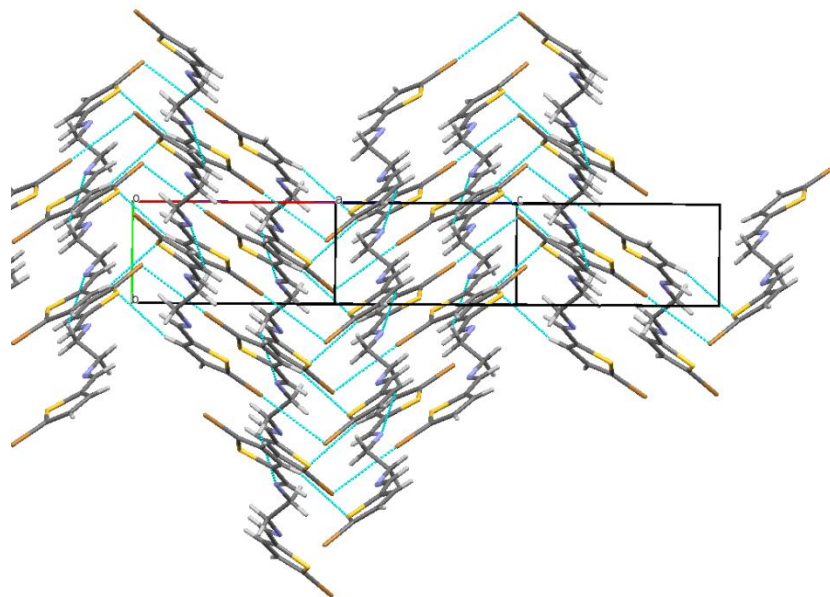


Figure 3.41: Crystal packing of the L₅.

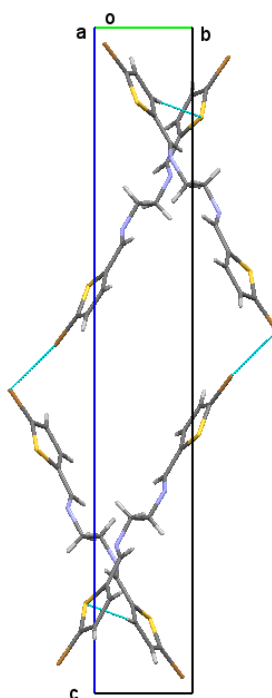


Figure 3.42: Crystal packing of the L₅

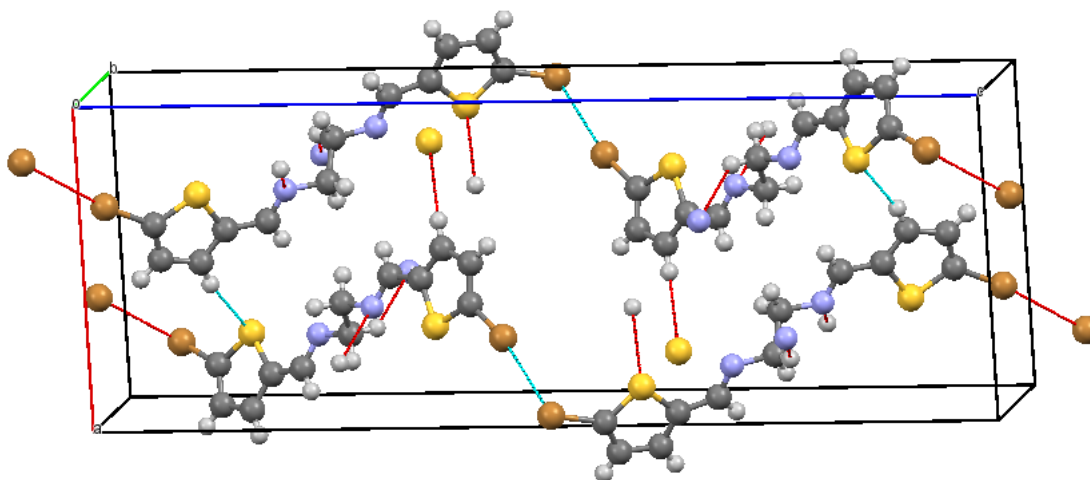


Figure 3.43: The crystal packing of L_5 . Only the hydrogen atoms involved in S...H bonding are marked by red bond, the S...S repulsion can be observed as green line

The symmetric unit contains four molecules. The crystal structure of L_5 is composed of two planar separated thiophene rings (S1/C3-C2/C1 and S2/C8-C9/C10) connected along C4 and C7 plane. having two phenyl (C7-C12/C13-C18) rings and dimethylaminoprop-2-en-1-one (O1/N1/ C19-C23 and O2/N2/C24-C28) moieties attached to C1, C2, C4, and C5 atoms respectively. Two thiophene (S1/C1-C3/C6 and S2/C3- C5/C6) and phenyl (C7-C12 and C13-C18) rings are each planar with maximum deviation of 0.009(1) °Å for S1 and C5 atoms from the root mean square plane. In the crystal molecules are linked *via* C21-H21A... O1, C22-H22A... O1, C27-H27A... O2 interaction to form chain arranged as observed in **Figure 3.43**.

3.7 Antibacterial activity

The antibacterial effect of ligands and their Cu(II) complexes were assessed against a variety of microorganisms including *E. coli*, *S. aureus*, *P. aeruginosa*, and *MRSA*. The minimum inhibitory concentration (MIC) of ligands and their complexes were also determined against these four test bacterial strains by broth microdilution technique.

The procedures described here are in accordance with the international recommendations provided by the Clinical and Laboratory Standards Institute (CLSI).

For MIC determination, the inoculum was prepared using a 4-6 h broth culture of each bacterial strain adjusted to a turbidity equivalent to a 0.5 McFarland standard (1.5×10^8 cfu/ml), then the bacteria suspension was diluted with nutrient broth to give a concentration of $\approx 5 \times 10^7$ cfu/mL. Two fold serial dilutions of compounds were prepared in nutrient broth in 96-well plates starting from (10.00 mg/mL DMSO) and (10.00 mg/mL distilled water) as stock solutions of ligands and copper(II) complexes respectively.

An equal volume of bacterial inoculum (1.0 μ L) was added to each well on the microtiter plate. In this manner, final concentrations of compounds range from 5000-9.76 μ g/mL and 5×10^7 cfu/mL bacteria in each well (last wells are broth only control wells). The inoculated microtiter plates were incubated at 37 °C for 24 h.

The MIC value was defined as the lowest concentration of compounds whose no turbid was comparable with the negative control wells (broth only, without inoculum). Where the growth was monitored visually.

The DMSO was used as a solvent for ligands and distilled water for the Copper complexes .

The test microorganisms *Escherichia coli* ATCC (25923), *P. aeruginosa* ATCC (27853), *Staphylococcus aureus* ATCC (25923) and *Staphylococcus aureus* (MRSA Positive) were obtained from the American Type Culture Collection (ATCC). The organisms were maintained on agar slope at 4 °C and sub-cultured for 24 h before use. DMSO (Merck). 96-well microtiter plates (TPP 92096) were used for microdilution tests.

All the Ligands and their complexes gave potential antibacterial effect against *E. coli*, *S. aureus*, *P. aeruginosa*, and MRSA (*Methicillin-resistant Staphylococcus aureus*) in the variable ratios of the concentrations.

3.7.1 Discussion about Figures (3.44-3.55)

- ❖ All the tested complexes of copper show lower activity than the free ligands.
- ❖ L₂, L₄, and L₅ as free ligands showed the same activity against *E.coli* bacteria, where the MIC appeared at 0.625 mg/ml, but the copper complex of L₂ having lower activity than others complexes. L₄ and L₅

and their copper complexes give the same result where the MIC reached 0.625 mg/ml in one hundred percent, as in **Figures 3.44, 3.45** and **3.46**.

- ❖ L₄ as free ligand shows the most activity against *S.aureus* bacteria compared with L₂ and L₅ where the MIC appeared at 0.15625 mg/ml as in **Figure 3.47**, followed by L₂ in activity, where the MIC appeared at 0.3125 mg/ml as in **Figure 3.48**.

In the other hand, the Copper complexes of L₂, L₄, and L₅ having the same activity and MIC appeared 0.938 mg/ml but the percentage of inhabitation were varying below one hundred percent .

- ❖ L₅ as free ligand shows the most activity against *Pseudomonas* bacteria compared with L₂ and L₄, where the MIC of it appeared at 0.3125 mg/ml as in Figure 3.50. And the L₂ and L₄ having the same activity and percentage of inhabitation, where the MIC appeared at 0.625 mg/ml as in **Figure 3.50**, and **3.51**.

In the other hand, the copper complexes of L₄ considered having the highest activity with 0.938 mg/ml in MIC value and 40% on its value, as in **Figure 3.52**, followed by copper complex of L₅, where the MIC appeared 1.875 mg/ml, and the copper complex of L₂ with MIC value at 3.75 mg/ml in 50%.

- ❖ L₄ as free ligand shows the most activity against *MRSA* bacteria compared with L₂ and L₅ where the MIC appeared at 0.15625 mg/ml as in **Figure 3.53**, followed by L₂ in activity, where the MIC appeared at 0.3125 mg/ml as in **Figure 3.54** .

In the other hand, the copper complexes of L_4 and L_5 having the same activity and MIC appeared 0.938 mg/ml and the percentage of inhabitation were above 50% . The copper complexes of L_2 having the lowest value of MIC it appeared at 3.75 mg/ml with the percentage around 20%.

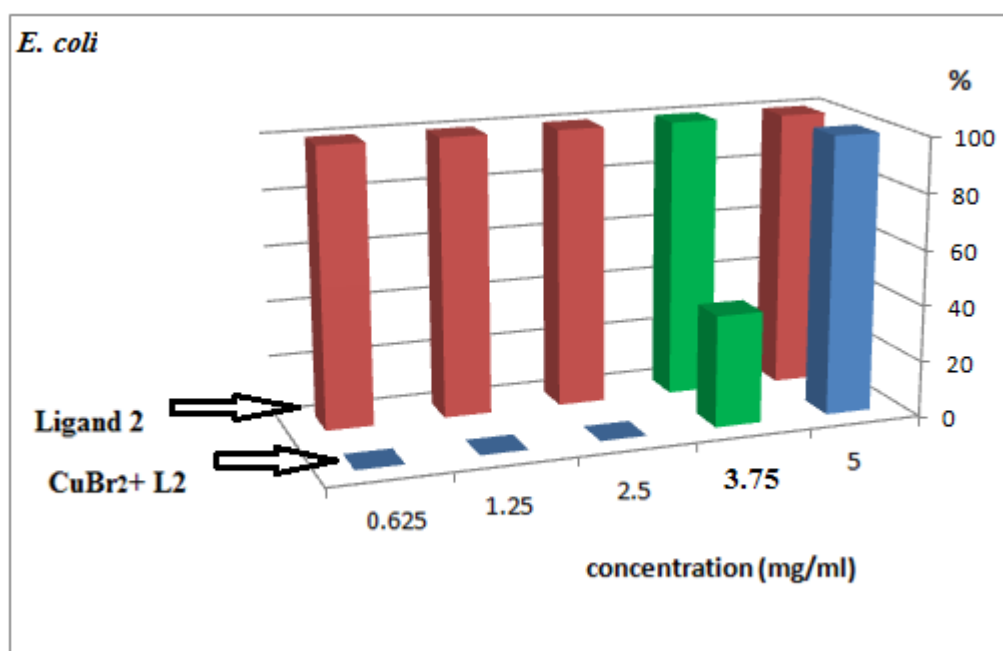


Figure 3.44: Antibacterial activity of L_2 & L_2CuBr_2 against (*E.coli*).

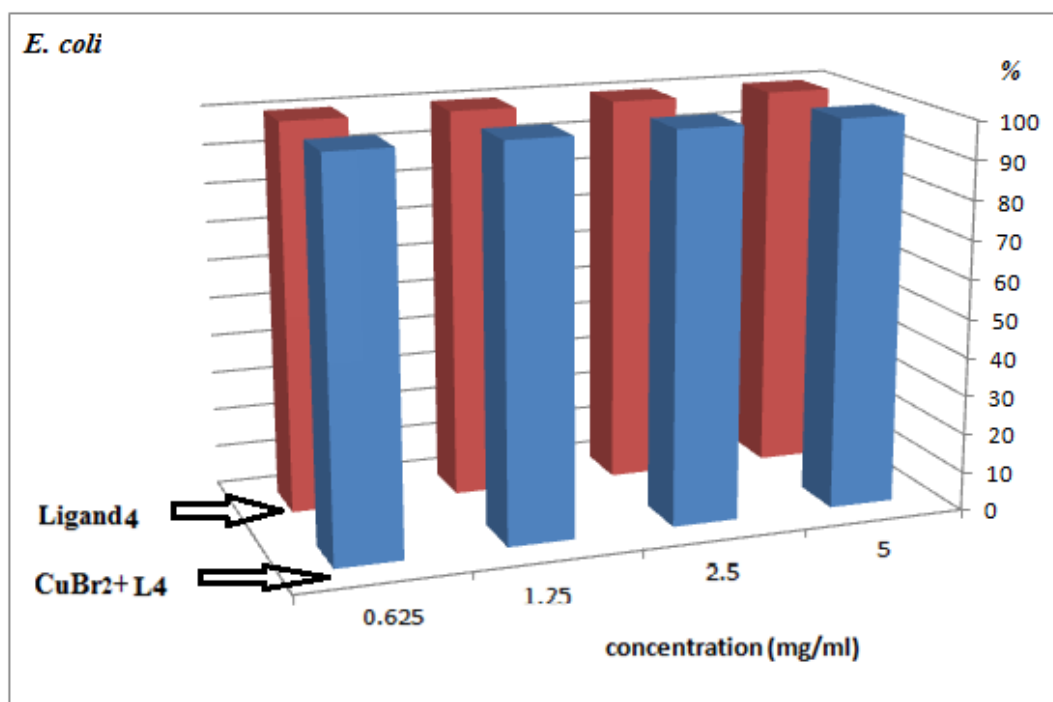


Figure 3.45: Antibacterial activity of L_4 & L_4CuBr_2 against (*E.coli*).

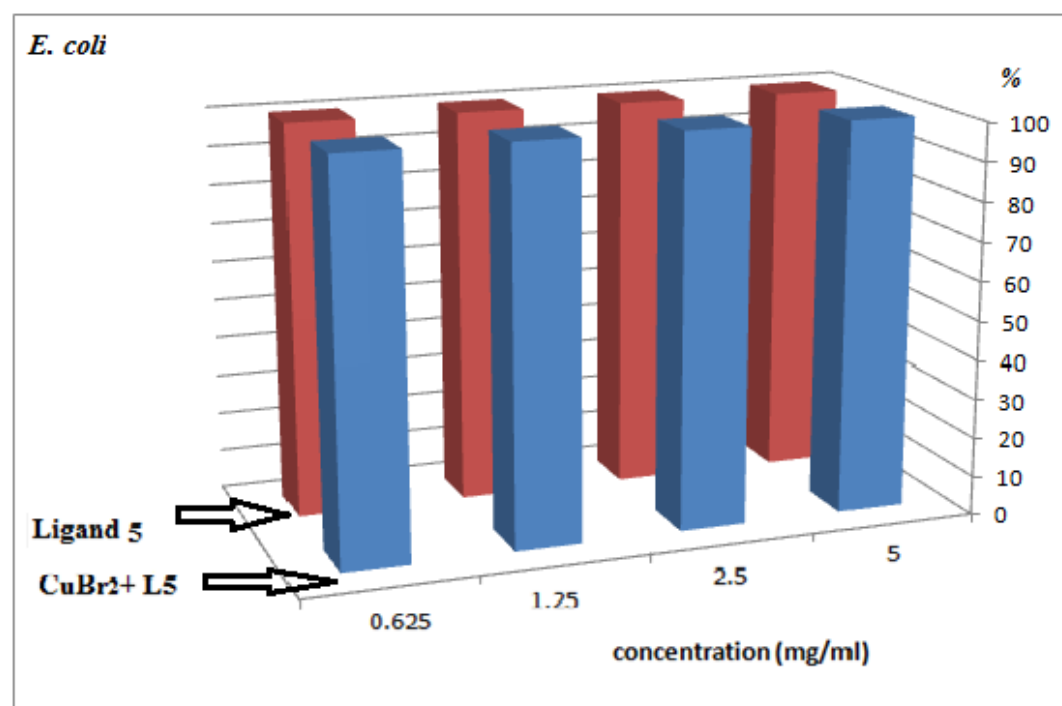


Figure 3.46: Antibacterial activity of L_5 & L_5CuBr_2 against (*E.coli*).

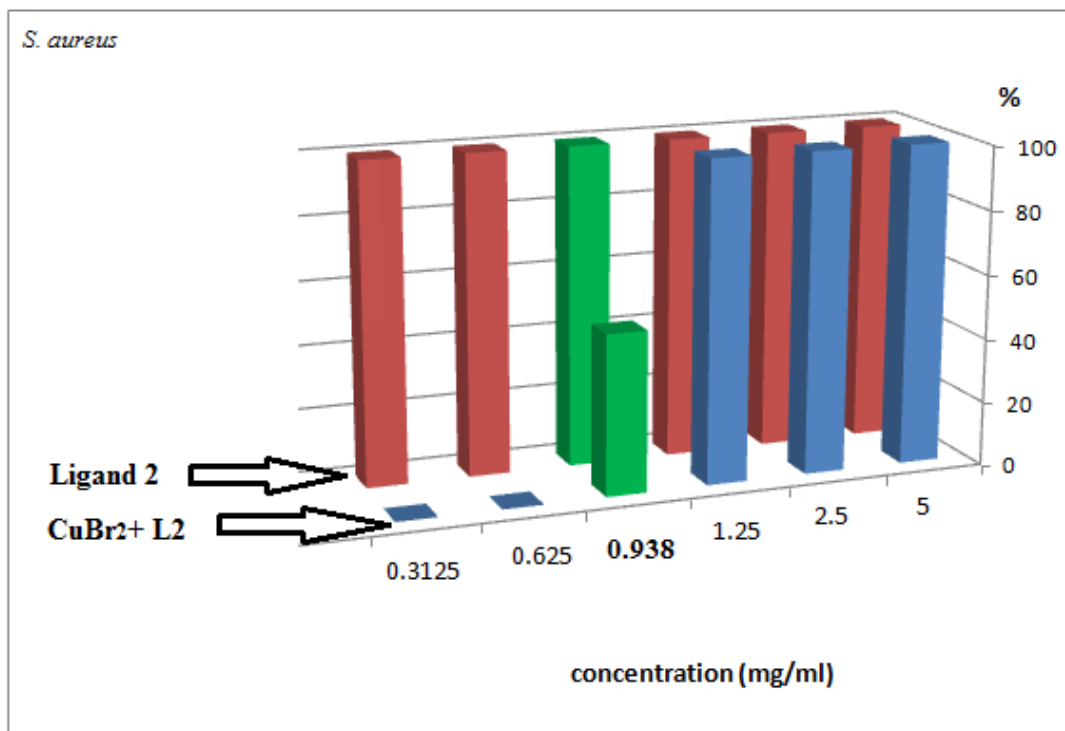


Figure 3.47: Antibacterial activity of L_2 & L_2CuBr_2 against (*S. aureus*).

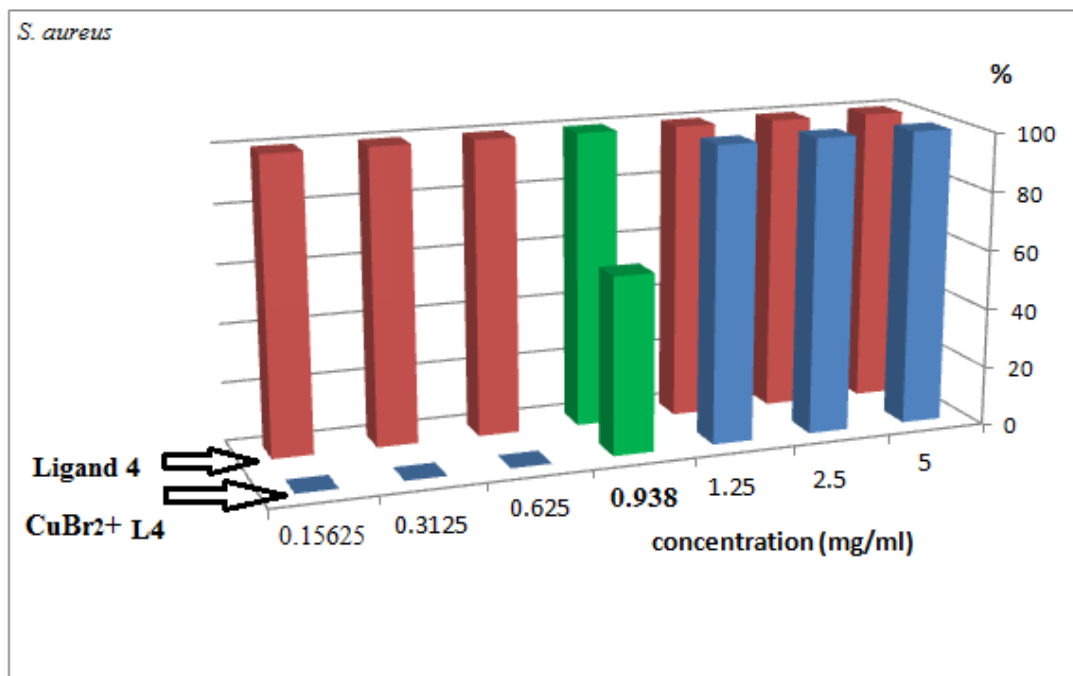


Figure 3.48: Antibacterial activity of L_4 & L_4CuBr_2 against (*S. aureus*)

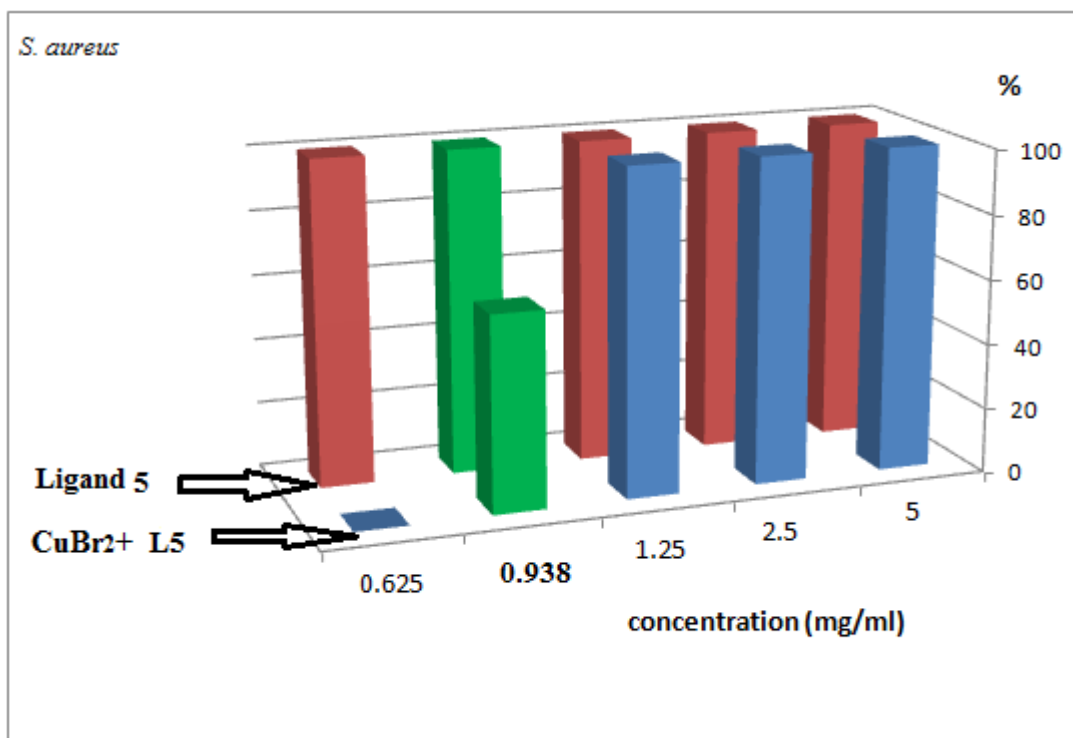


Figure 3.49: Antibacterial activity of L₅ & L₅CuBr₂ against (*S. aureus*).

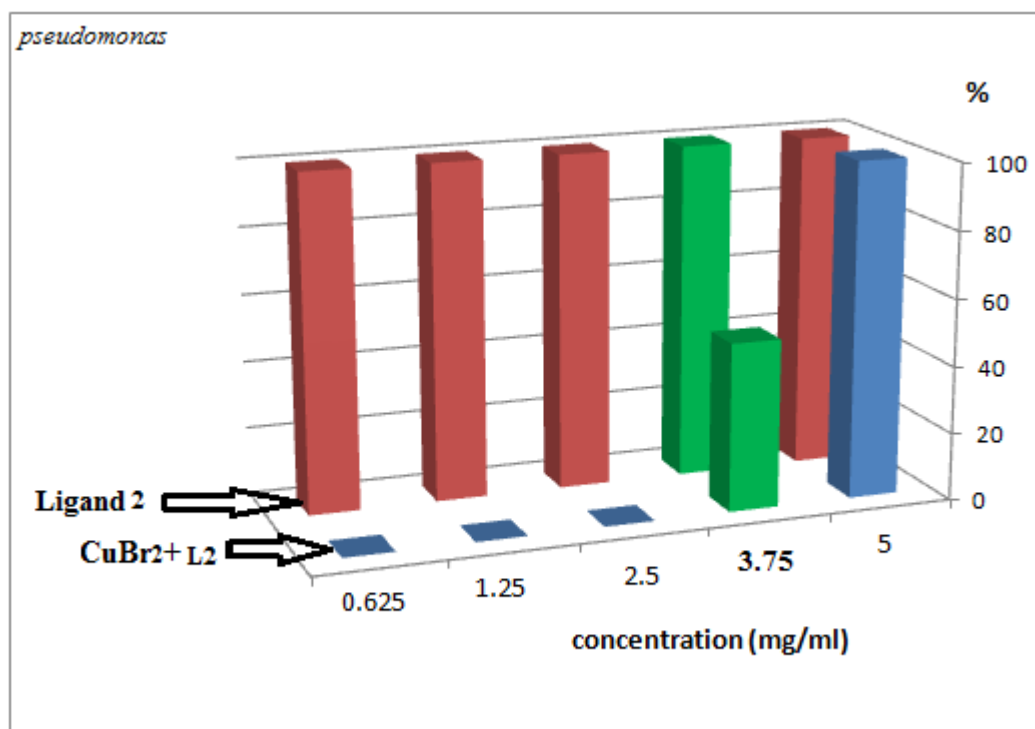


Figure 3.50: Antibacterial activity of L₂ & L₂CuBr₂ against (*Pseudomonas*).

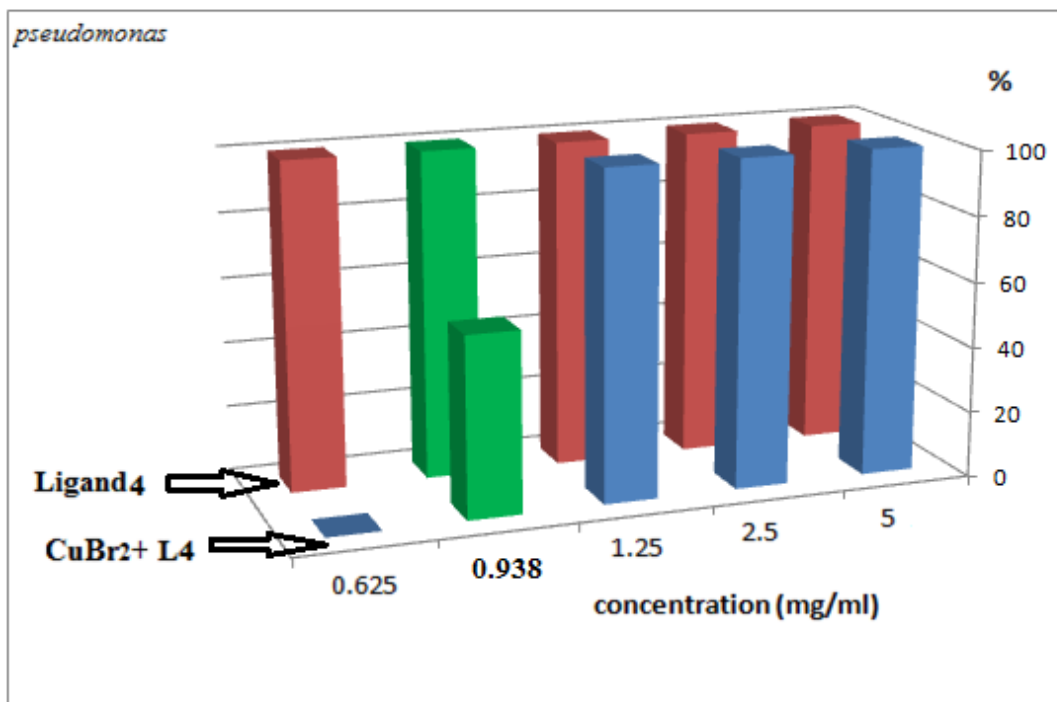


Figure 3.51: Antibacterial activity of L₄ & L₄CuBr₂ against (*Pseudomonas*).

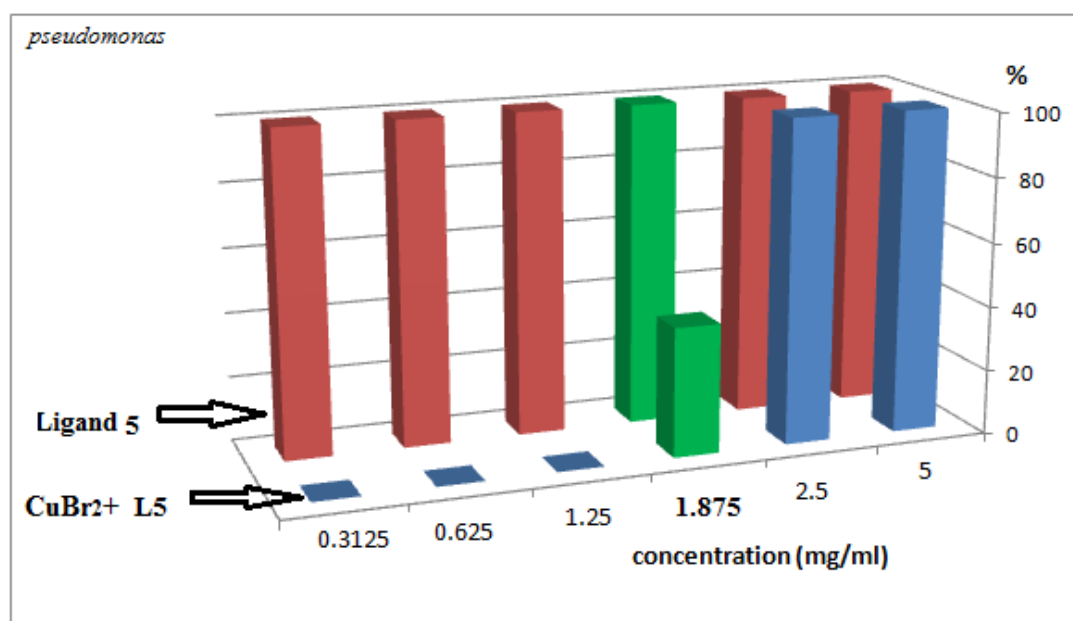


Figure 3.52: Antibacterial activity of L₅ & L₅CuBr₂ against (*Pseudomonas*).

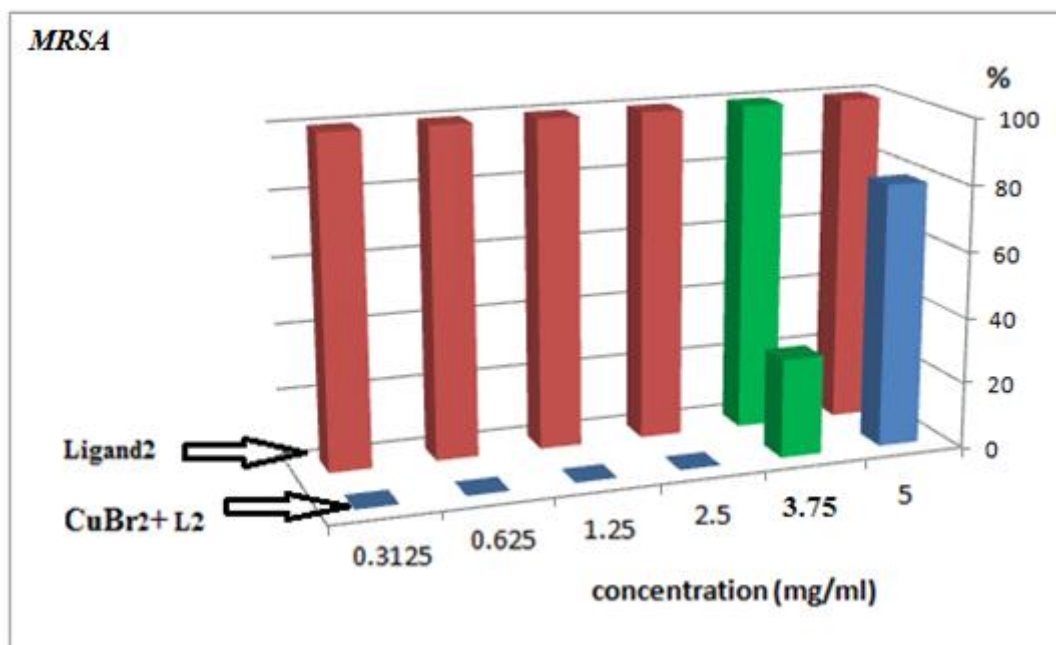


Figure 3.53: Antibacterial activity of L_2 & L_2CuBr_2 against (*MRSA*).

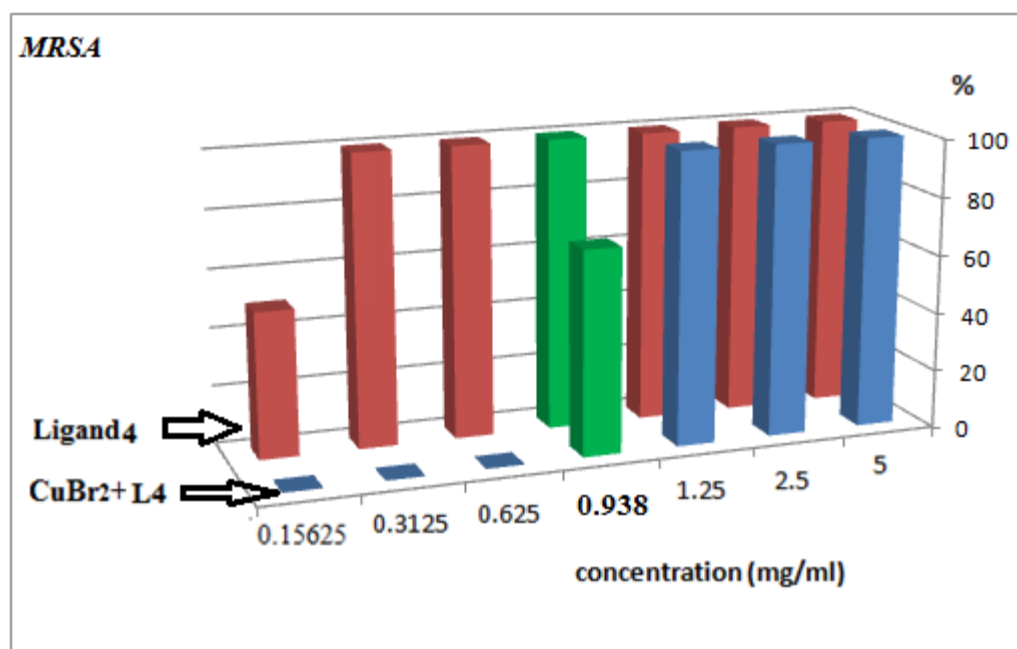


Figure 3.54: Antibacterial activity of L_4 & L_4CuBr_2 against (*MRSA*).

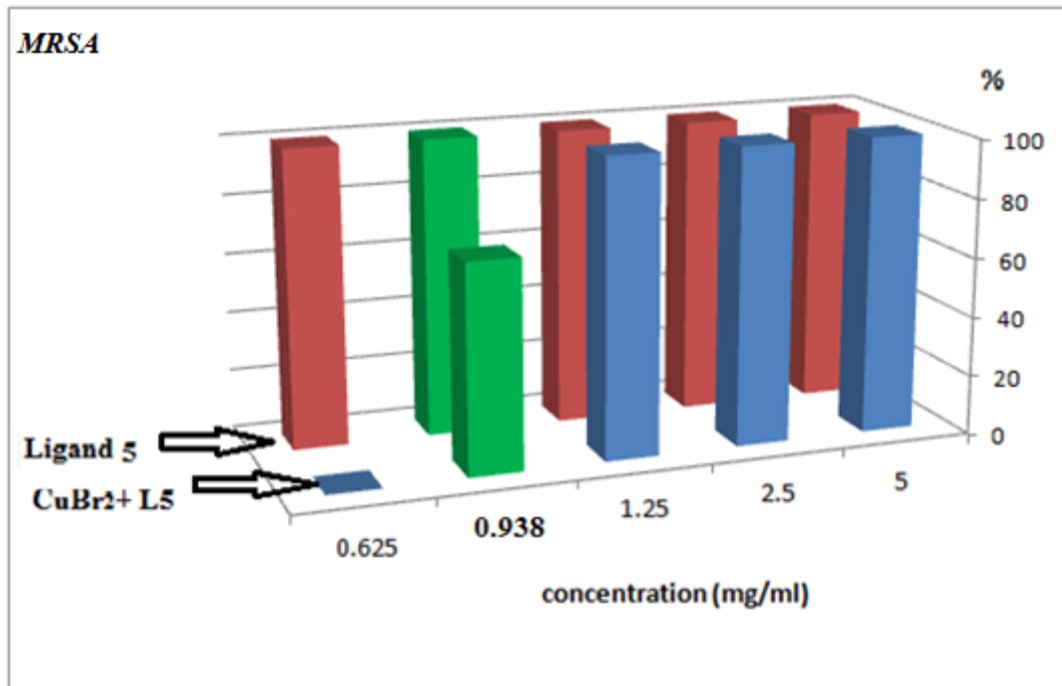


Figure 3.55: Antibacterial activity of L₅ & L₅CuBr₂ against (*MRSA*).

Chapter Four

Conclusion

In this project, six of polydentate Schiff's base ligands, copper (II) and cadmium(II) complexes were synthesized and characterized as follows:

✓ Schiff's base ligand **1**

[(E)-2-(piperidin-1-yl)-N-(pyridin-2-ylmethylene)ethanamine] formed readily in 75.5% yield. The structure was identified by IR, ¹H-NMR, and ¹³C-NMR spectroscopy.

✓ Schiff's base ligand **2**

[(E)-N-(3-bromobenzylidene)-2-(piperidin-1-yl) ethanamine]

was synthesized in 80.5% yield, and the structure was identified by IR, ¹H-NMR, and ¹³C-NMR spectroscopy.

This Schiff's base readily coordinates with CuBr₂. The free ligand and its complex with copper have the potential antibacterial activity against *E. coli*, *S. aureus*, *P. aeruginosa*, and *MRSA* bacteria.

✓ Schiff's base ligand **3**

[(N¹E,N²E)-N¹,N²-bis(2-chlorobenzylidene)cyclohexane-1,2-diamine]

was synthesized in 85.0% yield. And the structure was identified by IR, ¹H-NMR, and ¹³C-NMR spectroscopy.

This ligand was analyzed by XRD, this ligand is racemic, in which the cyclohexane ring adopts the expected didentate chair conformation suitable for mononuclear for mononuclear and dinuclear metal complexes, where this project was published.

✓ Schiff's base ligand **4**

[(N¹E,N²E)-N¹,N²-bis(3-bromobenzylidene)ethane-1,2-diamine] was in 80.3% yield. And the structure was identified by IR, ¹H-NMR, and ¹³C-NMR spectroscopy. This Schiff's base readily coordinates with CuBr₂ and CdCl₂. The thermal analysis was studied for this ligand and its complexes with CuBr₂ and CdCl₂. The free ligand and its complex with copper have the potential antibacterial activity against *E. coli*, *S. aureus*, *P. aeruginosa*, and *MRSA* bacteria.

✓ Schiff's base ligand **5**

(N¹E,N²E)-N¹,N²-bis((5-bromothiophen-2-yl)methylene)ethane-1,2-diamine] was synthesized in 88.2% yield. And the structure was identified by IR, ¹H-NMR, and ¹³C-NMR spectroscopy. This Schiff's base readily coordinates with CuBr₂ and CdCl₂.

The ligand analyzed by XRD, is revealed helix zig zag structure suitable for tetra dentate mononuclear and dinuclear metal complexes.

The free ligand and its complex with copper have the potential antibacterial activity against *E. coli*, *S. aureus*, *P. aeruginosa*, and *MRSA* bacteria.

✓ Schiff's base ligand **6**

[(N¹E,N²E)-N¹,N²-bis(2-chlorobenzylidene)ethane-1,2-diamine] was synthesized in 84.4 % yield. The structure was identified by IR, ¹H-NMR, and ¹³C-NMR spectroscopy. This Schiff's base readily coordinates with CuBr₂.

Our ligands and their complexes with copper have the potential antibacterial activity against *MRSA* bacteria, where the infections caused by these strains are more difficult in treatment with standard types of antibiotics and thus are more dangerous.

References

1. D. Patel, A. Patel, **Synthesis and Antibacterial Activity of M(II) N-[4 dimethyleamino] benzylidene benzene 1,2, diamine Complex**, *Journal of Pharmaceutical Science and Technology*. **4** (2011), 905-909.
2. A. Kraft, G. GmbH, **On The Discovery and History of Prussian blue**. *Bulletin. Historical Chemistry*. **33**(2008), 61-67.
3. G. Y. Yeap, S. T. Ishizawa , K. Suda, P. Boey, W. Mahmood, **Synthesis, Crystal Structure and Spectroscopic Study of Para Substituted 2-Hydroxy-3-Methoxybenzalideneanilines**, *Journal of Molecular Structure*. **658** (2003), 87.
4. A. Werner, **Beitrag zur Konstitution Anorganischer Verbindungen**. *Zietschraft of Anorngnica Chemie*. **3**(1983), 267-330.
5. M. Azam, I. Warad, S. I. Al-Resayes, N. Alzaqri, M.R. Khan, **Synthesis and Structural Characterization of Pd(II) Complexes Derived from Perimidine Ligand and Their in Vitro Antimicrobial Studies**, *Journal of Molecular Structure*. **1047** (2013), 48–54.
6. R. H. Crabtree, **The Organometallic Chemistry of the Transition Metals**. Wiley. 2005, 560.
7. M. Frezza, S. Hindo, D. Chen, A. Davenport, S. Schmitt, D. Tomco, and Q. Ping Dou, **Novel Metals and Metal Complexes as Platforms for Cancer Therapy**, *Current Pharmaceutical Design*. **16**(2010), 1813–182.

8. K. L. Haas and K. J. Franz , **Application of Metal Coordination Chemistry to Explore and Manipulate Cell Biology**, *Chemical Reviews*. **109**(2009), 4921–4960.
9. A. Prakash, D. Adhikari, **Application of Schiff bases and their metal complexes-A Review**, *International Journal of Chemistry and Technology Research*. **3** (2011), 1891-1896.
10. V. B. Kenche and K. J. Barnham, Alzheimer's disease & metals: **therapeutic opportunities**, *British Journal of Pharmacology*. **163**(2011), 211-219.
11. S. Tengattini, R. J. Reiter, D. Tan, M. P. Terron, L. F. Rodella and R. Rezzani, Cardiovascular Diseases: **Protective Effects of Melatonin**, *Journal of Pineal Research*. **44**(2008), 16-25.
12. R. Gomathi, A. Ramu, Synthesis, **Characterization of Novel Cu(II) Complexes of Isatin Derivatives as Potential Cytotoxicity, DNA binding, Cleavage and Antibacterial Agents**, *International Journal of Innovative Research in Science, Engineering and Technology*. **2**(2013), 4852-4865.
13. M. Hutton, Human Health Concerns of Lead, Mercury, **Cadmium and Arsenic**, Chapter 6, 53-68.
14. J. N. LePage , W. Lindner , G. Davies , D. E. Seitz , **Resolution of the Optical Isomers of Dansyl Amino Acids by Reversed Phase Liquid Chromatography with Optically Active Metal Chelate Additives**, *Journal of the Analytical Chemistry*. **51**(1979), 433-435.

15. A. M. Alaghazl, H. A. Bayoumi, **Synthesis, Spectral Properties and Potentiometric Studies on Some Metal Schiff Base Complexes Derived from 4-chlorophenyl-2-aminothiazole**, *International Journal of Electrochemical Science*. **8**(2013), 11860 –11876.
16. M. Hakimi, K. Moeini, Z. Mardani, F. Khorrami, **Crystal Structure and Characterization of a New Eight Coordinated Cadmium Complex**, *Journal of the Korean Chemical Society*. **57**(2013), 252-556.
17. A. Xavier, N. Srividhya, **Synthesis and Study of Schiff base Ligands**, *Journal of Applied Chemistry (IOSR-JAC)*. **57**(2014), 6-15.
18. M. A. Ashraf, K. Mahmood, A. Wajid, **Synthesis, Characterization and Biological Activity of Schiff Bases**, *International Conference on Chemistry and Chemical Process*. **10** (2011), 1-7.
19. S. Arulmurugan, H. P. Kavitha, B.R. Venkatraman, **Biological Activities of Schiff Base and its Complexes: A Review**, *Rasayan journal of chemistry*. **3**(2010), 385-410.
20. W. Al Zoubi, **Biological Activities of Schiff Bases and Their Complexes: A Review of Recent Works**, *International Journal of Organic Chemistry*. **3**(2013), 73-95.
21. Y. Ishii, K. Yamawaki, T. Ura, Y. Yamada, T. Ushida, M. Ogawa, **Hydrogen Peroxide Oxidation Catalyzed by Heteropoly Acids Combined with Cetylpyridinium Chloride. Epoxidation of Olefins and Allylic Alcohols, Ketonization of Alcohols and Diols, and Oxidative Cleavage of 1,2-diols and Olefins**, *Journal of Organic Chemistry*. **53**(1988), 3587.

22. B. E. Love, J. Ren, **Synthesis of Sterically Hindered Imines**, *Journal of Organic Chemistry*. **58**(1993), 5556–5557.
23. S. Kalaivani, N. P. Priya, S. Arunachalam, **Schiff Bases: Facial Synthesis, Spectral Characterization and Biological Studies**, *International Journal of Applied Biology and pharmaceutical Technology*. **3**(2012), 219-223.
24. S. Gaur, **Physico-Chemical and Biological Properties of Mn(II), Co(II), Ni(II) and Cu(II) Chelates of Schiff Bases**, *Assian Journal of chemistry*. **15**(2003), 250.
25. M. J. Gemi, C. Biles, B. J. Keiser, S. M. Poppe, S. M. Swaney, W. G. Tarapley, D. L. Romeso, Y. Yage, **Novel 1,5-Diphenylpyrazole Nonnucleoside HIV-1 Reverse Transcriptase Inhibitors with Enhanced Activity versus the Delavirdine-Resistant P236L Mutant: Lead Identification and SAR of 3- and 4-Substituted Derivatives**, *Journal of Medical Chemistry*. **43**(2000), 1034.
26. H. Schiff, **Mitteilungen aus dem Universitätslaboratorium in Pisa: Eine neue Reihe organischer Basen**, *Journal of Justus Liebigs Annalen der Chemie*. **131**(1864), 118–119.
27. E. J. Campbell, S. T. Nguyen, **Unsymmetrical Salen-Type Ligands: High Yield Synthesis of Salen-Type Schiff Bases Containing Two Different Benzaldehyde Moieties**, *Tetrahedron Letters*. **42**(2001), 1221-1225.
28. G. M. Santerre, C. J. Hansrote, T. I. Crowell, **The Reaction of Aromatic Aldehydes with N-butylamine Acid Catalysis and**

- Substituent Effects**, *Journal of American Chemical Society*. **80**(1958), 1254.
- 29.S. Patai, **The Chemistry of the Carbon- Nitrogen Double Bond**, Wiley: New York (1970).
- 30.K. Metwally, M. Abdel-Aziz , M. Lashine, I. Husseiny, H. Badawy, **Hydrazones of 2-Arylquinoline- 4-Carboxylic Acid Hydrazides: Synthesis and Preliminary Evaluation as Antimicrobial Agents**, *Journal of Bioorganic Medicinal Chemistry*. **14**(2006), 8675-8682.
31. R. Abu-El-Halawa, M. Al-Nuri, F. Mahmoud, **Synthesis and Antimicrobial Activity of New N-Methyl-N-(2-pyridyl) Aromatic and Heteroaromatic Hydrazones**, *Assian Journal of chemistry*. **19**(2007), 1658.
- 32.S. H. Khoo', J. Bond, D. W. Denning, **Administering Amphotericin B—a Practical Approach**, *Journal of Antimicrobial Chemotherapy*. **33**(1994), 203-213.
- 33.R. Laniado-Labori'n, M. N. Vargas, **Amphotericin B: Side Effects and Toxicity**, *Journal of Molecular Structure*. **26**(2009), 223–227.
- 34.S. Chandra, D. Jain, AK. Sharma, P. Sharma, **Coordination Modes of a Schiff Base Pentadentate Derivative of 4-aminoantipyrine with Cobalt(II), Nickel(II) and Copper(II) Metal Ions: Synthesis, Spectroscopic and Antimicrobial Studies**, *Journal of Molecules*. **14**(2009), 174-190.

- 35.P. Cozzi, N. Mongelli, A. Suarato, **Recent Anticancer Cytotoxic Agents**, *Journal of Current Medicinal Chemistry Anti-Cancer Agents*. **4**(2004), 93–121.
- 36.P. Prabhu, S. Pande, C. Shastry, **Synthesis and Biological Evaluation of Schiff's Bases of Some New Benzothiazole Derivatives as Antimicrobial Agents**, *International Journal Chemical Technology Research*. **3**(2011),185-191.
- 37.E. Brantley, V. Patel, S. Stinson, V. Trapani, C. D. Hose, HP. Ciolino, G. C. Yeh, **The Antitumor Drug Candidate 2-(4-amino-3-methylphenyl)-5-fluorobenzothiazole Induces NF-kappaB Activity in Drug-Sensitive MCF-7 cells**, *Anticancer Drugs journal*. **16**(2005), 137-143.
38. J. E. Coia, Clinical, **Microbiological and Epidemiological Aspects of Escherichia Coli O157 Infection**, *FEMS. Immunology and Medicinal Microbiology*. **20**(1998), 1–9.
- 39.A. Pietrangelo, E.coli Infection, *Healthline*, 2012.
- 40.L. R. W. Plano, **Staphylococcus Aureus Exfoliative Toxins: How they Cause Disease**, *Journal Investigative Dermatology*. **122**(2004), 1070–1077.
- 41.L. G. Harris, S. J. Foster, and R.G. Richards, **An Introduction to Staphylococcus Aureus, and Techniques for Identifying and Quantifying S, Aureus Adhesions in Relation to Adhesion to Bioma Terials: Review**, *European Cells and Materials*, **4**(2012), 39-60.

- 42.E. B. M. Breidenstein, C. de la Fuente-Núñez, R. E. W. Hancock, ***Pseudomonas aeruginosa: All Roads Lead to Resistance, Trends in Microbiology***. **19**(2011), 419–426.
- 43.N. Mesaros, P. Nordmann, P. Pleśiat, M. R. Delvallez, J. Van Eldere, Y. Glupczynski, ***Pseudomonas Aeruginosa: Resistance and Therapeutic Options at the Turn of the New Millennium, Clinical Microbiology Infection***. **13**(2007), 560–578.
- 44.A. Vipra, S. N. Desai, R. P. Junjappa, P. Roy, N. Poonacha, P. Ravinder, B. Sriram, S. Padmanabhan, ***Determining the Minimum Inhibitory Concentration of Bacteriophages: Potential Advantages, Advances in Microbiology***. **3**(2013), 181-190.
- 45.B. S. Sekhon, Inorganics/Bioinorganics: ***Biological, Medicinal and Pharmaceutical Uses, Journal of Pharmaceutical Education and Research***. **2**(2011), 1-20.
- 46.P. Kuhnert, P. Boerlin, J. Frey, ***Target Genes for Virulence Assessment of Escherichia Coli Isolates from Water, Food and the Environment, FEMS Microbiology Reviews***. **24**(2000), 107-117.
47. S. J. Cavalieri, ***Manual of Antimicrobial Susceptibility Testing, American Society for Microbiology***, 2005.
- 48.Abu-Obaid, A.I. Asadi, A. Alruwaili, H. Atieh, S. Khlaif, T. Ben Hadda, S. Radi, B. Hammouti, ***I. Warad, 5,5-dimethyl-2,2-di(pyridin-2-yl)hexahydropyrimidine, Molbank***. **1**(2015), 838.

- 49.S. Resayes, I. Warad, M. I. Choudhary, A.Wahab and S. Rasheed, **Heterocyclic Schiff's Bases as Novel and New Antiglycation Agents**, US Patent, 2014. USA2014/0221429A1.
- 50.I. Warad, M. Azam, S. I. Al-Resayes, M. S. Khan, M. Al-Nuri, S. Jodeh, A. Husein, S. F. Haddad, B. Hammouti, M. Al-Noaimi, **Structural Studies on Cd (II) Complexes Incorporating Di-2-pyridyl Ligand and the X-ray Crystal Structure of the Chloroform Solvated DPMNPH/CdI₂ Complex**, *Inorganic Chemistry Communications*, **43**(2014), 155-161.
- 51.M. AL-Noaimi, M. I. Choudhary, F. F. Awwadi, W. H. Talib, T. Ben Hadda, S. Yousuf, A. Sawafta, I. Warad, **Characterization and Biological Activities of Two Copper(II) Complexes with Dipropylenetriamine and Diamine as Ligands**, *Spectrochimica Acta Part A: Molecular and Biomolecular Spectroscopy*, **127**(2014), 225-230.
- 52.M. Al-Noaimi, O. Abdel-Rahman, I. I. FASFous, M. El-khateeb, F. Awwadi, I. Warad, **Ruthenium(II) Bipyridine Complexes Bearing Quinoline-Azoimine (NNN) Tridentate Ligands: Synthesis, Spectral Characterization, Electrochemical Properties and Single-Crystal X-ray Structure Analysis**, *Spectrochimica Acta Part A: Molecular and Biomolecular Spectroscopy*. **125**(2014), 375–383
- 53.T. B. Hadda, H. Bendaha, J. Sheikh, M. Ahmad, Ismail Warad, **Computational POM Evaluation of Experimental in Vitro**

- Trypanosoma Cruzi and Mycobacterium Tuberculosis Inhibition of Heterocyclic-2-Carboxylic Acid (3-cyano-1,4-dioxoquinolin-2-yl)amide Derivatives**, *Medicinal Chemistry Research*. **23**(2014), 1956-1965.
54. Warad, M. Al-Noaimi, S. Haddad, Y. Al-Demeri and B. **Hammouti**, **Rac-(E,E)-N,N₀-Bis(2-chlorobenzylidene)-cyclohexane-1,2-diamine**, *Acta Crystallographica Section E*. **69**(2013), o1075.
55. M. Azam, I. Warad, S. I. Al-Resayes, M. R. Siddiqui, M. Oves, **Synthesis, Physicochemical Properties, and *in Vitro* Antibacterial Screening of Palladium (II) Complexes Derived from Thiosemicarbazone**, *Chemistry & Biodiversity*. **10**(2013) 1109–1119.
56. M. Azam, I. Warad, S. Al-Resayes, M. Shakir, M. F. Ullah, A. Ahmad, F. H. Sarkar, **A Novel Ru (II) Complex Derived from Hydroxydiamine as a Potential Antitumor Agent: Synthesis and Structural Characterization**, *Inorganic Chemistry Communications*. **20**(2012), 252-258.
57. M. Azam, I. Warad, S. Al-Resayes, M. Zahin, I. Ahmad and M. Shakir, **Syntheses, Physico-Chemical Studies and Antioxidant Activities of Transition Metal Complexes with a Perimidine Ligand**, *Zeitschrift für anorganische und allgemeine Chemie*. **638**(2012), 1–7.

جامعة النجاح الوطنية

كلية الدراسات العليا

تحضير وتحليل وقياس النشاط ضد البكتيريا لمركبات مبتكرة مكونة من
اتحاد قواعد شيف مع ايونات العناصر الانتقالية

اعداد

ياسمين عزام الضميري

اشراف

أ.د. اسماعيل وراذ

قدمت هذه الرسالة استكمالاً لمتطلبات الحصول على درجة الماجستير في الكيمياء بكلية
الدراسات العليا، في جامعة النجاح الوطنية في نابلس، فلسطين.

2015

ب

تحضير وتحليل وقياس النشاط ضد البكتيريا لمركبات مبتكرة مكونة من اتحاد قواعد شيف مع

ايونات العناصر الانتقالية

اعداد

ياسمين عزام الضميري

اشراف

أ.د. اسماعيل وراد

الملخص

العمل الموصوف في هذه الأطروحة يتعلق بتحضير ستة قواعد الشيف المتعددة المنح

Copper polydentate Schiff 's bases وايضا تكوين معقداتها مع ثنائي بروميد النحاس

Bromide، وثنائي كلوريد الكاديوم Cadimium Chloride مع هذه القواعد.

وقد تم تحضير هذه القواعد بتفاعل التكثيف Condensation reaction بين الأمينات الأولية مع

الألدهيدات في الايثانول النقي في ظروف خاصة. وكذلك تم تكوين معقدات النحاس والكاديوم

بهذه الطريقة في نظام مغلق.

ونشير الى ان جميع المركبات درست خصائصها باستخدام القياسات الفيزيائية التالية:

IR, UV-VIS , EA, ¹H-NMR , ¹³C-NMR, TG/DTA.

وأیضا نشیر الى استخدام تقنية ال XRD ،حيث تمت دراسة قاعدتين من قواعد الشيف الستة

لمعرفة ودراسة شكلها بصورة دقيقة.

L₅(N¹E,N²E)-N¹,N²-bis((5-bromothiophen-2-yl)methylene)ethane-1,2-diamine

L₃[(N¹E,N²E)-N¹,N²-bis(2-chlorobenzylidene)cyclohexane-1,2-diamine].

ج

وأيضاً تم دراسة الأثر البيولوجي لقواعد الشيف ومعداتها مع النحاس وفعاليتها ضد أنواع مختلفة من البكتيريا *E. coli*, *S. aureus*, *P. aeruginosa*, and *MRSA*. حيث أظهرت القواعد العضوية نشاط أكبر من معداتها.

